

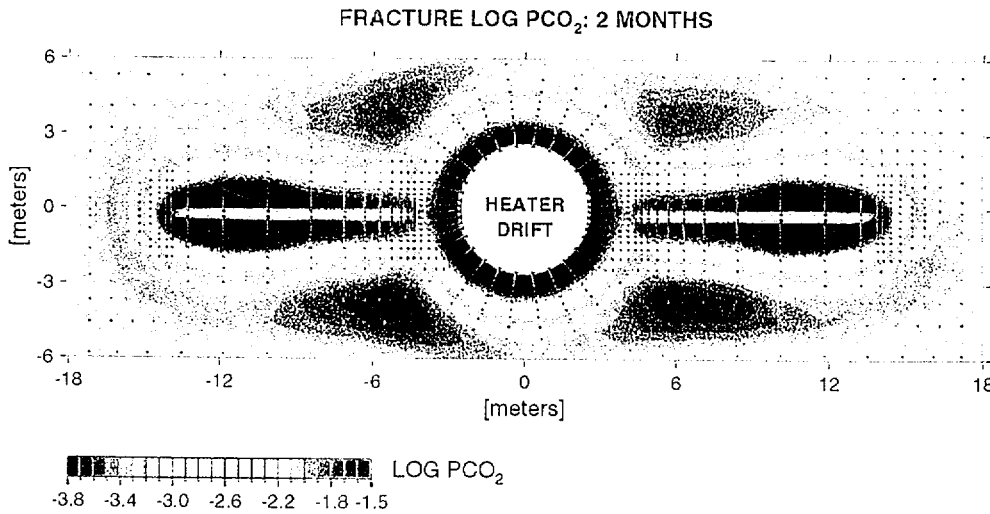
Level 4 Milestone SPY289M4  
September 10, 1998  
Version 1.1

Yucca Mountain Site Characterization Project

**Thermo-Hydro-Chemical Predictive Analysis  
For The Drift-Scale Heater Test**

Eric Sonnenthal, Nicolas Spycher, John Apps, and Ardyth Simmons

Lawrence Berkeley National Laboratory



Earth Sciences Division  
Lawrence Berkeley National Laboratory  
One Cyclotron Road MS 90-1116  
Berkeley, CA 94720

---

<b>1.</b>	<b>INTRODUCTION .....</b>	<b>4</b>
-----------	---------------------------	----------

---

<b>2.</b>	<b>WORK COMPLETED, ONGOING AND PLANNED .....</b>	<b>6</b>
2.1	Purpose and scope of this report.....	6
2.1.1	Major code capabilities of TOUGHREACT and use for this project .....	6
2.1.2	Model developments in progress.....	8
2.1.3	Model developments under consideration.....	8

---

<b>3.</b>	<b>BACKGROUND AND PREVIOUS WORK .....</b>	<b>9</b>
3.1	Purpose of DST.....	9
3.2	THC regimes in the repository and in the DST.....	10
3.2.1	Boiling zone.....	10
3.2.2	Condensation zone .....	10
3.2.3	Cooling phase.....	11
3.3	Insights on THC behavior from tests and geothermal analogues.....	11
3.3.1	Laboratory tests.....	11
3.3.2	Field tests.....	13
3.3.3	Geothermal analogues .....	14
3.4	Insights from previous modeling studies.....	15
3.5	Mineralogy of the fractured tuff.....	17

---

<b>4.</b>	<b>QA STATUS OF CODES AND DATA.....</b>	<b>19</b>
4.1	QA Status of Data Used in Report.....	19
4.2	QA Status of Codes.....	21

---

<b>5.</b>	<b>CONCEPTUAL MODEL OF THERMO-HYDRO-CHEMICAL PROCESSES FOR THE DST .....</b>	<b>22</b>
-----------	--	-----------

---

<b>6.</b>	<b>DEVELOPMENT AND ANALYSIS OF THERMODYNAMIC DATA FOR THE DST..</b>	<b>24</b>
6.1	Revision of Thermodynamic Data.....	24
6.1.1	Low Albite.....	26
6.1.2	Potash Feldspar.....	27
6.1.3	I/S Phases: Illite.....	27

6.1.4	I/S Phases: K-Smectite.....	27
6.1.5	I/S Phases: Ca-, Mg-, Na- Smectites .....	28
6.1.6	Kaolinite.....	28
6.1.7	Sepiolite .....	28
6.1.8	Quartz .....	29
6.1.9	Cristobalite .....	29
6.1.10	Amorphous Silica.....	29
<hr/>		
<b>7.</b>	<b>WATER AND GAS CHEMISTRY.....</b>	<b>30</b>
7.1	Water Chemistry .....	30
7.1.1	Statement of the Problem.....	30
7.1.2	Evaluation of Pore Water Analyses for Consistency.....	31
7.1.3	Preliminary Interpretation of Pore Water Equilibrium with Respect to Solid Phases.....	34
7.2	Gas Chemistry .....	37
7.2.1	Carbon dioxide.....	37
7.2.2	Nitrous oxide.....	37
7.2.3	Hydrogen.....	37
7.2.4	Other species, e.g. HCl, NH <sub>3</sub> , B(OH) <sub>3</sub> .....	38
<hr/>		
<b>8.</b>	<b>TOUGHREACT CODE: BASIS OF GEOCHEMICAL CALCULATIONS.....</b>	<b>38</b>
8.1	Geochemical and Mass-Transfer Calculations .....	39
8.2	Transport Calculations .....	42
<hr/>		
<b>9.</b>	<b>MODEL AND CODE TESTING.....</b>	<b>42</b>
9.1	Equilibrium Simulations: Heating and Boiling without Advection/Dispersion.....	42
9.2	Kinetic Simulations of Plug Flow Reactor Experiments.....	44
<hr/>		
<b>10.</b>	<b>DATA UNCERTAINTIES .....</b>	<b>47</b>
<hr/>		
<b>11.</b>	<b>EXPLORATORY GEOCHEMICAL SIMULATIONS.....</b>	<b>47</b>
11.1	Thermochemical Processes of the Altered Zone.....	48
11.1.1	Zone of Desiccation.....	48
11.1.2	Zone of Condensation and Reflux .....	52
11.2	Additional Geochemical Simulations .....	55
11.2.1	Heating.....	56
11.2.2	Boiling .....	57
11.2.3	Gas Condensation:.....	58

---

11.3	Discussion .....	59
------	------------------	----

---

<b>12.</b>	<b>DRIFT-SCALE TEST MODEL DESCRIPTION.....</b>	<b>59</b>
12.1	Grid, Thermohydrological Parameters, and Boundary Conditions.....	59
12.2	Geochemical Parameters.....	60
12.3	Mineral Abundances.....	63
12.4	Estimation of Pore Water Composition in the Tptpmn Unit.....	64

---

<b>13.</b>	<b>DRIFT-SCALE TEST SIMULATIONS.....</b>	<b>65</b>
13.1	DST-1, DST-1a.....	66
13.3	DST-3 .....	70
13.4.	DST-4 .....	71

---

<b>14.</b>	<b>CONCLUSIONS.....</b>	<b>73</b>
	ACKNOWLEDGMENTS .....	74

---

<b>15.</b>	<b>REFERENCES .....</b>	<b>74</b>
------------	-------------------------	-----------

---

<b>16.</b>	<b>FIGURES (APPENDIX A).....</b>	<b>93</b>
------------	----------------------------------	-----------

---

## 1. INTRODUCTION

This report presents a predictive analysis of the geochemical and isotopic alteration of minerals, fluid, and gas accompanying the underground Drift-Scale Heater Test (DST) begun in December 1997. The aim of this analysis is to incorporate the important geochemical and physical phenomena in a numerical model, using and assessing the current information on pore-water chemistry, mineralogy, thermodynamic and kinetic data, and heater test conditions. This work represents an initial effort to understand the system behavior, and the results should not be used by YMP researchers to provide quantitative estimates of the processes investigated. The DST will operate over a period of eight years; as data are collected the models and understanding of the system will undergo refinement and reevaluation. In overall terms, our objective is to provide a better understanding of the coupled thermo-hydrological-chemical (THC) system that could be applied with a higher level of confidence to constrain the behavior of the proposed repository for a period of ten thousand years or more.

In such a complex, highly coupled system, there are many variables that are only known approximately or not at all (e.g., thermodynamic data, rates of dissolution and precipitation, nucleation kinetics, reactive surface areas and surface properties, and mineral heterogeneity) in addition to uncertainties in the hydrological properties of fractured tuff. Therefore it is necessary to consider these analyses to be sensitivity studies along the path of understanding the system behavior. Given these caveats, constraints can be applied so that once geochemical data are collected, they can be used to obtain the overall rates of reaction, even if some of the detailed reaction parameters are unobtainable. One example we present is the use of Sr isotopic ratios to estimate the shift in the  $^{87}\text{Sr}/^{86}\text{Sr}$  isotopic ratio in water as a function of the dissolution of the anorthite component in feldspars.

A much better constrained aspect of coupled THC processes is the behavior of heat, fluid, and water vapor transport, in the absence of strong effects on permeability and porosity, accompanying the DST. Our model grid, input thermal and hydrological parameters, and boundary conditions are those developed for the thermo-hydrological model of the DST presented by Birkholzer and Tsang (1997). Their work, in turn, derives important parameters for unsaturated zone flow in matrix and fractures (e.g., Bandurraga and Bodvarsson, 1997; Sonnenthal et al., 1997a) from the site-scale unsaturated zone (UZ) flow model, and of course from various data and insights developed by others for the Yucca Mountain Project. Thus, the philosophy of this work is to combine the current capabilities regarding the physical behavior of the system with a conceptual model and numerical code to study geochemical effects on the system and the possible coupling to their thermohydrology.

The initial pore-water geochemistry is an important starting point in the simulation of water-rock interaction. Because no analyses have been made in the DST area, we present an analysis of the pore water geochemistry at Yucca Mountain and make an estimate of what could be a representative or average, pore-water chemistry for the Topopah Spring welded tuff. As for the thermo-hydrology, we build on the work presented to understand the controls on the ambient pore-water chemistry in the mountain (Apps, 1997; Yang et al., 1996a,b) and models for the strontium isotopic effects observed (Sonnenthal et al., 1997b).

Fundamental inputs to the numerical model are the thermodynamic and kinetic data. Here we present a new analysis of some of the relevant thermodynamic data for minerals under the conditions expected for the DST. We also build strongly on the kinetic and thermodynamic data (Hardin, 1998), fundamental reaction-transport experiments (Johnson et al., 1997a,b) and analysis of the geochemical system expected for the near-field environment and for the Single Heater Test (Glassley et al., 1997).

As of the start of this project in late 1997, there were no available numerical codes that could handle a general problem of multicomponent and multiphase transport, heat, equilibrium and kinetic mineral-water reaction, adsorption and exchange, and gas species transport for 2-D and 3-D dual-permeability problems for an arbitrary number of chemical species and mineral phases. Our work has involved the adaptation, enhancement, and testing of the TOUGHREACT code (Tianfu Xu and Karsten Pruess, 1997; 1998), in order to handle these important aspects of the DST, Single Heater Test, and the repository-induced THC processes. To build confidence in the code and our conceptual model of reaction-transport processes, we present several comparisons to experiments and to other modeling results under equilibrium and kinetic conditions. We also present sensitivity studies on the geochemistry of boiling systems to help us in our understanding of the DST simulation results.

Important aspects of the problem and numerical code are still being implemented and tested, such as a module to couple the feedbacks to flow via porosity, permeability changes in fracture and matrix, and the reverse feedback to the grain sizes, reactive surface areas, and textural relationships. This, along with an overview of our accomplished and planned work, is presented in the following section.

---

## 2. WORK COMPLETED, ONGOING AND PLANNED

### 2.1 Purpose and scope of this report

This report provides a predictive analysis of thermohydrochemical (THC) processes in the DST. The work was conducted under WBS 1.2.3.14.2 in Work Package 123E2275M2. Under this directive, the pre-test predictions are the first step in a comprehensive analysis to refine and update model predictions related to geochemistry/mineralogy-petrology data from the DST.

This section presents an overview of the tested numerical code capabilities (verification and validation), data assessed, and simulations undertaken.

#### 2.1.1 Major code capabilities of TOUGHREACT and use for this project

##### 2.1.1.1 Numerical Code

- Heat, fluid, water vapor transport (identical to Q-version of TOUGH2 v 1.11 EOS3).
- Dual permeability formulation (transport, flow, and diffusion between fractures and matrix, with separately defined mineral proportions and properties in each continuum);
- Equilibrium, kinetic, or mixed reactions for precipitation and dissolution;
- Any number of primary and secondary aqueous species (tested 13 primary, 29 secondary);
- Any number of minerals (tested 20 minerals);
- Diffusion and advection of species in aqueous and gas phases;
- Development and incorporation of a new thermodynamic database;
- Incorporation of different rate laws for precipitation and dissolution;
- Adsorption and ion exchange (implemented but not considered in this report);
- Consideration of CO<sub>2</sub> transport in gas phase. O<sub>2</sub> and redox have been considered for problems related to supergene enrichment (Xu et al., 1998a). Gas phase species currently considered in equilibrium with fluid.

- Isotopic ratios in fluid; calculation of  $^{87}\text{Sr}/^{86}\text{Sr}$  ratio in pore fluid.

#### **2.1.1.2 Data Analysis**

- Pore-water geochemistry;
- Thermodynamic data;
- Kinetic data;
- Ambient mineralogy.

#### **2.1.1.3 Verification and Validation**

- Verification by comparison to analytical solutions and other simulators for equilibrium and kinetic conditions at 25°C (Xu, 1996; Xu et al., 1998a, Xu et al., 1998b);
- Comparison to SOLVEQ/CHILLER equilibrium model result (Reed, 1982; Spycher and Reed, 1992) under heating and boiling conditions;
- Modeled quartz and TSw tuff plug flow reactor experiments by Johnson et al. (1997a).

#### **2.1.1.4 Model Simulations**

Using the exact thermohydrological predictive model (mesh, thermohydrologic properties, initial and boundary conditions, etc.) from the DST simulation by Birkholzer and Tsang (1997) we made:

- Simulations of mineral phases, proportions, fluid, and gas compositions in fractures and matrix (dual permeability) as a function of space and time in 2-D;

- Estimates of porosity changes—currently no coupling of porosity and permeability changes to flow field;
- Simulation of the Sr isotopic ratio in the fluid.

Model results are presented here for different time periods up to the full eight year planned heating and cooling phases of the DST. Because of the complexity of the geochemical systems and their sensitivity to numerical errors, transport effects, and thermodynamic/kinetic input data, the results should be considered as exploratory and will require further study to confirm whether they are representative of processes in the DST.

### **2.1.2 Model developments in progress**

- Coupling porosity and permeability changes to the flow field, updating reactive surface areas and crystal morphology in fracture and matrix continua;
- Completing a model for Sr isotopic ratios to include both exchange and precipitation effects;
- Evaluating the effects of boiling, condensation and transport on oxygen and deuterium isotopic ratios;
- Evaluating and testing conceptual models for chemical transport between fractures and matrix;
- Refining mineral distributions and heterogeneity in fractures and matrix;
- Expanding the number of participating mineral phases (in particular, zeolites).

### **2.1.3 Model developments under consideration**

- Coupling of gas species partial pressure to total pressure;

- Improving activity coefficient calculation methods;
- Incorporating additional kinetic rate laws;
- Evaluating system conditions at final dryout and initial rewetting;
- Incorporating the MINC model for a refined mesh in the matrix blocks;
- Incorporating temperature and species-dependent diffusion coefficients for aqueous and gas phase species.

---

### 3. BACKGROUND AND PREVIOUS WORK

The quantity of water entering the Engineered Barrier System (EBS) and its chemical behavior are essential to understanding the performance of the EBS and the influence of coupled THC processes on the alteration of the natural system. Water entering the EBS has the potential for contacting waste packages. The chemical composition of the water (e.g., pH, dissolved solids), which will be modified by repository thermal processes, has a direct bearing on corrosion rates and processes, and therefore may impact waste package performance. Hot water also has the potential for altering fracture mineral coatings, for dissolving mineral constituents such as silica and calcite at near-boiling temperatures close to the repository drifts, and for redepositing salts and mineral coatings in cooler regions farther away from the drifts. Potential changes in fracture coating mineralogy could change the transport properties of the rock over time. Circulating hot water could dissolve fracture mineral coatings in some areas and precipitate them in others, thus altering the permeability of the near-field environment. These rock-water interactions will operate over time scales far beyond our ability to monitor and observe them. However, data collected from *in situ* tests coupled with predictive models should advance our confidence in the ability to bound these processes.

#### 3.1 Purpose of DST

The DST, which began on December 3, 1997 in the Exploratory Studies Facility (ESF), is designed to gain a better understanding of coupled thermal, hydrological, mechanical, and

chemical processes likely to occur in the rock mass surrounding a potential repository at Yucca Mountain. Coupled processes in the DST will be monitored over an eight-year period as the test progresses through four years of heating, followed by four years of cooldown after the heaters are turned off. The DST has nine canister heaters, placed in a drift with a heated length of 47.6 m and flanked by 25 borehole wing heaters in each wall (CRWMS, 1997). The drift wall temperature will approach 200°C during the test (Birkholzer and Tsang, 1997). Sensors installed in over ninety instrumented boreholes monitor temperature, humidity, gas pressure, and mechanical displacement of the rock mass. Neutron logging, electrical resistivity tomography, cross-hole radar tomography, and air injection tests will be performed at intervals to measure moisture redistribution due to boiling, vaporization, and condensation of pore water (CRWMS, 1997). Liquid water and gas samples, collected opportunistically, will be analyzed to determine water-rock interaction. Passive monitoring and active testing data are intended to provide a base for modeling coupled thermal-hydrological-chemical processes, in order to advance understanding and reduce uncertainty in predicting repository performance.

### 3.2 THC regimes in the repository and in the DST

The evolution of the thermo hydrologic regime in the unsaturated zone surrounding the DST can be described in terms of processes occurring during the heating and cooling stages. During heating, THC reactions will occur in boiling and condensation zones. These are shown schematically for the potential repository at Yucca Mountain in Figure 3.1.

#### 3.2.1 Boiling zone

During the initial heating stage, rocks will be heated significantly above the boiling point, and evaporation and boiling of pore waters will take place. Along with evaporation and boiling, other processes are expected to occur. These include: 1) saturation with respect to calcium and magnesium sulfates and hydrated silicates; 2) transient dissolution of primary and some secondary minerals in response to a new equilibrium state imposed at elevated temperatures; 3) transient supersaturation and precipitation of secondary minerals resulting from the enhanced dissolution of primary minerals; 4) hydrolysis in response to elevated temperatures; and 5) partition of some volatiles and gases into the vapor phase, e.g., CO<sub>2</sub>, HCl, N<sub>2</sub>O, B(HO)<sub>3</sub> (and NH<sub>4</sub>Cl) (U.S. Department of Energy, 1995).

#### 3.2.2 Condensation zone

A condensation zone will occur beyond the volume of rock in which boiling takes place. Although the boiling point of water at Yucca Mountain is ~95°C, the condensation boundary temperature will be modified by capillary action and a lowered vapor pressure due to

dissolved salts. Within the condensation zone, the following are expected to take place: 1) dilution of pore waters with condensate; 2) enhanced dissolution of primary and secondary minerals in response to the new equilibrium state imposed by elevated temperatures; 3) uptake of volatiles and gases from the vapor phase; 4) above the drift, drainage of the aqueous liquid towards the boiling front, followed by possible repeated evaporation of the aqueous phase and precipitation of transported solutes; 5) some secondary precipitation of silica at declining temperatures in places where the aqueous liquid drains toward cooler regions (Glassley, 1997d).

### **3.2.3 Cooling phase**

The heated rock will begin to cool down after the heaters are turned off in the DST. During the cooling phase, the boiling front will retreat towards the drift walls. As the boiling front retreats, a coating of mineral precipitates will be deposited along fractures and perhaps to some degree into pores. Above the drift, the downward retreating front may induce redissolution of previously precipitated salts, and concentration of the salt load at the migrating front, that may lead eventually to fracture sealing (U.S. Department of Energy, 1995).

Water that interacts with repository materials will be a mixture of fracture water, pore water, and condensate that has interacted with rock fracture mineralogy (Glassley, 1997d). Evaporative concentration will produce different effects, depending upon conditions such as CO<sub>2</sub> fugacity. During repository heating, evaporative processes will dominate and the water composition will depend on the extent of evaporation (Glassley, 1997d). Most of this water will be derived from ambient percolation but some may be refluxed condensate. During cool-down, the water composition will be dominated by condensate and the actual composition will depend on the extent of rock-water interaction. Water of this more evolved nature is most likely to interact with repository materials (Glassley, 1997d). At the edges of the repository and toward the end of the cooldown period, the water composition will be more similar to that of fracture flow waters.

## **3.3 Insights on THC behavior from tests and geothermal analogues**

### **3.3.1 Laboratory tests**

Batch studies of hydrothermal alteration of wafers of Topopah Spring Tuff, both welded and devitrified, have been performed at temperatures of 90°, 120°, 150°, and 250°C for up to 120 days (Knauss, 1986; Knauss and Beiriger, 1984; Knauss et al. 1984, 1985, 1986, 1985a,b, and 1987; Knauss and Peifer, 1986; Oversby, 1984a,b, and 1985). These studies showed only minor changes in the composition of water in contact with the tuff at temperatures as great as

150°C, with slight alteration of the tuff over a few months. At higher temperatures reaction rates increased significantly. Accelerated experiments on crushed tuff at temperatures greater than 150°C produced the most extensive alteration, including the production of metastable phases. Knauss et al. (1984) found that at 150°C the dominant secondary phases produced by the experiment were mainly clays (gibbsite, illite, and Fe- and Mg-rich clay) and zeolites (mordenite and dachiardite), and at 250°C the dominant secondary mineral was dachiardite. SEM photographs indicated etch pits on feldspar and corrosion of biotite at these temperatures.

Laboratory experiments have also been conducted to study the alteration of zeolitized and vitric tuff. The upper and basal Topopah Spring vitrophyres contain reactive glass and secondary minerals, and these strata are potentially important to repository performance (although vitric and zeolitic horizons are not found in the ESF in areas of the heater tests). Knauss and Copenhaver (1995) reported an experiment that examined alteration of polished wafers of unaltered, densely welded Topopah Spring vitrophyre. At temperatures of 150°C and less, only glass dissolution was observed. In another experiment, Knauss and Copenhaver (1995) examined the alteration of naturally zeolitized samples from the same vitrophyre. These samples were stable to further alteration. From these experiments, it may be inferred that the reaction of water with glass will be slow at temperatures up to 150°C, compared to the experimental time scale.

Zeolites, due to their high water content, may have a significant effect on the heat and water balance in zones where they are abundant (Bish, 1995; Bish et al., 1996; Carey and Bish, 1996b). According to these studies, zeolite dehydration is reversible, such that rehydration will occur during cooldown. These studies indicated that dehydration of zeolites will cause some degree of shrinkage that increases porosity and permeability, and could affect the behavior of water perching at altered zones associated with the upper and lower Topopah Spring vitrophyres. Bish and Chipera (1994) showed that nearly two years of steam heating of zeolites did not alter them or transform them to other phases. They also reported in the same study that short-term heating of smectites to 150°C produces irreversible reduction in their swelling capacity.

Plug-flow reactor studies involving flow-through reaction of deionized water with Topopah Spring tuff at 240°C resulted in significant dissolution of alkali feldspar and cristobalite (DeLoach et al., 1997). The data from this experiment are significantly different from batch reactor studies at similar temperatures (as described above), in which alteration, rather than dissolution, predominated. Results of the plug-flow reactor experiments were simulated by Johnson et al. (1997a) using the reactive transport simulator GIMRT (Steeffel and Yabusaki, 1996). Results of the plug-flow reactor experiments were also modeled using TOUGHREACT in this study, as described in section 9.0.

Numerous studies have been conducted to investigate variations in matrix permeability with temperature. These studies showed that within-sample permeability variations associated with temperature changes are less than variations between samples of Topopah Spring welded tuff at one temperature (Lin and Daily, 1984, 1988, 1989, 1991; Lin, 1990; Lin and Roberts, 1996; Moore et al., 1985; 1986; Morrow et al., 1984; Reda, 1985). Lin and Daily (1984) also investigated the permeability of the welded tuff matrix to steam and found it to be comparable to water permeability. Lin et al. (1997) investigated the effect of differential pressure on fracture healing and showed a permeability decrease with increasing pressure, but the greatest decrease in pressure amplitude occurred during the initial heating cycle. Lin et al. (1997) reported that in fractured samples, dissolution and deposition of calcite and silica on fracture surfaces due to flowing of hot water caused fracture healing, and that healing is insensitive to fracture surface conditions. Their ongoing experiments demonstrate that fracture permeability decreases with time, with a rapid drop in permeability at high temperatures (Lin et al., 1997).

### 3.3.2 Field tests

Field tests conducted at G-Tunnel, the Fran Ridge Large Block Test, and the ESF Single Heater Test have been designed to look primarily at thermohydrologic and thermomechanical coupling phenomena. The G-Tunnel and Single Heater Tests were strongly over-driven, in that heat fluxes were about five times higher than would be the maximum average heat flux for the repository. Even so, some of the observations and results of these tests are important to bear in mind for understanding the scale of coupled processes with respect to THC models. In the first heater tests at G-Tunnel, (Lin et al., 1991; Ramirez et al., 1989 and 1991), moisture redistribution was observed with boreholes spaced 0.5 m apart; the maximum radius of the dryout zone was determined to be about 0.7 m. Some shedding of condensate to the sides of the heater was observed, but no water accumulation was observed in any borehole. In the Single Heater Test (SHT) (Lin, 1997) moisture redistribution was observed on the scale of about a meter. The dryout zone was apparently more centered on the heater than it was in the G-Tunnel tests. During the SHT water was collected after 70 days and twice more during the 270-day period of heating. Approximately 2000 L of water was boiled from the dryout zone, which had a maximum radius of about 0.9 m. Isotopic and inorganic chemical analyses of the water have been carried out.

Significant amounts of water have been mobilized as fracture flow in field-scale heater tests. In G-Tunnel, drying fronts proceeded along fractures during heating, and rewetting occurred near fractures during cooling. In the Fran Ridge Large Block Test, a reflux event lasting less than an hour involved a quantity of water sufficient to change the temperature of much of the block. Over such a short time period, this can only have occurred by fracture flow.

### 3.3.3 Geothermal analogues

Numerous geothermal systems possess some similarities to the hydrogeologic system at Yucca Mountain, but these have not been studied exhaustively from the perspective of coupled processes behavior and predictions for a Yucca Mountain repository. To gain a better understanding of water-rock interactions at the field-scale, the geothermal systems of the Taupo Volcanic Zone (TVZ) were modeled using geochemical codes such as EQ3/6 (Bruton et al., 1993a). TVZ silicic volcanic rocks are similar in composition to high-silica rhyolites at Yucca Mountain, and temperatures in accessible parts range from 25° to 300°C, producing a variety of secondary minerals similar to those anticipated to form under repository conditions at Yucca Mountain. Even though the TVZ is fully saturated, extensive regions of the rock mass fall in the temperature range of 20° to 100°C and effects of boiling are observed.

The EQ3/6 code package was tested at temperatures encountered in TVZ boreholes using analyses of solution compositions and mineral assemblages (Bruton et al., 1993a; 1994). An equilibrium approach was taken under the assumption that systems at temperatures greater than 200°C would be at equilibrium. In comparing mineral assemblages predicted for two geothermal wells with observed assemblages sampled by drilling, major phases such as quartz and calcite were calculated to be at near-equilibrium, whereas phases such as wairakite and epidote were not predicted as accurately. This discrepancy could have been due to kinetic considerations, inadequacy of thermodynamic data, boiling effects, model assumptions or other considerations.

Viani and Bruton (1992) took an equilibrium approach to modeling fluid-rock interaction at Yucca Mountain using the EQ3/6 code (Wolery, 1993; Wolery and Daveler, 1992) and interacted J-13 water with Topopah Spring welded, devitrified tuff. Their modeling indicated that the formation of secondary mineral assemblages at increasing temperatures would produce the same suite of minerals as found in diagenetic zones I and II (of Carlos et al. 1993) at Yucca Mountain. At 90°C the final simulated assemblage would consist of cristobalite, K-feldspar, dioctahedral smectite and muscovite (a proxy for illite/smectite).

An understanding of silica precipitation is important because geothermal systems commonly have an impermeable silica-rich rock that caps and sometimes surrounds the zone of convective fluid and heat flow. In the majority of geothermal systems, and in all vapor-dominated fields, such as The Geysers, the caprock is produced by self-sealing. This is most commonly attributed to the deposition of silica, but may also be due to hydrothermal formation of secondary mineral phases such as clays and zeolites, feldspars, calcite, pyrite, and hematite (Grindley and Browne, 1975). Silica deposition is likely to be greatest where the temperature decrease is most abrupt, particularly at the margins of the fields.

Rates of silica precipitation from thermal fluids have been analyzed and compared with laboratory-derived rate data (Carroll et al., 1995). Their comparison pointed to significant discrepancies between results obtained with different test conditions. Field measurements of amorphous silica precipitation rates were made in hydrothermal waters of the TVZ and were compared with rates measured in the laboratory using similar techniques (Carroll et al., 1996). Precipitation rates on the order of  $3 \times 10^{-7}$  mol/m<sup>2</sup>-day were obtained in the laboratory, which is within an order of magnitude reported by Rimstidt and Barnes (1980). Carroll et al. (1995) obtained similar results at buffered pH values of 3, 5, and 6 with slower precipitation at lower pH. Their results compared favorably with the pH dependence observed by Knauss and Wolery (1988). Carroll et al. (1995) also found that precipitation was more rapid in the presence of amorphous silica.

Precipitation rates measured in the field were 400 times faster than those obtained in laboratory experiments. Carroll et al. (1995; 1996) attributed this to several possible causes, including: 1) difference in solid phases between field (quartz) and laboratory tests (amorphous silica); 2) possible differences in effective surface area available for precipitation; 3) differences between closed-system transient adjustments in the laboratory experiments, and open-system steady-state processes in the field.

### 3.4 Insights from previous modeling studies

A plethora of simulations has been conducted over the past decade to attempt to quantify and bound coupled processes in the near-field environment and in the altered zone, which will extend tens of meters into the rock mass at different times over the period of repository heating and cooling. The simulations of coupled processes have been synthesized by Wilder (1996), Hardin and Chesnut (1997), and Hardin (1998). Two early simulations considered changes in water composition and changes in porosity due to THC processes. Glassley and Boyd (1994a) used the code FEHM and a 2-D, equivalent continuum approach to estimate the rates and magnitudes of changes in THC properties. His results showed a 2% change in porosity, measured in the change in moles of silica in the rock. The porosity change translated to a three-order of magnitude change in permeability. Steady state was achieved in a few thousand years for most mineral reactions involving aqueous fluids. Deposition of silica occurred near the repository, with dissolution farther away. In another study, Glassley and Boyd (1994b) simulated near-field water compositional changes due to evaporation, as contrasted to boiling. When the gas composition was not controlled, solution pH was near neutral and Eh was slightly oxidizing. As H<sub>2</sub>O activity decreased, Na, S, Cl, and F increased in the solution. SiO<sub>2</sub> was controlled by the solubility of quartz and chalcedony. When the gas composition was fixed at atmospheric O<sub>2</sub> and CO<sub>2</sub>, pH increased to 9.0 and Eh became reducing at higher temperatures. A follow-up study (Glassley, 1997a) modeled the chemical composition of waters up to 150°C before contacting repository materials and in the absence

of evaporation. In this study, calcite, quartz, and cristobalite became supersaturated in water that was in equilibrium with atmospheric CO<sub>2</sub>. Factors controlling mineral saturation were the extent to which equilibrium with atmospheric CO<sub>2</sub> was achieved, and the extent to which supersaturation of silica polymorphs occurred before they precipitated. The simulated waters became more dilute than J-13 water, due to the effect of mineral precipitation on solution chemistry. Porosity changes on the order of 3-4% occurred at inlet and outlet points in the model, as cristobalite, calcite, and smectite continued to dissolve while hematite, K-feldspar, and Ca-clinoptilolite formed.

Some of the simulations that may be instructive to comparisons in this report were conducted with specifications of the DST. In one study, Glassley (1997b) examined the THC alteration of flow pathways above and below the repository. Results of his simulations showed that most mineral reactions occurred over the first fifty years. For the mineral phases considered, dissolution rates were 10<sup>-10</sup> to 10<sup>-11</sup> mol/cm<sup>2</sup>/yr. This study furthermore predicted the following: 1) calcite dissolution would take place only where condensate forms, and is a strong function of fluid velocity; 2) amorphous silica dissolution is less below the drift than above it, and is not a function of fluid velocity; and 3) quartz and albite remained near saturation throughout. A second study (Glassley, 1997d) used the NUFT code and the GIMRT code to perform 2-D reactive transport predictions of the DST over a four-year period. For temperatures above 100°C, mineral changes were dominated by dehydration or alteration of existing vapor-phase minerals. From 40° to 100°C a large variation in chemistry took place, with strong compositional zoning reflecting the effect of flow length path on reaction progress (i.e., the shorter the flow path, the more dilute the solution). Glassley (1997d) noted that models of condensate development in fractures indicated the time-dependence of secondary mineral development and the spatial distribution of minerals. He concluded that the spatial distribution of precipitates is strongly sensitive to condensate flux and the spatial distribution of dissolution is only moderately sensitive to condensate flux.

Four THC modeling studies were presented by Hardin (1998) in his report of near-field models. The first was a reaction-path study using EQ3/6 for evolution of water in contact with the host rock. This study examined the uncertainty in reaction rate constants for water-rock interaction. Results showed that evolution of recharge water to the composition of J-13 depends principally on the rate of silica dissolution, but also on other rates of reaction, all of which are uncertain.

The second study simulated reactive transport of silica at the repository scale using FEHM. Changes in fracture porosity were coupled with permeability changes. Calculations showed that quantities of silica could be mobilized by repository TH processes to cause significant changes in local fracture porosity. Boiling occurred predominantly at the bottom of the isothermal heat pipe zone, where residual solids accumulated.

A third THC modeling study reported by Hardin (1998) involved fully coupled drift-scale THC calculations using the NUFT code with a dual permeability (DKM) formulation, which was modified to incorporate the behavior of silica. The model included coupled porosity and permeability and produced coupling between porosity and water potential and relative permeability curves. Reaction rates and chemical equilibria were temperature dependent. Chemical dissolution/precipitation reactions were modeled in both the fracture and matrix continua. The model predicted formation of a precipitation cap above emplacement drifts for all conditions considered, including ranges of the specific surface area available for silica dissolution, and reaction constants corresponding to different silica phases. The model showed that significant precipitate accumulated within a few years or tens of years after the start of heating. The model incorporated a lower bound on permeability reduction in the boiling zone to reflect the relationship between permeability and heat pipe formation, which showed upward migration of the zone of permeability reduction with time.

The fourth THC modeling study reported by Hardin (1998) performed coupled reactive transport simulations with the OS3D/GIMRT code (Steeffel and Yabusaki, 1996). The simulations focused only on fracture flow conditions. The objective of these simulations was to examine implications of the more certain aspects of chemical behavior, while acknowledging substantial uncertainty in rate constants for silica dissolution and precipitation reactions, as well as fracture mineral inventory. The simulations showed that dissolution of calcite would occur rapidly, whereas aqueous dissolution and precipitation reactions involving silicates would produce more significant changes in porosity, but over longer time periods, on the order of tens of years. Later in the thermal evolution of the repository, CO<sub>2</sub> would be displaced from the gas phase by water vapor as the air mass fraction approaches zero in the host rock. OS3D/GIMRT simulations showed that decreased CO<sub>2</sub> fugacity would have little impact on calcite and silica reactions at near-neutral pH. The presence of condensate that is less chemically aggressive to calcite would result in the physical spreading of precipitation and dissolution zones. The aqueous dissolution and boiling processes predicted by NUFT and by OS3D/GIMRT were shown to be incompatible above the emplacement drifts. Hardin (1998) stated the need for a model that would accommodate a full set of chemical reactions with evaporation, boiling and gas phase transport.

### **3.5 Mineralogy of the fractured tuff**

The Topopah Spring Tuff is relatively homogeneous from the chemical viewpoint, but varies in the relative abundances of silica polymorphs (quartz, cristobalite, and tridymite) (Bish et al., 1996). Within the repository horizon, which extends from below the zone of abundant (15%) lithophysae to the basal vitrophyre of the Topopah Spring Tuff, more than 98% of the mineral content of the bulk rock is comprised of tridymite, cristobalite, quartz, and alkali feldspar (Bish et al., 1996). The abundance of feldspar varies from 55 to 65%. Hematite and

smectite are common minor phases. The clay minerals at Yucca Mountain are predominantly interstratified illite/smectites (Bish, 1989) and are present in amounts from 1 to 10% in virtually every stratigraphic unit. The alkali feldspar (sanidine) compositions range from Or<sub>38</sub> to Or<sub>66</sub> (Broxton et al., 1989) with most in the range of Or<sub>45</sub> to Or<sub>55</sub>. Plagioclase compositions range from An<sub>14</sub> to An<sub>20</sub> with a minor compositional mode at An<sub>35</sub> (Broxton et al., 1989).

Carlos et al. (1991, 1995) reported on fracture mineralogy taken from drill core in the lower Topopah Spring Tuff above the basal vitrophyre. They noted three generations of fracture sets. The first generation fracture set was connected to (and related to) lithophysae and was sealed by tridymite that may or may not have transformed to cristobalite or quartz. This set was surrounded by a bleached zone. Another fracture set contained crusts of mordenite over Mn-oxides, predominantly lithiophorite (Al- and Li-bearing) and rancieite (Ca- and Mg-bearing), with some todorokite (Na-, Ca-, and K-bearing). Both of these fracture sets are nearly planar and are often slickensided, and were interpreted by Carlos et al. (1991, 1995) to be more than 11.5 Ma in age. A later fracture set that post-dated tectonic activity was sequentially lined by the zeolites stellerite and heulandite, smectite, and finally calcite. Glassley (1997c) noted that fracture mineralogy is consistent at the horizon of the DST with calcite (89%), alkali feldspar (0.2%), amorphous silica (5%), quartz (5%), and clay (0.1%). He used these relative abundances in predictive models.

Petrographic studies of the Topopah Spring Tuff in the area of the DST (this study) show it to be moderately to densely welded, devitrified, and vapor-phase altered. Phenocrysts make up less than 2% of the sample and on an average there are fewer than 2% voids. The dominant phenocrysts are sanidine and plagioclase, with lesser biotite, quartz, and Fe-oxides. Accessory minerals include zircon and apatite. The bulk of the groundmass consists of devitrification products, alkali feldspar, quartz, and cristobalite. The percentages of these were quantified by Roberts and Viani (1997a, b, see sect. 12.3). In some areas coarse granophyric crystallization has produced interlocking quartz and alkali feldspar. Relict glass shards and relict pumice are recognized in outline by nearly opaque clay and opaque oxide rims. Other relict vitric textures include spherulitic patches of silica, a feathery, fluid-looking groundmass, and a scalloped pattern of fine-grained, radial, fibrous quartz and/or alkali feldspar. These patterns are often nucleated on the surfaces of phenocrysts and relict pumice. Within lithophysal cavities, minute acicular crystals of quartz and alkali feldspar radiate from the walls. Vapor-phase crystallization includes quartz, quartz after tridymite, and alkali feldspar growing into void space.

Roberts and Viani (1997a,b) found that the abundances of quartz and cristobalite were inversely correlated. Tridymite and smectite were found in about 25% of the samples and clinoptilolite appeared in one sample. Fracture filling material observed included quartz, minor feldspar, calcite, hematite, manganese oxides, smectite, and a trace of tridymite. We

recently obtained thin sections of samples taken from these locations and have identified a zeolite lining fractures as well (Simmons and Glassley, 1998). Roberts and Viani (1997a,b) noted that grayish alteration areas in the matrix contained a greater percentage of quartz and tridymite and lesser amounts of cristobalite than in the unaltered matrix. This is the opposite to x-ray diffraction patterns of Glassley and Boyd (1995) in which cristobalite dominated over quartz in bleached zones surrounding many fractures of the first generation. Additional mineralogic studies of samples from the DST and the SHT are underway that may shed light on this contradiction (this study and at Los Alamos National Laboratory).

---

## 4. QA STATUS OF CODES AND DATA

### 4.1 QA Status of Data Used in Report

The data used as input to modeling in this report come from a variety of qualified and unqualified sources, making data developed from these sources and conclusions derived from these data non-Q. The QA status of specific input data sources is provided in Table 4.1. The data fall into several classes and the mixed nature of their qualification status can easily be seen:

1. Mineralogy – these data come primarily from non-Q borehole studies or from experimental data collected prior to the Yucca Mountain QA program, e.g. Delany et al., 1986. The exception is x-ray diffraction mineralogy of the DST (Roberts and Viani, 1997a, b; see Table 4.1). Mineralogy data collected from petrographic analyses in this study are preliminary but will be qualified in FY98.
2. Thermodynamic data are taken from the EQ3/6 data base (Wolery, 1992), which consist mostly of data from SUPCRT92 (Johnson et al., 1992) and from Pokrovskii and Helgeson (1995), Holland and Powell (1990); and from SOLTHERM.HP and SOLTHERM.JOH data bases (same data sources, courtesy of M.H. Reed, University of Oregon). All of these are unqualified data sources.
3. Water chemistry data and strontium isotopic compositions come from both qualified and unqualified sources and are shown in Table 4.1.
4. Gas chemistry data is taken from Conrad (1998), unqualified.

5. Hydrologic parameters and other specifications of the DST are taken from Birkholzer and Tsang (1997), which used qualified DST design parameters and hydrologic properties taken from the UZ Site-Scale Model (Bandurraga and Bodvarsson, 1997). The latter uses both qualified and unqualified data.
  
6. Kinetic data are unqualified (from Johnson et al., 1997a; Hardin, 1998; Rimstidt and Barnes, 1980).

The data developed as a result of new thermodynamic determinations are considered preliminary. The recalibration of pore water chemistry data is also preliminary and requires additional quality assurance checks. All of the model output data are considered scoping.

**Table 4.1. Study Data Summary and Q Status**

Borehole/Data Type Organization- Principal Investigator	Q Status	DTN/AN (if available)
XRD Mineralogy, LLNL, Roberts and Viani (1997a, b)	Y	DTN LL980106404244.050
J-13 well water, Various, Harrar et al., (1990)	N	Not available
G-1, G-3, G-4, UE25b-1H mineralogy LANL, Bish, Carlos, Broxton, various studies	N N N N	DTN LA000000000040.001 DTN LA000000000112.002 DTN LA000000000113.002 DTN LA000000000039.001
UZ Pore Water, USGS, Yang et al., 1996a	Q	DTN GS970108312271.001
Sr isotope data, USGS, Neymark et al., 1995	N	DTN GS941208319211.005
Sr isotope data, USGS, Paces et al., 1998	Q	DTN GS980308315215.009
		NA= Not Available; Y= qualified, N= unqualified data; TBQ = To be qualified

#### 4.2 QA Status of Codes

TOUGH2 version 1.11 (Pruess, 1991), the flow module of TOUGHREACT, has been tested extensively and has met the requirements for Software Qualification defined in LBNL Quality Implementing Procedure YMP-LBNL-QIP-SI.0 (Pruess et al., 1996; Wu et al., 1996). The qualification of TOUGHREACT is currently underway and the code cannot be considered QA at this time. Nevertheless, several benchmark tests have been performed as part of this study to verify the overall behavior of the geochemical reaction and transport modules of TOUGHREACT (Section 9.0). It is our intent to incorporate the results of these tests into software qualification of TOUGHREACT for the Yucca Mountain Project. In addition, reactive transport at 25°C has been extensively verified against analytical solutions and other simulations for a wide range of processes (Xu et al., 1998a, b; Xu, 1996).

Although EQ3/6 v.7.2b is qualified for use in the Yucca Mountain Project, neither SUPCRT92, nor the thermodynamic data embodied in SUPCRT92 have been qualified. The integrity of the data therefore depends on the traditional process of peer review and scientific testing. CHILLER (Reed, 1982; Spycher and Reed, 1992) has not been qualified for use on the Yucca Mountain Project, although it has been applied in the past to modeling boiling of pore waters at Yucca Mountain (Reed, 1988). It has been tested extensively for modeling

gas-water-rock interactions for the geothermal, mining, and oil industries. We do not intend to qualify it under Yucca Mountain Project software QA procedures.

---

## 5. CONCEPTUAL MODEL OF THERMO-HYDRO-CHEMICAL PROCESSES FOR THE DST

Different geochemical processes will take place in fractures and in the matrix, depending on the flow of water, water vapor, and heat in fractured tuff. There are several reasons for this. First, the fracture mineralogy is significantly different from that in the matrix, with common secondary mineralization of predominantly calcite, opal, clays, and zeolites (Paces et al., 1998). There is little secondary mineralization in the low permeability welded tuff matrix. Second, aqueous and gas phase transport by advection in open fractures can be orders of magnitude greater than in the matrix. Third, physical processes caused by heating of the unsaturated rock lead to more rapid dryout in fractures in the dryout region and strong condensation effects in fractures over a large region (Buscheck et al., 1997a,c). These effects can lead to large differences in the chemical compositions of fluids in fractures and adjacent matrix blocks.

Thus, it is foremost that we begin our conceptual model of the THC system with a good approximation of the physical aspects of the system. The dual permeability model has been shown to provide much better agreement than the equivalent continuum model (ECM) to the thermal and saturation results of the Single Heater Test (Birkholzer and Tsang, 1996; Tsang and Birkholzer, 1997). As a conceptualization of the primary mineralogical differences in the welded tuff, dual permeability allows the mineralogical aspects to be specific to fractures and matrix separately, with geochemical communication through imbibition and diffusion (Figure 5.1). There are also significant drawbacks to the dual-permeability concept, as it represents chemical diffusion between matrix and fracture continua as a flux associated with a linear concentration gradient. The choice of how liquid saturations are averaged at matrix-fracture interfaces can dramatically change the calculated diffusive chemical fluxes. The results of our testing have shown that this is exacerbated by the more rapid loss of water in fractures undergoing dryout as compared to the matrix.

Another consideration that is peculiar to the thermal tests and near-field of the repository is the transition over time to complete dryout of the region adjacent to the thermal source. Water-rock interaction models need an aqueous phase to be present in the simulated system to allow computations of reactions between water and rock. In addition, treating evaporation of the last remaining water (residual saturation) is not straightforward because there are limits to the applicability of such models at high ionic strengths. For the current conceptualization of

the thermal test regime, we consider that the most important mineralization and geochemical effects are those that occur above a certain liquid saturation level. For the simulations presented here, we assume that all geochemical interactions, and diffusive and advective chemical fluxes are zero below a liquid saturation of  $1 \times 10^{-5}$  (for one case,  $1 \times 10^{-4}$ ). At this point we save the final water chemistry so that under conditions of rewetting incoming fluids will mix with this residual fluid. This approximates the instant precipitation and dissolution of highly soluble salts at low water contents without being forced to calculate their actual identity under these extreme conditions.

The conceptualization of reacting minerals is that they are present in given amounts (from mineralogical studies or estimated) and that they are characterized by an unchanging reactive surface area. Assuming that the initial characterization of the reactive surface minerals in the system (effective relative to the rock texture, pore structure, etc.) is correct, which is unlikely, the surface areas available for reaction will certainly change over time. This will occur not only through dissolution and precipitation producing different amounts of the minerals, but also through coating of mineral grains by other mineral precipitates, resulting in areas that are unavailable to the pore fluid, except possibly through grain boundary diffusion or diffusion through mineral coatings (Sonnenthal and Ortoleva, 1994). Because the latter processes are diffusion-limited, they are likely to be effective only over much longer time-scales than for direct pore fluid-mineral reactions.

Rates of reactions and mineral assemblages are highly dependent on the pH, which for the conditions associated with the Drift-Scale thermal test is a strong function of the partial pressure of  $\text{CO}_2$  in the gas phase, as well as of the mineral-water reactions. A realistic model of the geochemical conditions of fluids and mineral alteration phenomena must consider interactions with  $\text{CO}_2$  in the gas phase, as well as typical water-rock interaction effects. Given this consideration, our conceptual model starts with the incorporation of gas species transport and  $\text{CO}_2$  equilibria between liquid and gaseous phases. This added realism, though, makes the solution of the reaction-transport problem much more difficult. Diffusion in the gas phase and gas flow velocities are much higher than that for aqueous species and fluid transport. Thus, there are significant numerical limitations, primarily in the time step size. Coupling the  $\text{CO}_2$  transport to mineral/water reactions also causes much more nonlinearity in the system as phases are affected by rapid flow velocities and the strong temperature dependence of  $\text{CO}_2$  partial pressure, which itself drastically affects pH. For these reasons, and the introduction of dual permeability concepts, the modeling we present here does not cover all of the minerals and aqueous species we may want to consider; however, we believe that the basis for this work will lead to a much better long-term analysis.

## 6. DEVELOPMENT AND ANALYSIS OF THERMODYNAMIC DATA FOR THE DST

### 6.1 Revision of Thermodynamic Data

Thermodynamic data of participating phases and aqueous species in natural systems are derived from a variety of sources, including low and high temperature heat capacity measurements, heats of solution data, using either lead borate or hydrofluoric acid, high temperature/pressure phase equilibria, and solubility data. Numerous internally consistent thermodynamic databases of naturally occurring minerals have been compiled from these disparate sources in recent years (e.g. Berman 1988; Holland and Powell 1985, 1990; Powell and Holland 1990; Gottschalk 1997), and they have been used extensively for geochemical modeling.

Thermodynamic data for aqueous species are similarly drawn from a variety of experimental methods including the use of electrochemical cells, calorimetric procedures and solubility studies. Major uncertainties remain from attempts to represent the thermodynamic data of aqueous species under standard state conditions, which require the application of suitable electrolyte models. Furthermore, not all species germane to the problem at hand have necessarily been identified, and their omission can result in cumulative systematic errors in reactive chemical transport models.

The EQ3/6 thermodynamic database, which is used as a basic source for this study, consists of the solubility products and dissociation constants of solid phases and aqueous species respectively, calculated at discrete temperature increments along the saturation surface for the aqueous phase between 0 and 300°C. A significant proportion of these data have been calculated using thermodynamic equations derived by Helgeson and his coworkers (Helgeson and Kirkham 1974a, b, 1976; Helgeson et al., 1978) in the SUPCRT92 code (Johnson et al., 1992). The latter code contains thermodynamic data for solid phases derived from a relatively early thermodynamic compilation by Helgeson et al. (1978) with subsequent corrections. Thermodynamic data for aqueous species in SUPCRT92 are presented in terms of the Helgeson, Kirkham, and Flowers (HKF) equation of state parameters, the parameters having been drawn from a series of papers by Helgeson and his co-workers (Helgeson et al., 1981; Shock and Helgeson, 1988, 1990; Shock et al., 1989; Sverjensky et al., 1997; Shock et al., 1997).

Since the publication of Helgeson et al. (1978), a number of new experimental studies have been reported, which mandate a revision of some of the thermodynamic data. The findings of some of these studies have already been incorporated, e.g. Pokrovskii and Helgeson (1995). But others of particular relevance to phase relations at Yucca Mountain have not.

The most important of these include a study of the low temperature aqueous solubility of quartz by Rimstidt (1997), revised thermodynamic data for coexisting illite and smectite (I/S) by Aja (1995) and Kulik and Aja (1997), solubility measurements of sepiolite and kerolite by Stoessel (1988), and a revised correlation of the thermodynamic properties of low albite and potash feldspar, based on field data of the  $[Na^+]/[K^+]$  ratio (Apps and Chang, 1992).

Fortunately, only a restricted subset of phases must be considered, and their thermodynamic properties accurately determined to model effectively the thermochemical environment of the DST in the Tptpmn Unit. In addition, all significant aqueous species must be included. The preliminary assessment of pore water compositions and potential thermodynamic controls (Section 7) indicates, however, that at a minimum, the following phases must be included:

- Low albite
- K-feldspar (microcline)
- I/S phases, i.e. illite and smectite
- Kaolinite
- Sepiolite
- Calcite
- Quartz
- Cristobalite
- Amorphous silica, i.e. opal-A

Several other phases could be important, but further evaluation will be necessary, either to refine their solubility products as a function of temperature, or to establish whether they are likely to be significant participants in thermochemical processes in either the DST or the proposed repository. They include several zeolites, particularly heulandite, stellerite, and mordenite as well as poorly defined amorphous alumino-silicates and opal-CT. Zeolites are in general infrequently observed in the matrix, but have been noted somewhat more commonly in fractures in the devitrified units and this might be attributed to devitrification of

the tuff to a mineral assemblage that is as stable or possibly more stable than the cited zeolites. Investigations are underway to clarify this issue.

One of the most important areas of concern in revising the ESQ3/6 database (DATA0) is the erroneous determination of the thermodynamic properties of  $\text{SiO}_2(\text{aq})$  by Walther and Helgeson (1977). In their study, they rejected two consistent data sets by van Lier et al. (1960) between 60 and 100°C, and Siever (1962) between 125 and 180°C in favor of incompatible data by Morey et al. (1962) and Mackenzie and Gees (1971) at 25°C. This interpretation contrasted with that by Apps (1970), who considered the datasets by Van Lier et al. and Siever to be valid (see Figure 6.1). Subsequently, Rimstidt (1997) conducted a careful study of quartz solubility between 25 and 95°C and obtained results that were consistent with Van Lier et al. and Siever. Rimstidt's interpretation is also substantiated by consistency between the thermodynamic properties of  $\text{SiO}_2(\text{aq})$  obtained from amorphous silica solubility. Walther and Helgeson (1997) calculated the HKF equation of state parameters for  $\text{SiO}_2(\text{aq})$  from a regression of selected solubility measurements, and these parameters were included in the SUPCRT92 database from which solubility products for many silicates and aluminosilicates in DATA0 were derived. Time constraints prohibit a redetermination of the HKF parameters for  $\text{SiO}_2(\text{aq})$  at this time. Instead a more pragmatic approach was taken in revising the solubility products of the phases listed above. These revisions, while not entirely consistent internally, are sufficiently accurate for preliminary model simulations of the DST. Any subsequent refinements will lead to minor differences that will have no quantitative significance.

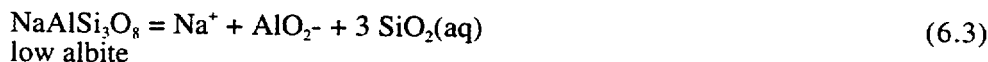
The nature of the revision depends on the original source of the Gibbs free energy of formation,  $\Delta G^\circ_{f, 298.15}$  of the solid phase at the reference temperature and pressure, i.e., at one atmosphere ( $10^5$  Pa) and 298.15 K. For those phases where  $\Delta G^\circ_{f, 298.15}$  was derived from aqueous solution measurements, a revision is undertaken by consulting the original source material. For those solid phases where  $\Delta G^\circ_{f, 298.15}$  is based on calorimetric determinations, the solubility products must be recomputed using revised quartz solubility data. For the phases listed above, the following procedures were adopted to determine their solubility products at 0, 25, 60, 100 and 150°C.

### 6.1.1 Low Albite

The recommended value for low albite from Berman (1988) was adopted, and the following equations used to compute the solubility products:



Solubility products for the first equation were computed using SUPCRT92 with data from a modified (Johnson et al., 1992) database. Solubility products for the second equation were computed from the solubility equation for quartz given by Rimstidt (1997). The solubility products from both equations were added to obtain the solubility products for the equation:

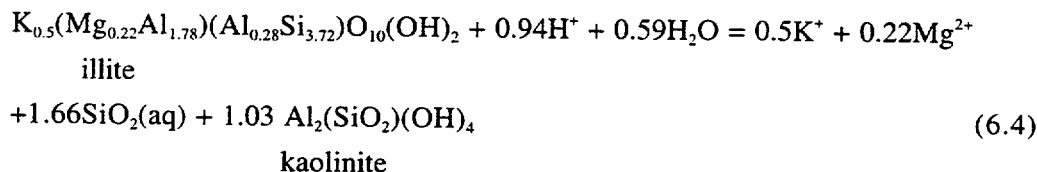


### 6.1.2 Potash Feldspar

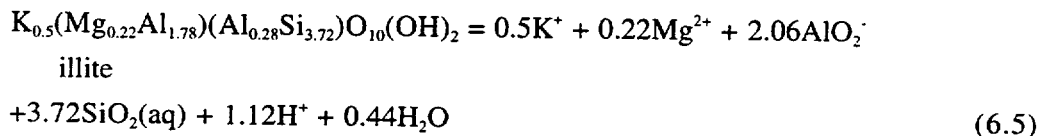
The same procedure as for low albite was adopted, using a corrected  $\Delta G^\circ_{f, 298.15}$  value for potash feldspar from Apps and Chang (1992).

### 6.1.3 I/S Phases: Illite

$\Delta G^\circ_{f, 298.15}$  and  $S^\circ_{298.15}$  for illite with the formula  $\text{K}_{0.5}(\text{Mg}_{0.22}\text{Al}_{1.78})(\text{Al}_{0.28}\text{Si}_{3.72})\text{O}_{10}(\text{OH})_2$  was corrected from values provided by Kulik and Aja (1997) using the following phase equilibrium relation determined experimentally by Aja (1995) at temperatures between 25 and 250°C:

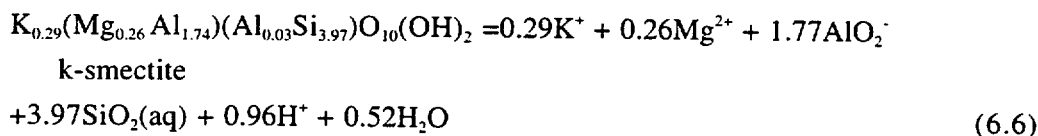


using the thermodynamic properties for kaolinite from Robie and Hemingway (1995), and the thermodynamic properties for  $\text{SiO}_2(\text{aq})$  computed from the data for  $\text{H}_4\text{SiO}_4$  by Rimstidt (1997). The revised values were entered in the SPRONS96.DAT database of SUPCRT92 together with molar volume and heat capacity data reported by Kulik and Aja (1997), and the solubility products calculated for the reaction:



### 6.1.4 I/S Phases: K-Smectite

$\Delta G^\circ_{f, 298.15}$  and  $S^\circ_{298.15}$  for K-smectite with the formula  $\text{K}_{0.29}(\text{Mg}_{0.26}\text{Al}_{1.74})(\text{Al}_{0.03}\text{Si}_{3.97})\text{O}_{10}(\text{OH})_2$  was computed in a similar manner to that of illite, and from the same literature sources cited for illite, and the solubility products calculated for the reaction:

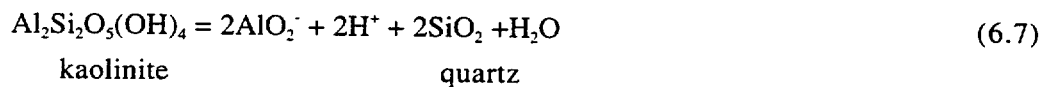


### 6.1.5 I/S Phases: Ca-, Mg-, Na- Smectites

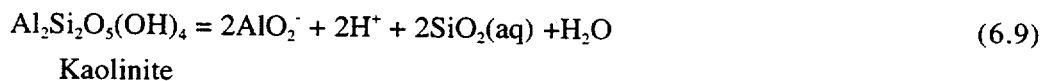
Solubility products for Ca-, Mg- and Na- smectites were calculated from those reported for "Montmor-K", "Montmor-Ca", "Montmor-Mg", and "Montmor-Na" in the DATA0.COM database of EQ3/6 v.7.2b by referencing K-smectite to "Montmor-K", and correcting the solubility constants for the remaining smectites after adjusting for minor differences in stoichiometry between the K-smectite cited above, and the montmorillonites reported in DATA0.COM, i.e.  $K_{0.33}Mg_{0.33}Al_{1.67}Si_4O_{10}(OH)_2$ , etc. For modeling purposes, these end member smectites serve to represent the contributions of each respective cation in the interlayer exchange positions of the smectite component of I/S. Ideally, a solid solution model should be incorporated in the model to describe the interlayer cation occupancy, and this will be done when time permits.

### 6.1.6 Kaolinite

In order to insure consistency with the I/S phase solubility products, the thermodynamic properties for kaolinite reported by Robie and Hemingway (1995) were entered in SPRONS96.DAT of SUPCRT92, and the solubility products computed by summing the computed solubility products from the following two equations:

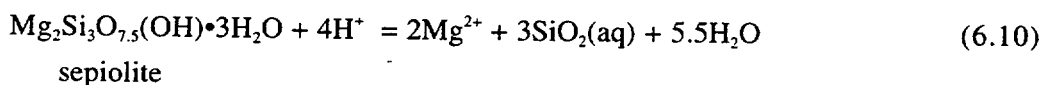


where the solubility equation for quartz is given by Rimstidt (1997), to give the solubility products for the reaction:



### 6.1.7 Sepiolite

The solubility products for the reaction:



were calculated directly from the reported values by Stoessel (1988).

### 6.1.8 Quartz

Solubility products for quartz were calculated from the solubility equation for quartz reported by Rimstidt (1997).

### 6.1.9 Cristobalite

The solubility products for cristobalite were calculated from:

$$\text{Log}K_s(\text{cristobalite}) = -970.05/T - 0.0787 \quad (6.11)$$

This equation is based on a regression by Apps (1970) of pressure-corrected cristobalite solubility data derived from measurements by Fournier and Rowe (1962).

### 6.1.10 Amorphous Silica

The solubility products for amorphous silica were calculated from:

$$\text{Log}K_s(\text{SiO}_{2(\text{am})}) = -679.19/T - 0.3848 \quad (6.12)$$

This equation is based on regression by Apps (1970) of amorphous silica solubilities from a number of sources in the literature, as shown in Figure 6.2. The consistency of these data sets strongly suggests that this metastable form of silica may be a synthetic equivalent of opal-A. The precipitation of amorphous silica is most likely to occur during evaporation of condensate during the DST, and is therefore an essential phase in thermochemical modeling simulations of the DST.

A summary of solubility products of the phases identified for incorporation in the model is given in Table 6.1.

**Table 6.1** Solubility products for the phases modeled in the DST (for reactions as shown in text).

	Temperature, °C				
	0	25	60	100	150
Low Albite	-21.694	-20.177	-18.362	-16.684	-15.094
Microcline	-24.861	-22.910	-20.619	-18.526	-16.549
Kaolinite	-43.073	-39.895	-36.336	-33.181	-30.212
K-Smectite	-43.004	-39.829	-36.275	-33.110	-30.093

	Temperature, °C				
	0	25	60	100	150
Ca-Smectite	-42.523	-39.519	-36.156	-33.159	-30.303
Na-Smectite	-42.628	-39.528	-36.049	-32.937	-29.956
Mg-Smectite	-42.583	-39.613	-36.049	-32.937	-29.956
Illite	-45.354	-41.926	-38.294	-34.994	-31.867
Quartz	-4.079	-3.739	-3.349	-2.992	-2.642
α-Cristobalite	-3.630	-3.332	-2.990	-2.678	-2.371
Amor. Silica	-2.871	-2.663	-2.423	-2.205	-1.990
Sepiolite	17.28	15.76	13.83	12.08	10.45

## 7. WATER AND GAS CHEMISTRY

### 7.1 Water Chemistry

#### 7.1.1 Statement of the Problem

The hydrochemical response of the DST must be modeled using a thermodynamic and kinetic database that has been calibrated against the pre-existing ambient hydrochemistry of the vadose zone at Yucca Mountain, and in particular, the Tptpmn Unit. Calibration is needed because extant thermodynamic and kinetic databases have been derived independently for conditions that do not necessarily match those at Yucca Mountain. Such conditions as phase metastability, surface free energy contributions, solid solutions, ion exchange, and adsorption may all affect the degree of correlation between theoretical prediction and field observation. Furthermore, despite extensive experimental investigations over several decades, thermodynamic data for some aqueous species and solid phases are still imprecise, incomplete or unknown. Furthermore, uncertainties in much of the thermodynamic data exceed by far, the degree of accuracy required for predictive modeling of the DST (e.g. see Apps and Chang, 1992). Hence the need for calibration, provided that the calibration process does not violate the uncertainties inherent in extant thermochemical data.

An analysis of pore water chemistry at Yucca Mountain is presently under way, using the species distribution code EQ3, v7.2b which forms part of the EQ3/6 package (Wolery, 1992).

An earlier investigation of the chemical composition of the pore waters recovered from drill core from UZ-14 at Yucca Mountain (Apps, 1997) suggested that the pore waters may have achieved local equilibrium with respect to primary and secondary minerals of the host rocks. This assumption was based on the relative invariance of log activity ratios representing the primary rock-forming oxide components. The analysis was based on an assumption that

calcite was at or near saturation throughout the vadose zone. However, the analysis was of just one data set of several collected by Yang et al. (1988, 1996a,b) from drill holes NRG6, NRG7a, SD-7, SD-9, SD-12, UZ-4 and UZ-16, and perched waters collected from several of the holes (Yang et al., 1996a). Because a larger number of samples would establish the degree of variability in pore water compositions at Yucca Mountain, and would assist in refining and calibrating the thermodynamic controls on pore water composition, the analysis was extended to include all available data. The analysis consists of two steps: (1) an evaluation of the consistency and quality of the chemical analysis, and (2) a preliminary interpretation of pore water equilibrium with respect to primary and secondary minerals.

### 7.1.2 Evaluation of Pore Water Analyses for Consistency

A number of tests can be performed to check the consistency and validity of chemical analyses. These checks are a necessary requirement before a thermodynamic evaluation can be performed. The following checks were performed on all chemical analyses reported by Yang (1992) and Yang et al. (1996a,b and corrections).

- Augmentation of the analyses by the addition of  $K^+$  at a concentration of 4.0 mg/L. In Yang's analyses,  $K^+$  was not reported for all but seven pore water analyses. Perched waters and those pore waters analyzed for  $K^+$ , showed a range from 4 to 16 mg/L. However, waters sampled below 100 m depth were usually toward the low end of the range.
- Omission of Al analyses. Those Al analyses reported were unrealistically high for pore waters, and appear to represent artifacts of the analytical procedure, representing the dissolution of suspended particulates by nitric acid.
- Correlation of  $SiO_2(aq)$  analyses for contamination introduced by the dissolution of clay particulates. These were corrected using a correlation plot, as illustrated in Figure 7.1, except for several anomalous values reported for pore water from UZ-14.
- The assumption that total  $HCO_3^-$  (in mg/L) is equal to the sum of  $HCO_3^- + (61/60)CO_3^{2-}$ . Alkalinity titrations are reported in terms of  $CO_3^{2-}$  above pH = 8.3, and  $HCO_3^-$  between pH = 8.3 and pH = 4.5. Although other species in solution above pH = 8.3 contribute to the alkalinity, e.g.  $HSiO_3^-$ ,  $NaHSiO_3(aq)$ ,  $CaCO_3(aq)$ , etc., the method of calculation is such that the true total  $HCO_3^-$  in solution can be approximated by the reported sum.

- An initial distribution of species at a reference temperature of 25°C using the given pH. The purpose of this calculation is to determine the charge imbalance, which includes those charged species resulting from hydrolysis. It is here assumed that the pH of the pore water was measured at this temperature in the laboratory immediately upon sampling.

Another useful check on the quality of the chemical analyses can be made by comparing the electrical conductivity computed from the chemical analysis of ionic species in solution with the measured electrical conductivity of that solution. This check was not performed in this study owing to time constraints, but has been evaluated empirically by Hem (1989).

The results of the above evaluation showed that the charge imbalances for many of the analyses were much larger than would be expected, i.e.,  $\leq 10$  percent of the mean charge, given the expected precision and accuracy of the analytical methods used. Apps (1997), in reviewing chemical analyses of J-13 well water (Harrar et al., 1990) concluded that the uncertainty in the measured pH values was so large that the reliability of the reported pH values of the pore waters might be questioned. Yang (1998, personal communication) in responding to this query has indicated that several pH measurements were made during the recovery of a pore water sample from a drill core, and that the pH values reported were of the initial measurements. Because the pore waters are commonly quite alkaline, they tend to absorb  $\text{CO}_2$  from the atmosphere, and this may have occurred to pore waters in the core periphery during recovery and subsequent storage. Accordingly, Yang has revised some of his reported pH measurements to reflect measurements on aqueous samples collected later in the pore water recovery process. These pH values are incrementally higher than those first reported.

In order to make an independent determination of the pH of the pore water, Apps (1997) assumed that the pore waters were just saturated with respect to calcite throughout all stratigraphic units. This assumption is supported by the presence of calcite in fractures throughout the vadose zone, except in the zeolitic interval of the Calico Hills Formation, where calcite is conspicuous by its absence, and which has been referred to as the "calcite barren zone" (Carey et al., 1997; Vaniman and Chipera, 1996). Furthermore, precipitation infiltrating Yucca Mountain may contact a caliche horizon and saturate with respect to calcite. Pore waters percolating through Yucca Mountain, if initially calcite saturated would, with one exception, tend to remain saturated as a result of rock and nitrate hydrolysis, and possibly evaporation. The exception occurs in the Calico Hills Formation, where zeolitic exchange of  $\text{Ca}^{++}$  and  $\text{Mg}^{++}$  for  $2\text{Na}^+$  would tend to favor undersaturation, consistent with the above mentioned field observations indicating the absence of calcite in that zone.

The analyses of all pore waters were evaluated using EQ3 v. 7.2b with the constraint that the pH be adjusted to ensure calcite saturation. All runs were conducted at the estimated ambient temperature at which the core sample was collected in the borehole. Temperatures ranged from 17.5°C at the surface to 36.0°C at the maximum depth in borehole UZ-14. The temperatures were interpolated and calculated to  $\pm 0.1^\circ\text{C}$  from either actual measured values or from values calculated for the Unsaturated Zone.

Results lead to a considerable improvement in the charge balance for most pore waters, particularly those whose pH was insufficiently high to record a measurable contribution from  $\text{CO}_3^{2-}$  and  $\text{HSiO}_3^-$  to the alkalinity titration above  $\text{pH} = 8.3$ . In most cases the calculated pH was elevated with respect to the measured pH. However, for a significant number of analyses, particularly those with higher pH and alkalinity, the charge imbalance was not improved. In many cases, the charge imbalance remained between +10 and +30 percent of mean charge.

For those analyses reporting an alkalinity component above  $\text{pH} = 8.3$ , i.e., those analyses reporting  $\text{CO}_3^{2-}$ , it is possible to compute the pH independently of the measured pH, and without recourse to a calcite saturation constraint. Many of the analyses falling into this category were recovered from the Calico Hills Formation, where the absence of calcite in the matrix and high ion exchange potential would suggest possible undersaturation with respect to calcite. In order to calculate the pH from the alkalinity, the total alkalinity above  $\text{pH} = 8.3$  must take into account the alkalinity contribution due to the dissociation of  $\text{SiO}_2(\text{aq})$ . Unfortunately, the qualified version of EQ3 is no longer equipped to make this correction (Wolery, 1992), and therefore it was made by graphical interpolation, assuming that the reported " $\text{CO}_3^{2-}$ " actually comprises both  $\text{CO}_3^{2-}$  and  $\text{HSiO}_3^-$ . Other species contributing to the alkalinity, other than  $\text{OH}^-$  in the affected pore waters, generally affected the alkalinity above  $\text{pH} = 8.3$  by only a few percentage points, i.e.  $\leq 5\%$ .

Forty-five analyses reporting alkalinity above  $\text{pH} = 8.3$  were accordingly corrected, and the pH and charge imbalance were calculated. Results lead to a considerable improvement in the charge imbalance, most showing imbalances of  $\leq 10$  percent. In most cases, however, calcite was supersaturated with saturation indices ( $\text{SI} = \log(Q/K)$ ) ranging from 0.0 to +1.2. This finding is inconsistent with the expectation that calcite would be undersaturated in the Calico Hills Formation, and challenges the presumption of calcite saturation (as opposed to supersaturation) in those pore waters where pH cannot be independently calculated from the alkalinity determination.

### 7.1.3 Preliminary Interpretation of Pore Water Equilibrium with Respect to Solid Phases

#### 7.1.3.1 Calcite

Uncertainty regarding the state of calcite saturation within the vadose zone calls into question several assumptions inherent in the interpretation of the vadose zone geochemistry from the pore waters, in modeling of the thermochemical response of the DST, and in modeling the long-term behavior of the post-closure hydrochemical regime of the repository. Several possible explanations require further review, but until this issue is resolved, modeling the DST will be based on the assumption that calcite is initially saturated within the Tptpmn Unit, and that the kinetics of calcite precipitation are unaffected by other dissolved species. The following are potential explanations:

- Species sorbed on the surface of the calcite hinder precipitation. An abundant literature testifies to the supersaturation of solutions with respect to calcite in soils, e.g. see Suarez et al. (1992) and Levy et al. (1995). Lebron and Suarez (1996) have quite convincingly demonstrated that dissolved organic matter can greatly hinder the rate of precipitation at soil temperatures, even at concentrations as low as 0.5 mg/L dissolved organic carbon (DOC). The total organic carbon concentration in water samples taken from 19 localities in the Yucca Mountain area between 1990 and 1992 (LaCamera and Westenburg, 1992) ranges from <0.1 to 1.5 mg/L. It is therefore possible that organic constituents inhibit calcite precipitation in the vadose zone at Yucca Mountain. It has long been known that calcite precipitation in seawater is hindered by the presence of  $Mg^{2+}$  (Mucci and Morse, 1983; Miyamoto and Pingitore, 1992), leading to the preferential precipitation of aragonite and/or high magnesium calcite. The pore waters at Yucca Mountain contain relatively high concentrations of  $Mg^{2+}$  (Yang et al., 1988, 1996a,b), but neither aragonite nor high magnesium calcite have been observed in either fractures or the matrix at Yucca Mountain; indeed, the calcite is reported to be almost pure (Carey et al., 1997). Amrhein (1998) suggested that  $HSiO_3^-$  may adsorb on calcite surfaces and hinder precipitation. This potential explanation is attractive, because it would reconcile the presumed saturation of calcite at lower alkalinities with the calculated supersaturation of pore waters at higher alkalinities. It might also explain the observed absence of calcite in the "calcite barren zone" (Carey et al., 1997) as being due, not to undersaturation of calcite, but to inhibition of calcite precipitation. However, no experimental results exist to support this hypothesis. Other inhibiting aqueous species include phosphate ( $H_2PO_3^-$ ) and fluoride ( $F^-$ ). Both species are present at low concentrations (0.05 and 2.0 mg/L, respectively), and are less likely to be primary inhibitors.

- The omission of Ca complexes from the EQ3 DATA0 database. At present, no dissociation constants are present in the database for the species  $\text{CaSiO}_3^-$ , or  $\text{CaHSiO}_3^+$ . Such species might be significant in alkaline solutions at  $\text{pH} \geq 9.0$ . They would depress the activity of  $\text{Ca}^{2+}$  and lower the apparent supersaturation of calcite.
- Erroneous solubility product of calcite. Repeated determinations of the thermodynamic properties and solubility product of calcite have established a high degree of confidence in currently recommended values for the solubility product by Plummer and Busenberg (1982) and Nordstrom et al., (1990), which is incorporated in the DATA0 database. However, a review is certainly merited.
- Apparent supersaturation induced by pore water evaporation during air drilling or storage. Artifacts resulting from collection, storage, and sampling procedures cannot be discounted. Their evaluation and quantification in the absence of other monitoring methods is questionable.

#### 7.1.3.2 Illite/smectite (I/S)

Carlos et al. (1995a,b) have reported the presence of illite/smectite in the matrix throughout most of the vadose zone in drill cores USW G-1, G-2, and G-3 at Yucca Mountain. The I/S ratio, which is a measure of the maximum temperatures to which I/S is subjected, has also been investigated. These ratios indicate that regions of the lower part of the vadose zone have been subjected to elevated (hydrothermal) temperatures since deposition over 10 million years ago. In response to a debate concerning the status of I/S as a single phase or as two phases, Garrels (1984) demonstrated that I/S should be treated as two distinct phases rather than one. This he illustrated with an activity diagram of  $\log[\text{K}^+]/[\text{H}^+]$  versus  $\log[\text{SiO}_{2(\text{aq})}]$  showing the calculated phase boundaries of I/S with respect to coexisting minerals, and upon which he plotted well-characterized groundwater compositions known to co-exist with I/S assemblages. In Figure 7.2, the same activity diagram is plotted, including the phase boundary separating illite from smectite determined by Garrels from the ground water analyses. On this figure are also plotted the calculated parameters derived from EQ3 distributions of chemical analyses of perched waters from Yucca Mountain, as reported by Yang et al. (1996a).

The  $\log[\text{K}^+]/[\text{H}^+]$  versus  $\log[\text{SiO}_{2(\text{aq})}]$  data clearly reflect the same trend recognized by Garrels (1984), although the slope of the phase boundary is slightly steeper. The increased steepness is entirely consistent with more recent estimates of stoichiometry of the I/S phase pair by Aja

(1995) and Kulik and Aja (1997), i.e.  $K_{0.29}(Mg_{0.26}Al_{1.74})(Al_{0.03}Si_{3.97})O_{10}(OH)_2$  and  $K_{0.5}(Mg_{0.22}Al_{1.78})(Al_{0.28}Si_{3.72})O_{10}(OH)_2$  for K-smectite and illite, respectively. The scatter off the phase boundary into the illite field might also be explained by the increasing activity ratio of  $[Mg^{2+}]/[H^+]^2$  in solution for those analyses, and reflects the fact that the I/S phase boundary is pseudo-trivariant at a given P and T. The exchangeable cation site in the smectite is probably occupied by  $0.5Ca^{2+}$  and or  $Na^+$  rather than by  $K^+$  as is represented by the above equation, but Figure 7.2 suggests strongly that the compositions of the perched waters, and by inference, the pore waters, may in part be controlled by the I/S phase pair. Of particular relevance is the  $SiO_{2(aq)}$  activity, which in many pore waters exceeds the saturation of cristobalite, one of the principal minerals of the divitrified welded tuffs.  $Mg^{2+}$  and  $Ca^{2+}$  may also display binary control by smectite and other secondary phase in the system, i.e. sepiolite and calcite. Further investigation of these supposed controls is in progress.

### 7.1.3.3 Sepiolite

Sepiolite and/or palygorskite is commonly associated with pedogenic calcite and opal-CT in southern Nevada and adjacent regions of the desert southwest (Gardner, 1972; Hay and Wiggins, 1980; Machette, 1985; McFadden and Tinsley, 1985), and has also been observed in saline lake bed deposits of the Amargosa desert (Khoury et al., 1982; Eberl et al., 1982). Sepiolite and palygorskite have also been found lining fractures in the vadose zone at Yucca Mountain (Carlos et al., 1995a), although Carey et al. (1997) were not able to identify either of these phases on fracture surfaces exposed in the ESF. Stoessel (1988) conducted an extended solubility study of both sepiolite and kerolite at 25°C and correlated his measurements with earlier work at higher temperatures. His solubility product values were used in preference to those in the EQ3 DATA0 database to test whether sepiolite is close to saturation within the vadose zone. Preliminary results from UZ-14 and UZ-16 pore water data by Yang et al. (1996a,b) show that the pore waters are for the most part at or near saturation with respect to sepiolite in units above the Calico Hills Formation. However, the waters become strongly undersaturated with respect to sepiolite in the latter. As noted above, sepiolite + I/S may control  $[Mg^{2+}]/[H^+]^2$ , thereby explaining the substantial invariance of this parameter in UZ-14 above the Calico Hills Formation (Apps, 1997). Traces of sepiolite may be present within the volume of rock occupied by the DST and should therefore be included in the model as a potential reactant phase, although its persistence, even at boiling water temperatures, is equivocal.

## 7.2 Gas Chemistry

### 7.2.1 Carbon dioxide

It is expected that ambient  $\log P_{\text{CO}_2}$  (bar) before turning on the heaters in the DST will range from  $-2.5$  to  $-3.5$ . The most likely value is about  $-3.5$ , in conformity with atmospheric conditions, because excavation of the ESF and DST facility has allowed the ingress of atmospheric carbon dioxide. Upon heating,  $\log P_{\text{CO}_2}$  could rise to near zero in the desiccation zone adjacent to the heaters, if the rock were to behave as a closed system. However, such a scenario is considered unlikely, and  $\log P_{\text{CO}_2}$  is not expected to rise appreciably above  $-1.5$ . The actual value depends on several hydrologic parameters that will require quantification as modeling proceeds.

### 7.2.2 Nitrous oxide

As discussed in Section 11 of this report, nitrous oxide could be generated in the dryout zone through the partial decomposition of nitrate, thus:



Because nitrate decomposition could cause the residual pore waters to become more alkaline and affect the release of carbon dioxide, it is worth monitoring for the presence of nitrous oxide in the gas phase. The concentration is expected to be low, but has been detected in a borehole elsewhere at Yucca Mountain (ONC#1) at a concentration of approximately 500 ppmv (Stellavato and Montazer, 1998). Its detection and evolution over time would provide useful insights into the desiccation process and the evolution of the pore water chemistry during desiccation.

### 7.2.3 Hydrogen

Hydrogen can be released during the cataclasis of minerals in rocks. This process arises from the rupturing of Si-O-Si bonds and subsequent hydrolysis, thus:



The evolved hydrogen would be a measure of the extent of cataclasis caused by induced thermomechanical stresses during heating. Although the quantity of hydrogen evolved will

be small, and may not be detectable, it would be worth testing for this gas as a measure of cataclastic deformation.

#### 7.2.4 Other species, e.g. HCl, NH<sub>3</sub>, B(OH)<sub>3</sub>

Calculations indicate that the concentrations of HCl, NH<sub>3</sub>, NH<sub>4</sub>Cl, and B(OH)<sub>3</sub> in the gas phase, surrounding the desiccation zone, would be negligible. Most NH<sub>4</sub><sup>+</sup> infiltrating Yucca Mountain is probably bacterially decomposed or taken up by plants in the root zone, and I/S clays probably take up that part which penetrates below the root zone. Therefore the concentration of NH<sub>4</sub><sup>+</sup> at the repository horizon is expected to be vanishingly small. This has recently been confirmed by Yang (1998, personal communication), and therefore the amount of NH<sub>3</sub> or NH<sub>4</sub>Cl released to the atmosphere would also be negligible, even though the pore waters are alkaline. Similarly, the evolution of HCl to the gas phase will remain negligible, unless the pH of the pore waters were to become acid at the final stages of desiccation, where the pore waters would be highly saline and consist primarily of residual sodium potassium chloride. Even then, the total mass released would be negligible and be immediately re-absorbed by condensate.

Boric acid, B(OH)<sub>3</sub>, would volatilize in the zone of desiccation, particularly as temperatures reached 200°C, and would condense with the condensate. It is possible that it would accumulate in the aqueous phase as refluxing occurs, and could be a measure of the extent of rock alteration. Therefore, the measurement of B(OH)<sub>3</sub> in solution during the course of the DST may be a useful indication of rock alteration. Such monitoring should be explored on an experimental basis.

---

## 8. TOUGHREACT CODE: BASIS OF GEOCHEMICAL CALCULATIONS

The module TOUGHREACT has been developed by Tianfu Xu and Karsten Pruess at LBNL to model non-isothermal multiphase reactive transport (Xu et al., 1997). TOUGHREACT considers homogeneous and heterogeneous reactions for an arbitrary number of primary chemical species and minerals under equilibrium and kinetic conditions, including adsorption and cation exchange. Also considered is the transport of an arbitrary number of species such as CO<sub>2</sub> and O<sub>2</sub> in the gas phase at equilibrium with the aqueous solution. As further discussed below, it is assumed that the partial pressures of the gaseous species are relatively low, such that they do not affect the total gas pressure.

An important aspect of TOUGHREACT is that its core structure is the TOUGH2 code, enabling it to treat various geochemical processes in the framework of dual

permeability/porosity, multiple interacting continua (MINC), and equivalent continuum formalisms for fractured porous media, along with the transport of water, air, and heat. The geochemical and transport calculation methods incorporated in TOUGHREACT are summarized below. These have been enhanced as part of this study to deal with boiling conditions such as those arising from the DST.

## 8.1 Geochemical and Mass-Transfer Calculations

The geochemical module incorporated in TOUGHREACT solves simultaneously a set of chemical mass-action and mass-balance equations to compute the extent of reaction and mass transfer between a set of given aqueous species, minerals, and gases at each grid block of the flow model. Details on the coupling between the flow model (TOUGH2) and the geochemical module are described by Xu et al. (1997). Equations for flow and chemical reactions are solved sequentially rather than in a coupled fashion (e.g. Steefel and Lasaga, 1994). This sequential approach has proven to be more time- and memory-efficient than a fully-coupled formulation for problems of large size such as the 2-D and 3-D realizations needed for the Yucca Mountain Project.

The setup of mass-action and mass-balance equations in the geochemical module of TOUGHREACT is, in general, similar to the formulation implemented in other geochemical models (e.g. Reed, 1982; Wolery, 1992; Kharaka et al., 1988; Parkhurst et al., 1980; Ball and Nordstrom, 1991; Allison et al., 1991), with additional provisions for mineral dissolution and precipitation under kinetic constraints and a volume-dependent formulation for gas equilibrium, as described below. The chemical system is described in terms of primary aqueous species (the independent variables). Minerals, gases, and secondary aqueous species are defined in terms of reactions involving only the primary species. It can be shown that if the dispersivities of all aqueous species are assumed equal, only the transport of primary species (in terms of total dissolved concentrations) need to be considered to solve the entire reactive flow/transport problem (Steefel and Lasaga, 1994).

The system of non-linear equations describing chemical mass-balance and mass-action is solved by a Newton-Raphson iterative procedure. Activity coefficients of aqueous species are computed by an extended Debye-Hückel equation (e.g. Parkhurst, 1990). Activity coefficients of neutral species are currently assumed equal to one, and the activity of water is computed using a method by Garrels and Christ (1965). A more rigorous treatment of activity coefficients will be incorporated in future versions of the code.

Equilibration with mineral phases is computed by adding a mass-action equation, for each saturated mineral, into the system of non-linear equations as follows:

$$\log(K_i) = \log(Q_i) \quad (8.1)$$

where  $K_i$  denotes the equilibrium constant and  $Q_i$  the product of the ion activities in the reaction that expresses mineral  $i$  in terms of the primary aqueous species. A term representing the amount of primary aqueous species consumed or produced by equilibration of minerals is added to the mass-balance equation for each primary species involved in mineral reactions, and is solved simultaneously with the concentrations of all primary species.

Kinetically retarded mineral precipitation and dissolution reactions are implemented in the code by incorporating a rate law which is dependent on the magnitude of the saturation index ( $Q/K$ ) of each considered mineral (Aagaard and Helgeson, 1982; Velbel, 1989) as follows:

$$r = \text{sgn}(1 - Q/K) k S [1 - (Q/K)^m]^n \quad (8.2)$$

$$\text{and } k = k_0 \exp[-E_a/R(1/T(K) - 1/298.15K)] \quad (8.3)$$

where  $\text{sgn}(1 - Q/K)$  is the sign of the expression  $(1 - Q/K)$ ,  $r$  is the mineral precipitation (negative) or dissolution (positive) rate,  $k$ ,  $E_a$ , and  $S$  are the rate constant, activation energy, and reactive surface area, respectively,  $T$  is temperature, and  $R$  the ideal gas constant. We assume that the exponents  $m$  and  $n$  equal one. The effect of pH and other aqueous species activities on reaction rates is not considered.

Over a finite time step  $\Delta t$ , the change in the concentration of each primary species  $j$  due to mineral precipitation or dissolution under kinetic constraints is computed from the sum of the rates,  $r_i$ , of all  $j$ -containing minerals  $i$  as follows:

$$\Delta C_j = \sum r_i \Delta t \quad (8.4)$$

These concentration changes are incorporated into the mass-balance equation of each primary species involved in mineral reactions, using Equations (8.2) and (8.3), and solved simultaneously with the concentrations of all primary species (i.e. the  $\Delta C_j$  terms are included into the jacobian matrix rather than computed externally). Instead of adding a separate rate equation for each mineral in the jacobian matrix,  $\Delta C_j$  in terms of Equation (8.2) substituted in (8.3) is added to each mass-balance equation. Therefore, the size of the jacobian matrix does not increase with the addition of minerals to the system, in contrast to the case when minerals are assumed to precipitate or dissolve at equilibrium.

Minor gas species such as  $\text{CO}_2$  are included in the model as ideal mixtures of ideal gases in equilibrium with aqueous and mineral phases. A mass-action equation is added to the system

of simultaneous equations for each saturated gas present, except for H<sub>2</sub>O and air (the carrier gases) which are handled separately through the flow module in TOUGH2. The gas mass-action equation takes the form:

$$\log(K_i) = \log(Q_i) - \log(P_i) \quad (8.5)$$

where  $K_i$  and  $Q_i$  are as defined for Equation (8.1) and  $P_i$  is the gas partial pressure. The latter is replaced with the ideal gas law,

$$P_i = n_i / V_g RT \quad (8.6)$$

where  $n_i$  denotes the number of moles of gas species  $i$ ,  $R$  is the ideal gas constant,  $T$  is temperature, and  $V_g$  is the gas total volume (all trace gas species and carrier gas). By expressing  $V_g$  in terms of the gas saturation  $s_g$ , the porosity of the medium  $\phi$ , and the (fixed) volume of each grid block in the flow model  $V_{block}$ , equation (8.5) is rewritten as:

$$P_i = n_i / (V_{block} \phi s_g) RT \quad (8.7)$$

The gas saturation is computed externally by TOUGH2 for the carrier gas (H<sub>2</sub>O and air). Substitution of Equation (8.6) into (8.4) allows for solving the amount of trace gas species ( $n/V_{block}$ ) together with the concentrations of all primary species.

The partial pressures of gas species calculated in this fashion are not fed back to TOUGH2 for solving the water and gas flow equations. Therefore, this calculation method is valid only for minor gases with partial pressures significantly lower than the total gas pressure (i.e. lower than the pressure of the carrier gas). For cases where the partial pressures of minor gases become significant, chemical equilibrium with the aqueous phase is computed correctly but the gas and water flow velocities computed by TOUGH2 are likely to be underestimated.

For saturated flow conditions ( $s_g = 0$ ), the partial pressure of dissolved gases is computed directly through Equation (8.3) (i.e.  $\log(P_i) = \log(Q_i / K_i)$ ).

Provisions for handling real mixing of real gases will be included in future versions of the code. For low gas pressures (near atmospheric) such as those prevailing in the unsaturated zone at Yucca Mountain, the effect of gas non-ideality is assumed to be negligible, especially when compared to other uncertainties inherent to modeling any subsurface processes (Section 10).

## 8.2 Transport Calculations

As mentioned above, if the dispersivities of primary and secondary aqueous species are assumed equal, only the transport of total dissolved components need to be considered to solve the entire reactive flow/transport problem (Steefel and Lasaga, 1994). This is the approach used in TOUGHREACT. Primary aqueous species and trace gases are transported by advection and diffusion using the water and gas velocity field computed by TOUGH2. Transport computations are carried out component by component using the same integral finite-difference approach as in TOUGH2 (Pruess, 1991). For this study, a sequential non-iterative approach (Xu et al., 1997) is used between the flow and reaction-transport modules.

---

## 9. MODEL AND CODE TESTING

As a recently developed code in which a wide range of physical phenomena and chemical processes are considered, it is important that verification and validation tests be made. In this section we present some of the important tests we have made for this project. At the current stage of this investigation, these tests should not be regarded as exhaustive. Other tests have been done by the primary authors of TOUGHREACT (Section 4.2) and will be presented for software QA. Further improvement and verification of TOUGHREACT is ongoing and, therefore, the results presented in this report are preliminary.

Several model simulations were performed to assess the results of the TOUGHREACT code for simulations of water-rock interaction under equilibrium and kinetic conditions. Equilibrium simulations were performed to compare the mineral assemblages and chemical compositions under "batch reactor" conditions to that given by the well-tested equilibrium code CHILLER (Reed 1982; Spycher and Reed, 1992). Kinetic simulations were compared to plug flow reactor experiments and model simulations on quartz and Topopah Spring welded tuff (Johnson et al., 1997a).

### 9.1 Equilibrium Simulations: Heating and Boiling without Advection/Dispersion

Simple computations using 1 and 2 grid blocks were performed to check gas, mineral, and aqueous phase equilibria in closed systems with no or limited advection/dispersion of chemical reactants. Heating and boiling simulations were conducted with TOUGHREACT and benchmarked against the results of CHILLER. CHILLER computes multicomponent chemical equilibria between an aqueous phase, minerals, and gases, and was specially designed for boiling and heating problems. CHILLER includes an option for incrementally adding heat into the chemical system to simulate boiling, which makes it practical for comparison with similar heat-"titration" simulations using TOUGHREACT.

A heating simulation was performed with TOUGHREACT using one grid block and fully saturated conditions. Heat was added to the water-only system to raise its temperature from 25 to 200°C. The pressure was maintained above the water saturation pressure so that no gas phase was formed. An equivalent simulation was conducted with CHILLER. For both cases, identical thermodynamic data bases were used: data from SUPCRT92 as reported by Johnson et al. (1992) upgraded with aluminum data from Pokrovskii and Helgeson (1995) (data compiled in SOLTHERM.JOH data base, courtesy of M.H. Reed, University of Oregon).

The composition of the water for this benchmarking exercise was taken from Yang et al. (1996a) (Sample UZ-16 at 1296.8 feet depth). The simulations were set to maintain equilibrium with calcite, albite, k-feldspar, kaolinite, and cristobalite. Two other minerals, sepiolite and anhydrite, were allowed to precipitate. No other minerals were allowed to form.

Results are shown on Figure 9.1, where output data from TOUGHREACT are shown with solid lines and CHILLER results are shown with symbols. The aqueous phase compositions and CO<sub>2</sub> fugacities computed by both programs are in very good agreement. The same is true for precipitated (positive) and dissolved (negative) mineral amounts. There is a small divergence in computed calcite amounts between 50 and 150° C (exaggerated by a factor of 100 on Figure 9.1a). This divergence does not affect the computed concentrations of aqueous species. It may be related to a difference in residual error in the carbonate mass balance (the calcite amount is quite small) and possibly also to a difference in computed activity coefficient for calcium and/or carbonate species as a function of temperature.

Benchmark boiling simulations were accomplished with the same water composition and mineral assemblage as for the heating test. Heat was incrementally added into the initially saturated (no gas) solution at 100°C, but this time the pressure was maintained near 1 atmosphere to allow a gas phase to form. In this case, the CHILLER and TOUGHREACT simulations were more difficult to benchmark because CHILLER computes boiling using pressure (with volume undefined, thus variable) while TOUGHREACT uses a fixed volume. Variable volume simulations were approximated with TOUGHREACT by setting a two-block grid, with one of the blocks representing the initially saturated (no gas) solution, and the other block set with a very large volume filled mostly with air. At a pressure near 1 atmosphere and temperature of 100°C, heat was "titrated" into the first block to simulate boiling, with the gas phase expanding into the second block, and pressure remaining constant because of the large volume of this block.

Results of both simulations are shown on Figures 9.2 through 9.4. These figures were plotted with the X-axis representing heat increasing from left to right, thus showing temperature increasing until the onset of boiling (100°C), then the boiling weight fraction at the constant temperature of 100°C (pressure is maintained near 1 atm.). The CHILLER simulation reveals

a more pronounced effect from early CO<sub>2</sub> degassing than the TOUGHREACT simulation (Figure 9.2). This results in a CO<sub>2</sub> pressure trend and a final pH different from those computed with TOUGHREACT, as well as a more pronounced effect on mineral dissolution and precipitation amounts (Figure 9.3). However, both simulations show consistent aqueous chemistry trends with a similar evaporative concentration trend for chloride (a useful conservative tracer in this case) (Figure 9.4). The simulations also indicate similar mineral precipitation and dissolution trends, including the precipitation of anhydrite at the later stages of boiling (Figure 9.3). The greater CO<sub>2</sub> degassing effect in the CHILLER simulation may be related to the absence of a volume constraint in the calculation method (closed system with expanding volume) and likely also to the different activity coefficient calculation methods incorporated in each program.

TOUGHREACT results show a lesser CO<sub>2</sub> degassing effect, with CO<sub>2</sub> pressures still slightly increasing after the onset of boiling. These results could be representative of a case where an extreme CO<sub>2</sub> degassing effect may not occur due to the ubiquitous presence of atmospheric CO<sub>2</sub>.

## 9.2 Kinetic Simulations of Plug Flow Reactor Experiments

Details of the plug flow reactor experiments on quartz and tuff, and GIMRT simulations, can be found in Johnson et al., (1997a). Here we describe the most important aspects to be considered for modeling conditions, and to compare to TOUGHREACT results.

### 9.2.1 Quartz

This experiment used crushed quartz grains having a range in grain size from 75 to 125  $\mu\text{m}$ , packed in a tube 3.1 cm in length and of inside diameter 0.66 cm. The temperature was held constant at 239° C and the average flow rate measured over the duration of the experiment (12.7 days) was 24.8 mm/day, under saturated flow conditions. The inlet fluid was distilled water. The initial porosity was not known exactly, and an average of values from 40 to 45% was given as 42.5%.

The outlet concentration of Si reached a roughly constant value of 105.4 ppm before the first measurement was made (16.2 hours). Because the equilibrium concentration of Si in equilibrium with quartz at 239° C is 156.8 ppm, the experiment can be considered as pure dissolution under kinetic conditions (Johnson et al., 1997a).

The latter authors also presented results of GIMRT (Steeffel and Yabusaki, 1996) simulations, assuming a constant flow field. The average outlet concentration in the experiment was best matched using the kinetic data given by Tester et al. (1994) and using a calibrated reactive

surface area of between 335 and 368 cm<sup>2</sup>/g for an initial porosity range of 40 to 45%. For comparison, Johnson et al. (1997a) reported a BET measured surface area range from 368 to 650 cm<sup>2</sup>/g.

A 1-D TOUGHREACT simulation was performed using a 31 volume element mesh with dimensions and interface areas identical to that of the plug flow experiment, plus one boundary element to set the appropriate outlet conditions. A constant injection rate (mass flux) was applied corresponding to the volume flux of 24.8 mm/day at 239° C, calculated using an estimated density<sup>1</sup> of 0.817 g/cm<sup>3</sup>. The permeability of the packed quartz grains was not given, and was therefore calculated assuming a cubic array of truncated spheres (Weyl, 1959) having a grain size of 100 μm with a truncation factor set to that needed to yield a porosity of about 42.5% (~ 0.97). A permeability of 6.51 x 10<sup>-12</sup> m<sup>2</sup> was calculated from the minimum pore throat diameter and number of pores per unit area of this grain texture using the modified Hagen-Poiseuille equation as described by Ehrlich et al. (1991). The kinetic rate for dissolution adopted was 0.2724 x 10<sup>-7</sup> mol/ m<sup>2</sup>s as derived from Tester et al. (1994), and used by Johnson et al., (1997a).

The results of this simulation are close to that given by Johnson et al. (1997a). Using a specific surface area of 350 cm<sup>2</sup>/g which is approximately the best fit surface area from Johnson et al. (1997a) we obtain an outlet concentration of 104 ppm Si, as compared to the 105.4 ppm measured in the experiment. The average porosity at the end of the simulation was 44.68%, compared to 44.55% found by Johnson et al. (1997a).

## 9.2.2 Topopah Spring Tuff

The experiment on Topopah Spring welded tuff, described by Johnson et al. (1997a), consisted of crushed tuff in a tube of length 26.3 cm and diameter 0.66 cm. The experiment was run for 36 days at a constant temperature of 240° C and an average flow rate of 25 ml/day. The initial porosity was estimated to be 42.5%. Roughly steady-state concentrations were attained after about a day, although there was a general decline in Si (aq) over time.

The mineral assemblage used in the TOUGHREACT and GIMRT simulations was quartz, cristobalite (α), amorphous silica, K-feldspar, albite, anorthite, kaolinite, paragonite, muscovite, gibbsite, boehmite, diaspore, and pyrophyllite. Except for anorthite, the same dissolution rate constants as those presented in Johnson et al. (1997a) were employed. The rate constant given for the anorthite component was several orders of magnitude greater than for the k-feldspar and albite components, and given that the calcium is in solid solution with the other feldspars (predominantly in exsolved albite) the rate was adjusted to the same order

<sup>1</sup> The fluid density was calculated using the temperature dependence given by Person and Garven (1992), and assuming a typical linear compressibility of pure water as 4.522 x 10<sup>-5</sup> bar<sup>-1</sup>.

of magnitude as albite. The same surface areas for dissolution were used; however, the GIMRT code incorporates a relation of precipitation surface area to porosity that is not implemented in TOUGHREACT, so that the precipitation kinetics are different. For this reason, and differences in thermodynamic data, the results can only be compared qualitatively.

Here, we compare the measured outlet concentrations to the TOUGHREACT and GIMRT simulations. We compare the results at approximately 22 days, instead of 36 days, because this corresponds approximately to the maximum number of time steps that TOUGHREACT reached before the final simulation time of 36 days. Because the simulation concentrations do not change over time (no phase was exhausted and there is no feedback to the flow field in terms of porosity or permeability changes), the shorter time period makes no difference in the results.

Table 9.1 shows the outlet concentrations from the experiment and the model simulations. The first two TOUGHREACT (TR-1 and TR-2) simulations show the effect of changing from the original thermodynamic database used in TOUGHREACT that is derived from SUPCRT92 (TR-1) to the updated database presented in this report (TR-2). The third simulation (TR-3) illustrates the effect of suppressing quartz precipitation, as was indicated by the lack of quartz precipitates in the experiment, and the known difficulty for quartz nucleation (Rimstidt and Barnes, 1980).

**Table 9.1.** Comparison of measured outlet concentrations from a TSw tuff plug flow reactor experiment and GIMRT simulation (Johnson et al., 1997a) and TOUGHREACT simulations.

Cation	Meas. (ppm)	GIMRT-A	TR - 1	TR - 2	TR - 3
Si	356.951	252.17	191.9	186.9	309.2
Na	14.003	9.76	30.1	27.3	16.8
K	2.253	1.09	3.36	3.03	1.86
Ca	0.043	0.0103	0.044	0.036	0.089
Al	7.17	7.03	8.36	6.90	2.21

Although the TOUGHREACT results are not identical to GIMRT outlet concentrations, the analysis shows that the model describes the experimental data as well as GIMRT. Differences in the cation ratios in the output fluid are due mainly to the different precipitation kinetics employed for the secondary phases.

## 10. DATA UNCERTAINTIES

Any modeling of heat and fluid flow in the subsurface is subject to large uncertainties resulting from the inherently heterogeneous nature of subsurface materials. In addition, calculation methods and assumptions also contribute to the uncertainty of modeling results. For coupled flow and reactive transport simulations, this uncertainty is compounded by the fact that the simulations rely largely on the thermodynamic and kinetic data input into the model. These include the dissociation constants  $K$  in Equations 8.1 and 8.2, and rate constants, activation energies, and very uncertain surface areas in Equation 8.2. The calculation methods and parameters used for computing activity and fugacity coefficients also affect modeling results. All these data have significantly large uncertainties which directly affect modeling results.

The mineral saturation indices ( $\log [Q/K]$ ) determine whether a mineral precipitates or dissolves either at equilibrium (Equation 8.1) or under kinetic constraint (Equation 8.2). To provide an example of the effect of  $\log(K)$  data on computed saturation indices, simple speciation calculations were performed using thermodynamic data from two commonly used data bases: Johnson et al., (1992) (SUPCRT92) with revised aluminum data by Pokrovskii and Helgeson (1995), and data from Holland and Powell (1990) (compiled data in SOLTHERM.JOH and SOLTHERM.HP databases, courtesy of M.H. Reed, University of Oregon). Saturation indices were computed with SOLVEQ (Reed, 1982) for several minerals from 25 to 200°C and the same water composition as for the tests described in Section 9.1. Differences between computed  $Q/K$  values were up to a several orders of magnitude for many aluminosilicate minerals. For two common rock forming minerals at Yucca Mountain, albite and K-feldspar,  $\log (Q/K)$  differences up to 1 and 0.7, respectively, were calculated. Similar conclusions on the discrepancy between thermodynamic data for these minerals have been expressed by Apps and Chang (1992).

The uncertainty of published kinetic data for many minerals is even greater than for dissociation constants, which compounds the uncertainty on reaction rates expressed through Equation (8.2). Only careful experimental and field studies combined with modeling (such as in the plug flow experiments) will allow refinement of thermodynamic controls and the effective rates of reaction.

---

## 11. EXPLORATORY GEOCHEMICAL SIMULATIONS

In this section, we discuss the results of a series of preliminary simulations of chemical processes in the DST in either the dryout (desiccation) zone immediately surrounding the

heaters or in the region of condensation. These simulations allow a conceptual understanding of the chemical evolution of a system as a function of some specified physical or chemical variable. This variable can be a reaction progress parameter, such as the extent of evaporation, boiling or cooling, or some externally defined chemical potential, such as the partial pressure of carbon dioxide, which can be varied over a range realistically expected during the course of the DST. The advantage of such simulations is that they are easy to perform, and facilitate interpretation of more complex THC simulations involving both spatial and temporal domains.

The section comprises two separate studies. The first is made using EQ3 v7.2b, a qualified distribution-of-species code. The code is used to conduct simple calculations to study the chemical behavior of the residual brine during evaporation in the desiccation zone, assuming partial equilibrium with the host rock minerals. The code is also used to evaluate condensate chemistry as a function of variable ambient partial pressure of carbon dioxide. In the second section, more ambitious reaction progress simulations are conducted using the unqualified code CHILLER, which is advantageously configured to permit studies of the evolution of systems during either boiling or condensation.

The results of the two sets of simulations are broadly comparable, after due consideration is given to differences in the way in which the simulations were conducted, and minor differences in model assumptions.

## **11.1 Thermochemical Processes of the Altered Zone**

### **11.1.1 Zone of Desiccation**

In the zone immediately adjacent to the waste containers or surrogate waste (electric heaters), temperatures are expected to rise to a maximum of 200°C. This will lead initially to boiling of the rock pore water, and eventually to complete evaporation and drying. Because the pore water is relatively dilute, the initial boiling temperature will be at approximately the temperature at which pure water boils at the elevation of the ESF, i.e., approximately 95°C. With progressive concentration of residual salts, the temperature will rise, until crystallization of the dissolved residue and complete desiccation takes place. Between 95 and 200°C, some dehydration of small quantities of smectite in illite/smectite (I/S) assemblages may occur, and decomposition of calcite precipitates is possible. However, both such processes are expected to be minor.

In order to provide an initial scoping of the chemical processes in the zone of desiccation, a series of calculations were conducted to determine potential precipitates likely to be observed during boiling and the equilibrium partial pressure of carbon dioxide at various stages of

concentration<sup>2</sup>. Two sets of simulations were made. The first assumes that no carbon dioxide is released from the pore water during concentration, i.e. the system is considered closed, and the second assumes that the partial pressure of carbon dioxide is controlled externally at  $10^{-2}$  bar, i.e. the system is considered open with respect to  $P_{CO_2}$ . Furthermore, it is assumed in both cases that calcite, cristobalite, high albite, sanidine, and sepiolite are initially at saturation and remain so. The assumed phase saturations are based on a preliminary assessment of thermodynamic controls on the pore water composition at Yucca Mountain (Apps, 1997), on the assumption that the primary mineral products of devitrification are cristobalite and sanidine, and that cristobalite, high albite and sanidine are convenient end-member phases present in the EQ3/6 v.7.2b database. However, evidence from a transmission electron microscope study of a devitrified tuff similar in provenance and composition to that of the TSw units at Yucca Mountain suggests that the sanidine laths in the axiolitic and spherulitic intergrowths of the welded units may have recrystallized to potash feldspar (microcline?) and low albite (Tarshis, 1982).

The two simulations represent the extremes of closed versus open systems. In reality, the desiccating zone will likely remain partially open, depending on a variety of complex hydrological and hydrochemical factors, quantifiable only with non-isothermal reactive chemical transport modeling of the vadose zone at Yucca Mountain, as well as the acquisition of new data from the DST.

The initial conditions are summarized in Table 11.1, and the results are presented graphically in Figures 11.1, 11.2 and 11.3. Figure 11.1 displays the evolution of the principal chemical constituents of the pore water as a function of the concentration factor due to boiling. Significant differences in chemistry between open and closed systems occur with respect to Mg, Ca, and  $HCO_3^-$ . In the closed system, the concentration of Mg increases sharply with boiling, as the solubility of sepiolite increases with declining pH, as shown in Figure 11.2. This suggests that sepiolite would dissolve, releasing  $SiO_2(aq)$  and  $Mg^{2+}$  to the solution. The  $Mg^{2+}$ , in turn, would contribute to the precipitation of secondary smectite.  $HCO_3^-$  in the closed system increases in conformity with concentration due to evaporation, depressing the Ca concentration in relation to the open system. In Figure 11.2, the corresponding variations in pH and  $P_{CO_2}$  are recorded. In the closed system,  $P_{CO_2}$  rises dramatically with concentration of dissolved salts, attaining approximately one bar ( $10^5$  Pa) with a 16 fold concentration. The pH in both cases declines with evaporation, but the closed system pH falls further, as would be expected. These results do not take into account the possible dilution of  $CO_2$  by steam in an

---

<sup>2</sup> EQ3 V. 7.2b (Wolery, 1992) was employed in the calculations using the unmodified database issued with the code. The database requires modification to be suitable for application to problems germane to the DST and subsequent modeling of the proposed waste repository hydrogeochemistry. Modeling results are therefore preliminary.

open system, which could lead to transient declines in  $P_{CO_2}$  and positive pH excursions. These results differ from preliminary TOUGHREACT simulations presented in this report.

**Table 11.1** EQ3 Modeling of Evaporation at 100°C

Constituent	Initial Composition (mg/L)	Constraint (Closed)	Constraint (Open)
H <sup>+</sup>	-	UEBAL <sup>1</sup>	UEBAL
Na	9.	Conc.Factor	Conc. Factor
K	-	Sanidine high	Sanidine high
Mg	12.	Sepiolite	Sepiolite
Ca	65.	Calcite	Calcite
Al	-	Albite high	Albite high
SiO <sub>2</sub> (aq)	46.	Cristobalite (beta)	Cristobalite(beta)
HCO <sub>3</sub> <sup>-</sup>	66.	Conc. Factor	Conc. Factor
SO <sub>4</sub>	79.	Conc. Factor	Conc. Factor
Cl	77.	Conc. Factor	Conc. Factor
NO <sub>3</sub>	12.	Conc. Factor	Conc. Factor

<sup>1</sup>UEBAL indicates that selection of ionic species used to achieve electrical neutrality in the aqueous phase.

Figure 11.3 indicates that the specified mineral assemblage is unstable with respect to calcium montmorillonite, and that the boiling stage would enhance the decomposition of the primary minerals to form secondary clays. Under open system conditions, anhydrite (CaSO<sub>4</sub>) is also likely to precipitate after the pore waters have evaporated to less than one quarter their initial volume. The total quantity of anhydrite, however, will be negligible, and would not have a significant effect on the porosity or permeability of the devitrified tuff matrix.

Thin section descriptions by Broxton et al. (1982) of the welded devitrified tuffs at Yucca Mountain suggest that "clay" (presumably illite/smectite) may be in part due to the alteration of extremely fine axiolitic or spherulitic sanidine/cristobalite intergrowths. It is possible that the excess free energy contribution imparted by the enhanced surface area of these intergrowths destabilized them in favor of coarser intergrowths. However, a more critical examination will be needed to clarify this matter. The rate of alteration of the primary feldspars and cristobalite in the rock could be dependent on the specific surface area, which varies depending on the coarseness of the primary and secondary mineral textures. Because the rate of alteration of the welded tuffs is estimated to be only of the order of 1 to  $10 \times 10^{-9}$ /yr., or a few percent of the rock over a ten million year period, (Johnson and DePaolo, 1994), the extent of alteration to clay before desiccation of the inner thermal zone within four years is not expected to increase by more than a factor of two. Recognition of such alteration during the course of the DST is expected to be subtle, and will require perseverance in its identification.

The potential precipitation of small amounts of anhydrite and residual salts in DST desiccation zone samples will likewise be difficult to discern by optical methods. Thus, alteration of this zone is expected to be trivial over the lifetime of the DST test. Under actual proposed repository conditions, longer duration thermal alteration will cause dehydration of the small amounts of clay minerals present, i.e., I/S and sepiolite, and decarbonation of calcite. The latter processes will be of minor consequence because of the small concentrations of participating minerals.

Although the above simulations are believed to be reasonable, there exists the possibility that elevated temperatures may accelerate nitrate decomposition according to the following equations (Cooper and Smith, 1963; Mehran and Tanji, 1974):



In sum:



Nitrate decomposition will drive up the pH of the residual pore waters and decrease the partial pressure of  $\text{CO}_2$ . Thus the evolution of the pore water pH and  $P_{\text{CO}_2}$  will be somewhat different from that illustrated in Figure 11.2. Evidence for nitrate decomposition might be detected in the field through the measurement of emitted nitrous oxide ( $\text{N}_2\text{O}$ ). Laboratory testing under closed system conditions might also allow the kinetics of nitrate decomposition to be quantified.

Physio-chemical phenomena affecting the desiccation zone, which are of scientific rather than technological interest, include the nature of capillary pressure changes during desiccation, the residual quantity of adsorbed water remaining, whether chemical reactions can proceed through surface diffusion through the adsorbed water surface layer, and at what rate. As an example of the last item, consider the reaction between  $\beta$ -cristobalite and calcite to form wollastonite:



$\beta$ -Cristobalite      Wollastonite

$\log P_{\text{CO}_2}$  resulting from this reaction is plotted in Figure 11.4 as a function of temperature and compared with the anticipated range of  $\log P_{\text{CO}_2}$  anticipated during desiccation. The above reaction becomes significant in releasing carbon dioxide to the vapor phase only at temperatures above 120°C. The kinetics of such a reaction are expected to be extremely slow, unless diffusion through the adsorbed water layer were to accelerate the rate.

The preceding discussion presupposes that no anthropogenic or natural materials are introduced into the heated drifts, and that an air gap exists between the heat source and the rock faces of the DST. If, as may be proposed, a capillary barrier material is introduced in the proposed repository, or the drifts are lined with concrete reinforcing panels, other issues concerning their thermochemical response should be addressed.

### **11.1.2 Zone of Condensation and Reflux**

During the initial phase of boiling adjacent to the walls of the drift, steam will migrate into the drift, and into the host rock. Steam flow is expected to occur predominantly along fractures where condensation will occur due to cooling by the host rock. Condensation will in turn heat the rocks and accelerate interdiffusional mixing of the ambient pore water with the condensate. Imbibition of the condensate will also occur where the rock is not fully saturated with the aqueous phase. Depending on the location of the condensation front, pore water diluted with condensate will migrate under the force of gravity, either away from the heat source, or towards it. Condensate in fractures above the heat source will flow back towards the heaters and be evaporated and condensed repeatedly. Continuous refluxing of the condensate will induce transport of dissolved constituents and their precipitation and accumulation at the boiling front, which will migrate during progressive heating and cooling cycles of the DST.

At issue is the impact of the progressive accumulation of precipitates in fractures at the boiling front. If the accumulation of such precipitates were to lead to sealing of fractures and a drastic decline in the porosity and permeability of the rock matrix above the emplaced waste, this would significantly impact the hydrologic regime and modify the long term hydrologic behavior of the repository. Field evidence under approximately analogous conditions where a basalt sill intruded a devitrified tuff at the Nevada Test Site (Matyskiela, 1997) suggests that matrix porosity reduction of nearly 100 percent and a reduction of permeability of approximately three orders of magnitude is possible. The DST will be in operation for a maximum period of eight years, and therefore the long-term progressive sealing of rock fractures might not be detectable. However, cyclic processes of refluxing should be observable, and detailed features of the process, such as the rate and nature of rock mineral dissolution, diffusive mixing of pre-existent pore water with condensate, and gas

phase transport and gas phase component partial pressures, could be monitored during heating as well as cooling phases.

Complicating the process of condensate transport is the as yet uncertain extent to which pressure solution (or stress corrosion) of the fracture and grain asperities may influence the kinetics of mineral dissolution under field conditions. The DST could provide vital clues as to the significance of rock stress corrosion under field conditions, and it may be of sufficient duration to permit the establishment of a realistic trend in permeability reduction.

With respect to preliminary modeling of the condensate chemistry, it is instructive to calculate the composition of the condensate after equilibration with the host rock primary and secondary minerals. Modeling was conducted at 100°C under the constraints given in Table 11.2, which includes the assumption that saturation is maintained with respect to rock forming minerals. The effect of varying CO<sub>2</sub> partial pressure on the chemistry was examined through variation of the ambient log P<sub>CO<sub>2</sub></sub> from -3.5 to -1.0.

**Table 11.2** EQ3 Modeling Of Condensation at 100°C

Constituent	Constraint
H <sup>+</sup>	UEBAL
Na <sup>+</sup>	Conc. Factor
K <sup>+</sup>	Sanidine high
Mg <sup>++</sup>	Sepiolite
Ca <sup>++</sup>	Calcite
Al <sup>+</sup>	Albite high
SiO <sub>2</sub> (aq)	Cristobalite (beta)
HCO <sub>3</sub> <sup>-</sup>	LOG P <sub>co2</sub> (var)

The results of the modeling are presented in Figures 11.5, 11.6, and 11.7. Figure 11.5 illustrates the condensate chemistry. As expected, the progressive increase in P<sub>CO2</sub> leads to a substantial increase in HCO<sub>3</sub><sup>-</sup> content, and a corresponding decrease in Ca<sup>++</sup> content to maintain saturation with respect to calcite. An increase in Mg concentration with increasing P<sub>CO2</sub> can be correlated with the decrease in pH (Figure 11.6).

If the condensate compositions are allowed to evaporate to dryness, the approximate distribution of calcium smectite, calcite, and amorphous silica in the fracture precipitate can be calculated. This is illustrated in Figure 11.7. It can be seen, that regardless of the carbon dioxide partial pressure, the precipitate is dominated by amorphous silica. Somewhat less than ten percent of the precipitate would be calcite and less than one percent would be smectite. The predominance of silica as a fracture precipitate compared with other aluminosilicate mineral phases is due to the extremely low solubility of aluminum in the condensate. In contrast, alteration within the rock matrix will be dominated by *in situ* replacement of feldspars by aluminosilicate clays, i.e. kaolinite and/or illite/smectite.

Highly soluble salts, consisting primarily of sodium bicarbonate (NaHCO<sub>3</sub>) will also concentrate and eventually precipitate at the boiling front, but episodic invasion of condensate will ensure their rapid dissolution and repeated redistribution. The concentration of these salts in rock matrix pores could lead eventually to the formation of matrix zeolites, such as clinoptilolite or mordenite, in preference to clay minerals. Alteration of this type is unlikely to be significant during the DST time frame, and might not be significant over longer periods if deuteric recrystallization of sanidine to more stable feldspars, low albite and potash feldspar, has occurred. Further investigation of this potential phenomenon is merited in order to predict the long-term hydrochemical behavior of the repository.

## 11.2 Additional Geochemical Simulations

Geochemical simulations in addition to those presented in Section 11.1 were performed to further illustrate and scope the water-rock-gas interaction processes that are likely to affect the DST. The purpose of these computations was not to predict exact water chemistry, but to reveal trends useful in interpreting the results of coupled flow-transport-reaction simulations of the DST. In addition, these simulations are presented to illustrate the difference between a system allowed to react with a typical rock-forming assemblage and a system allowed to react with silica and carbonates only. The processes examined include temperature change, CO<sub>2</sub> degassing and evaporative concentration due to boiling, and gas condensation.

Equilibrium simulations were performed with the program CHILLER (Section 4.2 and 9.1), using the same water composition as for the benchmark tests in Section 9.1 (sample UZ-16, 1296.8 feet from Yang et al., 1996a; Table 11.3). The composition of this water falls between the range of calcium chloride or sulfate type waters that typically occur above the Topopah Spring Tuff, and the more sodium carbonate-bicarbonate type waters deeper into the Calico Hills Formation. This intermediate composition is believed to be reasonable for exploratory work.

Simulations of heating, boiling, and gas condensation were conducted using a simple chemical system (Table 11.3) under two limiting conditions: Case 1 equilibrium with calcite and cristobalite only, and Case 2 equilibrium with calcite, cristobalite, albite (low phase), k-feldspar, and kaolinite (typical rock-forming minerals at Yucca Mountain). In both cases, anhydrite was allowed to precipitate on its own, while sepiolite, a magnesium phase, was allowed to form only in the second case. Illite and smectites are not included because these phases cause the system to be over-defined under the conditions of forced equilibrium. For the sake of simplicity, no other mineral phases were considered. The chemical system was assumed to be closed (i.e. no mass exchange with the outside, but a gas phase is allowed to form in boiling simulations). The goal of this exercise was to investigate pH, mineral precipitation, dissolution, and other chemical trends for these two limiting cases, understanding that a real case with kinetically retarded mineral reactions (i.e. reactions with aluminum silicates) is likely to fall between these two limits. Cristobalite (alpha phase) was chosen as the silica mineral because its solubility falls between that of amorphous silica (more likely to form at lower temperature) and that of quartz (kinetically retarded at low temperatures).

**Table 11.3.** Water Composition for CHILLER Simulations.

Constituent	Concentration	
	A	B
pH	7.4	8.5
Cl <sup>-</sup>	50	75**
SO <sub>4</sub> <sup>-2</sup>	18	18
CO <sub>3</sub> <sup>-2*</sup>	336	295
SiO <sub>2</sub>	47	23
Na <sup>+</sup>	98	160
K <sup>+</sup>	4*	0.25
Ca <sup>++</sup>	32	3.8
Mg <sup>++</sup>	20	2.8
Al <sup>+++</sup>	0.01*	0.0008

(Temperature 25°C, all concentrations in ppm)

A) Original composition from sample UZ-16 (1296.8 feet) (Yang et al., 1996a). B) Composition after equilibration at 25° C with Case-2 minerals; used in both Case-1 and Case-2 simulations (see text).

\* Total carbonate as CO<sub>3</sub><sup>-2</sup>

\* Estimated, not initially available.

\*\* Adjusted for charge balance of the solution.

For both cases 1 and 2, the initial water at 25°C was forced to equilibrate with all mineral phases except for sepiolite, which precipitated on its own, and anhydrite. This raised the water pH from the measured value of 7.4 to a pH of 8.5 (Table 11.3). The higher pH is likely to be more representative of waters in the Topopah Spring Tuff (Apps, 1997).

Figures 11.8 through 11.10 show the result of simulated heating to 100°C followed by boiling at 1 atmosphere pressure. Both Case 1 and Case 2 are presented. CO<sub>2</sub> measurements taken around the DST area on February 8, 1998 (Conrad et al., 1998) are included in Figure 11.8 for information.

### 11.2.1 Heating

Heating causes the pH to decrease (Figure 11.8) due to the dissociation of water with increasing temperature and to the retrograde solubility of calcite (Case 1),



and also to the reaction of silica and kaolinite to form albite (Case 2),



for this aqueous species may be questionable. Without this species, calculated dissolved silica concentrations in Case 1 are near 3000 ppm.

After approximately 90 percent boiling in Case 2, anhydrite precipitates from the concentrative effect of H<sub>2</sub>O vaporization on calcium and sulfate. Precipitation of anhydrite was not observed in Case 1 (at ending simulated boiling fraction of 99.7 %) because pH is high and calcium is used by calcite. Obviously, upon complete boiling (dry-out, not modeled here) silica and other salts in solution are expected to precipitate in both cases, and most likely also anhydrite in Case 1.

The different pH trends between cases 1 and 2 during boiling demonstrate the important effects of CO<sub>2</sub> degassing and pH-buffering by typical rock-forming minerals. The difference between these two simulations illustrates the chemical shifts that could be expected from differing reaction rates for minerals, and thus reinforces the fact that results of coupled flow-transport-reaction simulations of the DST will be quite dependent on kinetic data.

### 11.2.3 Gas Condensation

Results of gas condensation simulations are shown on Figures 11.11 through 11.13. The gas from the Case 2 boiling simulation at 99.7 percent fraction boiling (last boiling step) was cooled from 100°C to 25°C at near 1 atm. pressure to simulate condensation. The composition of the original gas phase at 100°C, before condensation, was approximately 100 ppmV CO<sub>2</sub> (PCO<sub>2</sub> near 10<sup>-4</sup> bar for both Case 1 and Case 2, Figure 11.8), the rest being H<sub>2</sub>O gas. Equilibration of the condensate with Case 1 and Case 2 mineral assemblages was maintained from 100°C down to 25°C.

The gas condensed entirely from the start of simulations below 100°C at near 1 atmosphere pressure. The calculated pH of the condensate at 100°C is 6.2 at equilibrium with a Case 1 mineral assemblage, and 7.4 at equilibrium with Case 2 minerals (Figure 11.11). Additional calculations with a higher starting gas CO<sub>2</sub> content (log PCO<sub>2</sub> = -1.3 at 100°C) yield similar pH for each case at the onset of condensation near 100°C, because most of the added CO<sub>2</sub> forms a gas phase at this temperature (i.e., most of the added CO<sub>2</sub> does not dissolve). However, this gas phase prevails down to 25°C (no complete condensation possible at 1 atm.), and provides for increased CO<sub>2</sub> dissolution upon cooling compared to the cases with a lower initial CO<sub>2</sub> partial pressure. As a result, the final pH for Case 1 at 25°C is near 6, while it is near 7 for Case 2, contrasting significantly with the final pH values near 6.7 and 8.5, respectively, shown at 25°C on Figure 11.11.

Cooling the condensed gas from 100°C to 25°C results in different mineral precipitation and dissolution patterns for cases 1 and 2 (Figure 11.12). In the first case, significant amounts of

calcite dissolve, while a small amount of calcite precipitates in the second case. More cristobalite forms in Case 2 from the dissolution of albite. The concentrations of aqueous species vary accordingly (Figure 11.13). Again, the difference between the two cases underlines the importance of kinetic constraints and their anticipated large effect on the accuracy of results of DST simulations.

### 11.3 Discussion

More sophisticated simulations of the desiccation and condensate zones using the reaction progress simulator, EQ6, or CHILLER are merited. Such simulations can be conducted in either the reaction progress or time domains (Delaney et al., 1986; Wolery, 1993; Wolery and Daveler, 1992) for the application of EQ3. In the reaction progress domain, simulations assume homogeneous equilibrium in the aqueous phase, and reversible equilibrium with respect to product minerals. When conducting reaction progress simulations in the time domain, kinetic equations for mineral dissolution and precipitation are also required. For such simulations to be meaningful, it is essential that both the thermodynamic and kinetic data be validated for the conditions pertaining to the Yucca Mountain hydrochemical environment, and especially for the Tptpmn Unit. The validation process is currently under way, and sufficient progress has been made to formulate a preliminary understanding of the thermodynamic and kinetic controls on pore water compositions within the stratigraphic sequence of the vadose zone.

---

## 12. DRIFT-SCALE TEST MODEL DESCRIPTION

### 12.1 Grid, Thermohydrological Parameters, and Boundary Conditions

The DST grid, thermal and hydrologic parameters and boundary conditions, and heating schedule used for the simulation of reaction-transport processes were taken directly from the DST thermohydrological model presented by Birkholzer and Tsang (1997). We do not repeat all of the thermohydrological parameters used here, as these can be found in the detailed report by the latter authors. It is important to note that the hydrological parameters are calibrated parameters developed by inverse modeling of the SD-9 borehole using an infiltration rate of 3.6 mm/yr (Bandurraga and Bodvarsson, 1997). While these parameters have been calibrated against matrix saturations and water potentials, there are many assumptions and hydrological parameters for fractures that are highly uncertain. Thus, it is likely that these parameters, as well as the conceptual models for unsaturated flow in the fractured tuffs, will be refined further.

The 2-D dual permeability mesh consists of 4484 elements, as shown in Figure 12.1. A close-up of the mesh around the heater drift and wing heaters is shown in Figure 12.2. The heating schedule is the base case presented by Birkholzer and Tsang (1997) with 100% output for the first year, 50% for the following 3 years, followed by a cooldown period of 4 years.

We assume that there is no infiltration over the period of the experiment. Infiltration has been shown to have little effect on the thermohydrology over the time-period (8 years) of the experiment (Birkholzer and Tsang, 1997). The inside wall of the heater drift is considered to be a no-flux boundary for water, gas, and aqueous and gaseous species.

## 12.2 Geochemical Parameters

We present results from four simulations using different mineral assemblages (Tables 12.1, 12.2, and 12.3). The first simulation consists of calcite, quartz, cristobalite, and amorphous silica and considers CO<sub>2</sub> transport in the gas phase with a reduced set of primary aqueous species. The second simulation considers a much wider range of minerals and aqueous species, in addition to CO<sub>2</sub> transport, and also includes effects of anorthite dissolution on <sup>87</sup>Sr/<sup>86</sup>Sr ratios. The third simulation uses a mineral assemblage based in part on the plug flow reactor experiment modeling (Johnson et al., 1997a). This simulation also includes CO<sub>2</sub> transport in the gas phase. The fourth simulation considers only the silica phases without CO<sub>2</sub> transport.

Tables 12.1 through 12.3 present the mineral assemblages and volume rate constants, reactive surface areas, and aqueous species used in the first three simulations presented here. The fourth simulation uses the same parameters as in Table 12.1, but without calcite, calcium, carbonate species, and CO<sub>2</sub>. Volume fractions (Vf) are calculated assuming a matrix porosity of 0.11 in the Tptpmn, and 0.10 in fractures (the latter is solely for consideration of the fractured wall-rock, as actual fracture porosities used in the thermohydrologic calculations are much lower). All kinetic parameters and surface areas were derived originally from Johnson et al. (1997a) and Hardin (1998), except where noted. Some parameters were assumed to be the same as for other similar mineral phases or endmembers.

**Table 12.1.** Starting mineral assemblage and possible secondary phases considered. Reaction rate law parameters (precipitation and dissolution) for the drift scale test simulations (DST-1, DST-1a). Calcite is considered an equilibrium mineral. Primary aqueous species are considered in reactions and for transport.

Minerals	Vf (matrix)	Vf (fractures)	k <sub>0</sub> (mol/m <sup>2</sup> s)	E <sub>a</sub> (kJ/mol)	S (m <sup>2</sup> /kgH <sub>2</sub> O)	Aqueous Species
Quartz	0.1018	0.0995	1.2589e-14	87.5	71.07	H <sub>2</sub> O

Minerals	Vf (matrix)	Vf (fractures)	$k_0$ (mol/m <sup>2</sup> s)	$E_a$ (kJ/mol)	S (m <sup>2</sup> /kgH <sub>2</sub> O)	Aqueous Species
Cristobalite	0.2292	0.2241	3.1623e-13	69.08	71.07	H <sup>+</sup>
Am. SiO <sub>2</sub> *	0.0	0.0	7.944e-13	62.8	142.14	Ca <sup>2+</sup>
Calcite	0.0	0.02	equil.	equil.	equil.	Na <sup>+</sup>
						Cl <sup>-</sup>
						SiO <sub>2</sub> (aq)
						HCO <sub>3</sub> <sup>-</sup>

\* Precipitation rate law from Rimstidt and Barnes (1980):  $\log k = -7.07 - 2598/T(K)$ . Reactive surface area set twice that of the other silica phases. Precipitation of quartz and cristobalite was suppressed.

Table 12.2 shows the input geochemical parameters for minerals in simulation DST-2. In addition, a small component of Sr has been substituted into the Ca site in anorthite in amounts equivalent, in stoichiometric quantities, to the total Sr content of TSw middle nonlithophysal (~18 ppm; Neymark et al., 1995) and the approximate <sup>87</sup>Sr/<sup>86</sup>Sr ratio of the bulk tuff (~0.718; Neymark et al., 1995). The initial pore water Sr isotopic composition is given from the mean calcite isotopic ratio in the same unit in the ESF (0.7126; Paces et al., 1998). The total porewater Sr content (240 ppm) was derived from the average Sr content in UZ-14 perched water (Rousseau et al., 1996), which is considered to be close to the average in the TSw porewaters (Sonnenthal et al., 1998). It is assumed that only anorthite dissolution shifts the water isotopic ratio, and that no other mineral phases are contributing Sr. This is a simplification given the moderate Sr contents of calcites at this level (~ 100 ppm, on average; Denniston et al., 1997; Vaniman and Chipera, 1996). Pore water Sr isotopic ratios can then be recalculated using Sr' and <sup>86</sup>Sr as defined below:

$$^{87}\text{Sr}/^{86}\text{Sr} = \frac{\text{Sr}'}{^{86}\text{Sr}} - 1 \quad (12.1)$$

where

$$\text{Sr}' = \text{Sr}_{\text{total}} \left( 1 - \left[ ^{84}\text{Sr} + ^{88}\text{Sr} \right] \right) \quad (12.2)$$

This relation assumes that there is no radioactive decay of <sup>87</sup>Rb to <sup>87</sup>Sr and that the masses of the different Sr isotopes are identical. The proportions of <sup>84</sup>Sr and <sup>88</sup>Sr are also assumed constant (<sup>84</sup>Sr = 0.0056, <sup>88</sup>Sr = 0.8253; Faure, 1977).

**Table 12.2.** Starting mineral assemblage and possible secondary phases considered in TOUGHREACT simulations. Reaction rate law parameters (precipitation and dissolution) for drift scale simulation (DST-2). Calcite and anhydrite are considered equilibrium minerals. Primary aqueous species considered in reactions and for transport.

Minerals	Vf (matrix)	Vf (fractures)	$k_0$ (mol/m <sup>2</sup> s)	$E_a$ (kJ/mol)	S (m <sup>2</sup> /kgH <sub>2</sub> O)	Aqueous Species
Quartz	0.1018	0.0995	1.2589e-14	87.5	71.07	H <sub>2</sub> O
Cristobalite- $\alpha$	0.2292	0.2241	3.1623e-13	69.08	71.07	H <sup>+</sup>
Am. SiO <sub>2</sub> *	0.0	0.0	7.944e-13	62.8	142.14	Ca <sup>2+</sup>
Calcite	0.0	0.02	equil.	equil.	equil.	Na <sup>+</sup>
Anhydrite	0.0	0.0	equil.	equil.	equil.	Cl <sup>-</sup>
Microcline	0.3009	0.2942	1.0e-12	57.78	142.4	SiO <sub>2</sub> (aq)
Albite-low	0.2498	0.2441	1.0e-12	67.83	104.2	HCO <sub>3</sub> <sup>-</sup>
Anorthite (Sr)	0.0083	0.0087	1.0e-12	67.83	124.6	SO <sub>4</sub> <sup>2-</sup>
Kaolinite	0.0	0.0	1.0e-13	62.80	142.4	K <sup>+</sup>
Illite	0.0	0.005	1.0e-14	58.62	142.4	Mg <sup>2+</sup>
Sepiolite	0.0	0.0	1.0e-14	58.62	142.4	AlO <sub>2</sub> <sup>-</sup>
Smectite-Na	0.0	0.0	1.0e-14	58.62	142.4	Sr <sup>+,+2</sup>
Smectite-K	0.0	0.0	1.0e-14	58.62	142.4	<sup>86</sup> Sr <sup>+2</sup>
Smectite-Ca	0.0	0.0	1.0e-14	58.62	142.4	
Smectite-Mg	0.0	0.0	1.0e-14	58.62	142.4	

\* Precipitation rate law from Rimstidt and Barnes (1980):  $\log k = -7.07 - 2598/T(K)$ . Reactive surface area set twice that of the other silica phases. All other kinetic minerals were given the same rate law for precipitation as dissolution (Equation 8.2), except quartz and cristobalite for which precipitation was suppressed.

The mineral assemblage and kinetic parameters for the DST-3 simulation are presented in Table 12.3. The initial amounts of illite and calcite in fractures were estimated.

**Table 12.3.** Starting mineral assemblage and possible secondary phases considered in TOUGHREACT simulations. Reaction rate law parameters (precipitation and dissolution) for drift scale simulation (DST-3). Calcite and anhydrite are considered equilibrium minerals. Primary aqueous species considered in reactions and for transport.

Minerals	Vf (matrix)	Vf (fractures)	$k_0$ (mol/m <sup>2</sup> s)	$E_a$ (kJ/mol)	S (m <sup>2</sup> /kgH <sub>2</sub> O)	Aqueous Species
Quartz	0.1018	0.0995	1.2589e-14	87.5	71.07	H <sub>2</sub> O
Cristobalite- $\alpha$	0.2292	0.2241	3.1623e-13	69.08	71.07	H <sup>+</sup>
Am. SiO <sub>2</sub> *	0.0	0.0	7.944e-13	62.8	142.14	Ca <sup>2+</sup>
Calcite	0.0	0.02	equil.	equil.	equil.	Na <sup>+</sup>
Anhydrite	0.0	0.0	equil.	equil.	equil.	Cl <sup>-</sup>
K-feldspar	0.3009	0.2942	1.0e-12	57.78	142.4	SiO <sub>2</sub> (aq)
Albite-low	0.2498	0.2441	1.0e-12	67.83	104.2	HCO <sub>3</sub> <sup>-</sup>
Anorthite	0.0083	0.0087	1.0e-12	67.83	124.6	SO <sub>4</sub> <sup>2-</sup>
Kaolinite	0.0	0.0	1.0e-13	62.80	142.4	K <sup>+</sup>
Illite	0.0	0.005	1.0e-14	58.62	142.4	Mg <sup>2+</sup>
Sepiolite	0.0	0.0	1.0e-14	58.62	142.4	AlO <sub>2</sub> <sup>-</sup>
Kerolite	0.0	0.0	1.0e-14	58.62	142.4	
Paragonite	0.0	0.0	1.0e-14	58.62	142.4	
Muscovite	0.0	0.0	1.0e-14	58.62	142.4	
Gibbsite	0.0	0.0	3.1623e-13	62.8	142.4	
Boehmite	0.0	0.0	3.1623e-13	62.8	142.4	
Diaspore	0.0	0.0	3.1623e-13	62.8	142.4	
Pyrophyllite	0.0	0.0	3.1623e-13	62.8	142.4	
Beidellite-Mg	0.0	0.0	1.0e-14	58.62	142.4	

\* Precipitation rate law from Rimstidt and Barnes (1980):  $\log k = -7.07 - 2598/T(K)$ . Reactive surface area set twice that of the other silica phases. All other kinetic minerals were given the same rate law for precipitation as dissolution (Equation 8.2), except quartz and cristobalite for which precipitation was suppressed.

The aqueous species diffusion coefficient was assumed to be  $1 \times 10^{-9}$  in matrix and fractures. The tortuosity was set to 0.2 in fractures and matrix. The diffusion coefficient for CO<sub>2</sub> in the gas phase was set to  $1 \times 10^{-7}$  (Moridis and Apps, 1997).

### 12.3 Mineral Abundances

The abundances of mineral endmembers albite and anorthite were recalculated based on the An content of the albite given by Johnson et al. (1997b). Mineral abundances in samples from instrumented boreholes in the DST access drift were determined by x-ray diffraction by Roberts and Viani, (1997a,b). Mineral proportions compared well with those reported by Bish

et al. (1996). On average in these samples, albite (23.3%), sanidine (33.3%), and cristobalite (23.5%) were dominant in the groundmass, with lesser amounts of quartz (11.9%).

#### 12.4 Estimation of Pore Water Composition in the Tptpmn Unit

In conducting computer simulations of the DST, it is desirable to start with an aqueous solution composition that is representative of the pore waters present in the Tptpmn Unit. Unfortunately, no pore water analyses from the Tptpmn Unit are currently available, because pore water recovery using a triaxial press is not feasible (Yang et al., 1988), and recovery by ultracentrifugation is still in progress. The problem is further complicated by the variability in pore water compositions, both areally, and as a function of depth in the vadose zone. In order to estimate as representative a pore water as possible, without introducing an unacceptable level of personal bias or prejudice, the concentrations of the principal analytical constituents were determined in the following manner:

- Pore water chemical constituent analyses determined by Yang et al. (1996a,b; Yang 1998, personal communication) for UZ-16, SD-9 and SD-12 were plotted as a function of depth and stratigraphic unit.
- For each chemical constituent, a box was drawn in which the two closest analyses above and two closest analyses below the Tptpl Unit were located at the corners.
- A horizontal line was drawn at the mid point between the upper and lower boundaries of the Tptpl Unit, and the mid point between the intersection of this line with the sub-vertical boundaries of the box taken as the representative composition.
- The process was repeated for all constituents except pH and for all three well datasets.
- The average of all three wells for each constituent was determined.
- An EQ3 input file was created from the resulting average chemical analysis, and EQ3 was run at 25°C, balancing charge on  $\text{HCO}_3^-$  with the pH specified at 8.2 (the interpolated measured values from UZ-16, SD-9 and SD-12 were 8.3, 7.3, and 8.2 respectively).

Charge balance was achieved by adjustment of  $\text{HCO}_3^-$  from 191.0 to 218.62 mg/L. Calcite was supersaturated, where  $\text{SI}(\text{calcite}) = +0.495$ , and  $\log P_{\text{CO}_2} = -2.886$ . The interpolated chemical analyses for the mid point of the Tptpl Unit from all three boreholes and the average values are given in Table 12.4. We assumed that the chemical composition of water in the Tptpmn is the same as in the Tptpl. The average analysis appears to be reasonable, but

subsequent analyses of Tptpmn Unit pore water may have a somewhat higher Ca and Mg concentration, and somewhat lower Na, because the substantial chemical changes due to zeolitic exchange in the upper part of the calico Hills Formation may have biased the analysis.

**Table 12.4.** Water Composition for TOUGHREACT Simulations

	Total concentrations in mg/L			
	UZ-16	SD-9	SD-12	Average (used for simulations)
Ca	33	19	30	27
Mg	10	4	2	5
Na	59	99	115	91
HCO <sub>3</sub> <sup>-</sup>	162	212	200	191 (219*)
Cl <sup>-</sup>	51	24	47	41
NO <sub>3</sub> <sup>-</sup>	23	10	7	13
SO <sub>4</sub> <sup>-</sup>	32	62	27	40
SiO <sub>2</sub>	60	60	60	60
Al	-	-	-	1 x 10 <sup>-6**</sup>
K	-	-	-	4**
pH	8.3	7.3	8.2	8.2

\* Adjusted for charge balance

\*\* Estimated

### 13. DRIFT-SCALE TEST SIMULATIONS

Results of TOUGHREACT simulations are presented in this section. Five simulations, DST-1, DST-1a, DST-2, and DST-3 are presented. DST-1 was run for a 2 month heating cycle. DST-1a was run for the entire 4 year heating cycle, without the cooldown phase. DST-2 was run for a 2-month heating period. DST-3 was run for 2 months of heating followed by nearly one month of cooldown. DST-4 was run for the full 8 year heating and cooling cycle of the Drift-Scale Test.

### 13.1 DST-1, DST-1a

These simulations present a fairly simple mineralogy consisting of calcite and the silica phases only. Transport of CO<sub>2</sub> in the gas phase gives important controls on the pH, which then affects the solubility of these minerals. This provides a good limiting scenario in which the aluminosilicates are nonreactive.

Figure 13.1 shows the simulated fracture temperature distribution around the heater area. The dryout region is confined to about half a meter at the wing heaters and less at the wall of the heater drift. The chloride concentration in fracture waters (Figure 13.2) clearly shows the small region where concentrations have increased by nearly 500 times, from the ambient concentration of about 40 mg/liter. In contrast, the increased fracture saturation owing to condensation of water vapor resulted in large area of dilute fracture waters, down to a minimum of about 3 mg/liter.

The partial pressure of CO<sub>2</sub> ( $P_{CO_2}$ ) in the gas phase shows more than two orders of magnitude variation, with the highest values in the moderate temperature region (~50°C) where there is some slight condensation (Figure 13.3). In the main condensation region (in the range of 90 to 98°C), the  $P_{CO_2}$  has decreased substantially due to increased CO<sub>2</sub> volatility with temperature. This CO<sub>2</sub> volatilization causes the pH to increase (Figure 13.5) away from the heaters. A large  $P_{CO_2}$  halo, compared to effects seen in chloride concentrations, illustrates the increased transport of CO<sub>2</sub> in the gas phase relative to species traveling in the liquid phase. Calcite precipitates in the dryout region (Figure 13.4) but is dissolving in the outer moderate temperature areas in condensate regions where pH is lower (Figure 13.5). In this outer region, the pH has decreased from the initial value of about 8.2 to nearly 7.0, while in the areas of higher boiling the pH has increased to a maximum of about 8.5. In other warming regions, calcite is precipitating due to pH increase and its decreasing solubility with temperature. In the dryout region (assuming a small residual saturation), pH has increased to nearly 9.0. Within the matrix there is only calcite precipitation (not shown), due to the heating effect and the lack of significant condensate imbibition. Also, calcite is not present initially in the matrix mineral assemblage and cannot therefore provide a buffer if pH should decrease.

Figure 13.6 shows the strong dissolution of cristobalite in the condensate area. Amorphous silica is observed to precipitate near the final dryout saturation (not shown). However, high pH in the region results in an increased solubility of silica, thus delaying amorphous silica precipitation. Another factor leading to high aqueous silica concentrations is the very rapid decline in liquid saturation due to boiling at a rate greater than the precipitation rate of amorphous silica can remove SiO<sub>2</sub>(aq) from solution.

The maximum decrease in fracture porosity over 2 months is about  $4 \times 10^{-4}$  (volume fraction) in the dryout region, almost entirely due to calcite precipitation. This is a negligible change

such that very little precipitate should be observed. The decrease in the volume fraction of cristobalite due to dissolution reaches a maximum of about  $4.5 \times 10^{-5}$ , which is also very minor. However, this considers that all precipitation and dissolution occurs on the fracture walls, whereas it likely permeates the adjacent matrix, as observed by Matyskiela (1997). At the low fracture porosities observed, the change in permeability could be more significant at the fracture walls, as it is related to the square of the fracture aperture, and the square of the pore throat diameter.

A simulation with input parameters identical to those used in Simulation DST-1 (Table 12.1) was run for the full 4-year heating cycle and is included here as Simulation DST-1a. This simulation was run using a slightly modified version of TOUGHREACT from the version used for Simulation DST-1. The modifications to the TOUGHREACT code were a change in the minimum saturation for the calculation of chemical reactions from  $1 \times 10^{-5}$  to  $1 \times 10^{-4}$  and a change in the gridblock interfacial weighting for diffusive transport to the harmonic mean of the product of the porosity and liquid saturation, instead of solely liquid saturation. The first change affects those concentrations in the final dryout region and has little effect elsewhere, as both of these liquid saturations are exceedingly small. The second modification changes slightly the diffusivity across gridblock interfaces for this problem, but has little effect on the results of these simulations.

The primary reason for including the DST-1a simulation in this report is to show the expanding region of increased  $P_{CO_2}$  in the condensate area up to about 40 meters away from the center of the heater drift after four years (Figure 13.7). As the  $P_{CO_2}$  has a strong effect on pH and thus calcite dissolution, this region should be an important area to look for alteration of calcite crystal surfaces on fracture walls.

Over a longer time period than shown here, cooldown would redissolve any calcite precipitated in areas where refluxing is significant, because there is no other source for calcium in this simulation. Amorphous silica would precipitate where  $SiO_2$ -rich fluids cooled below the saturation temperature. However, without allowing quartz or cristobalite precipitation there would initially be regions of elevated pore water silica concentrations. Over longer periods of time, slow nucleation and crystallization of amorphous silica would occur, decreasing silica concentrations.

## 13.2 DST-2

This simulation includes the feldspar endmembers (albite, anorthite, and microcline), illite, the smectite endmembers (Na, Mg, Ca, and K), sepiolite, kaolinite, calcite, anhydrite, and the silica polymorphs.





is significant feldspar dissolution (anorthite component) the isotopic ratio is shifted to about 0.716 to 0.718. This effect would be diluted by any calcite dissolution (with an isotopic ratio close to that of the initial pore water), however this does indicate the rates of feldspar dissolution (effective: rate constant times surface area) in the model are significant enough to shift the isotopic ratio of the pore waters. Whether these effective dissolution rates are reasonable can then be constrained not only by the pore water chemistry but also by the isotopic ratio and total Sr content of any collected condensate waters.

### 13.3 DST-3

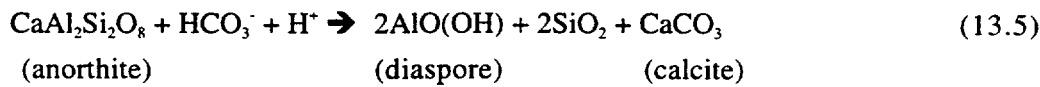
This simulation uses a mineral assemblage similar to the plug flow reactor experiment assemblage of Johnson et al. (1997a), with the additional Mg-phyllsilicates sepiolite and kerolite, plus calcite and anhydrite. For this simulation we consider a short heating period (2 months) at full power followed by short cool down period of about 25 days.

Results of this simulation are presented as a function of time for one grid node (number 1167) located within the condensation zone, approximately 55 cm below the wing heater and 10 m from the heater drift. Computed physical and chemical parameters are presented for both the fracture and matrix media (Figures 13.22 through 13.26).

The same pattern of pH increase due to CO<sub>2</sub> degassing is observed as in other simulations. This time, however, the pH remains below 10 at most locations in both fractures and matrix. This is attributed to the different selected mineral assemblage, which includes, among other minerals, diaspore and boehmite (two crystallographic forms of AlO(OH)), and muscovite (Table 12.3).

The trend of decreasing concentrations of chloride and sulfate in the fracture medium contrasts sharply with the unchanging concentration of these species in the matrix (Figure 13.26). This can be attributed to condensation in the fractures of water vapor from the fractures and matrix closer to the heater. At the location examined, the decreasing chloride and sulfate trends are noticeable from the start of the simulation up to day 60 when heating is turned off. At that time condensation stops, and evaporation and drainage of excess water occurs leading to a sharp water saturation decrease (Figure 13.24) and rise in chloride and sulfate concentrations in fractures (Figure 13.26).

For the first 30 to 40 days of heating, the same pattern of anorthite dissolution is observed as for simulation DST-2. However, this time, anorthite dissolution seems to lead mostly to precipitation of diaspore, and to a lesser extent kaolinite. An equivalent of reaction 13.3 involving diaspore instead of kaolinite can be written as:



At the examined location, the precipitation of diaspore appears to take over the formation of kaolinite after approximately 25 days in the fracture medium and 30 days in the matrix (Figure 13.25). Other minerals also form in both the fracture and matrix media, including boehmite and muscovite. Interestingly, albite initially dissolves in both media but after 25 days it starts precipitating in significant amounts only in the matrix.

Between approximately day 25 and 40, the total carbonate in solution becomes depleted (Figure 13.26), as previously observed in simulation DST-2, and the amount of precipitated calcite levels-off in both matrix and fractures. Accordingly, the calcium concentration in solution starts increasing due to continued anorthite dissolution. Between approximately day 40 and 60, a pH reversal is observed in both the matrix and fracture media (less pronounced in the latter). This may be the result of a slight reversal in the balance between carbonate depletion through calcite precipitation and CO<sub>2</sub> degassing, and CO<sub>2</sub> influx from other hot areas such as the heater drift.

After heating stops at day 60, the temperature immediately drops in both matrix and fractures (Figure 13.22). After approximately 25 days of cooling, the system temperature is still elevated (near 70°C). During the cooling period, the pH starts increasing again in both fractures and matrix (Figure 13.23), most likely as the result of further CO<sub>2</sub> degassing (the system is still hot) without a balancing CO<sub>2</sub> influx from hotter areas. As mentioned above, steam condensation (and generation) stops once the heat is turned off. The fractures drain as a result, which causes a sharp drop in their water saturation (Figure 13.24) as well as an increase in the concentration of chloride and other conservative species due to the lack of dilution from steam condensation and continued evaporation.

#### 13.4. DST-4

This simulation considers only the three silica phases (cristobalite, quartz, and amorphous silica) and the aqueous species SiO<sub>2</sub>, Na<sup>+</sup>, Cl<sup>-</sup>, H<sup>+</sup>, in addition to H<sub>2</sub>O. All parameters are identical to those given in Table 12.1 and used for Simulation DST-1. This simulation was run with the same TOUGHREACT version as that used for Simulation DST-1a. Because this system is simpler chemically than the other simulations, and does not consider CO<sub>2</sub>, it is significantly less computationally intensive. This simulation was run for the full 8-year planned duration of the DST, including the heating and cooling phases. Depending on the actual behavior of CO<sub>2</sub> during the DST and the rates of reaction of mineral phases other than the silica phases, the results of this simulation may not be as realistic as if CO<sub>2</sub> and the other mineral phases were considered.

The total volume percent of cristobalite dissolved in fractures after eight years is shown in Figure 13.27. The greatest amount of cristobalite dissolution is seen around the test area in a region that had the highest fluxes of condensate and was maintained at the boiling temperature while having high liquid saturation and low dissolved silica concentrations. Areas closer to the drift that were actively drying out show less cristobalite dissolution because dissolved silica concentrations increased to higher levels, thus slowing cristobalite dissolution and eventually resulting in precipitation of amorphous silica (Figure 13.28). Temperatures around the drift walls and at the wing heaters were still over 70°C after eight years. Therefore, dissolved silica concentrations are elevated with respect to ambient temperatures and additional amorphous silica precipitation would be likely from further cooling for several years until the area has completely cooled and equilibrium is attained with respect to this phase.

A grid node was selected from the 2-D model output for analysis over the full 8 year period. It is in the condensate region, but in an area which never reached a boiling or a dryout condition. Temperatures and liquid saturations are shown in Figures 13.29a-c for both fractures and matrix. On these figures, changes in slope are directly related to the drop in power output at one year and the final cooldown (zero power output) after four years. The first drop in power is not observed in the temperatures as this grid node was still in a region that was very cool, although the resulting loss of vapor flux is clearly evident in the fracture liquid saturation. In Figure 13.29b there is also a slope change to greater liquid saturations after about two years. This is a result of the expansion of the dryout zone closer to this point and the associated increased vapor flux. Matrix saturation rises steadily due to imbibition and thermal expansion of the water, and then declines steadily during the 4-year cooldown phase.

The aqueous species concentrations shown in Figures 13.30a and b directly reflect the liquid saturation and temperature histories. In both fractures and matrix, the unreactive aqueous components (in this simulation)  $\text{Na}^+$  and  $\text{Cl}^-$  decline as a result of dilution by steam condensation. The dissolved silica concentration also declines initially by dilution, but as temperatures increase the greater reaction rate of cristobalite outpaces the dilution effect and silica concentrations rise in the matrix and less so in the fractures. At cooldown (4 years)  $\text{Na}^+$  and  $\text{Cl}^-$  increase sharply in the fractures for about 1.5 years mainly due to diffusive exchange with higher concentration matrix pore waters. Dissolved silica concentrations continue to increase in the fractures and then stabilize as a result of reaching equilibration with respect to cristobalite (Figure 13.31a and b). At this gridblock there was no amorphous silica precipitation and no quartz dissolution.

## 14. CONCLUSIONS

The prediction of changes in water chemistry and mineral assemblages for the DST requires the incorporation of well-constrained parameter sets for the reaction kinetics and thermodynamics of mineral precipitation and dissolution, as well as for gas species transport and equilibria (especially  $\text{CO}_2$ ). In addition, it is important that the calculations reflect a conceptual model for water, water vapor, and heat flow that captures the important physical aspects of the system and can be similarly used to describe the initial and dynamic geochemical system and phenomena. The dual permeability model provides a suitable framework for the treatment of reaction-transport processes in fractured porous media; although a more refined discretization such as MINC could resolve concentration and mineralogical gradients more accurately.

The initial conditions are an important aspect to the prediction of the response of a system to a thermal perturbation. The initial pore water chemistry is not known for the DST area, and few analyses exist for the Topopah Spring Tuff. Thus, a detailed analysis of the existing pore water data was necessary to give the most informed estimate of the possible water chemistry. The analysis performed in this work has shown that, except for chloride and sulfate, the ambient pore water chemistry is controlled by secondary minerals in the unsaturated zone and availability of atmospheric  $\text{CO}_2$ .

This study reveals that the transport dynamics (advection and diffusion) of  $\text{CO}_2$  in the gas phase, the mineral assemblage, and the thermodynamic and kinetic parameters considered in the model are crucial in controlling the system pH, pore water chemistry, and overall rates of reaction. These data are currently quite uncertain. It is therefore essential that more data from the ongoing DST be incorporated in future modeling efforts for calibration purposes so that longer-term predictions can be achieved with some degree of reliability.

For the simulations presented in this study, a common trend is the strong dissolution of cristobalite and variable amounts of calcite precipitation in fractures. Amorphous silica and anhydrite precipitate in the dryout regions, but high pH causes an increase in silica solubility until nearly the last remaining residual saturation is evaporated. Feldspar dissolution is also quite strong. At this stage of the investigation it is not clear whether the rates of reaction used in this study are representative of field conditions at Yucca Mountain, especially when considering the possibility of mineral coatings reducing the effective surface area for reaction. To fully realize this in a model, a more precise characterization of feldspar and clay morphology, chemistry, and texture will be important. Modeling does indicate that the rates of plagioclase dissolution (albite + anorthite) should result in a significant shift in the strontium isotopic ratio if the anorthite component is dissolving as strongly predicted given the kinetic rates, solubility, and surface areas employed. This will be easily tested if

condensate waters are collected for strontium isotopic analysis, allowing a further constraint on the effective reaction rates.

In addition to constraining model input data with more field observations from the DST, improvement of the numerical model will increase the reliability of predictions. We are currently incorporating coupling of flow to permeability and porosity changes, consideration of mineral textures as a function of reaction, and enhancing the thermodynamic and kinetic models.

In summary, the coupled flow-transport-reaction modeling results presented in this study reflect complex physical, chemical and hydrological processes which rely on an equally complex set of input data, most of them with a high degree of uncertainty. Therefore, the results presented here should be considered preliminary until the acquisition of new data from the ongoing DST permits better model calibration and thus allows for more reliable long-term predictions.

## ACKNOWLEDGMENTS

This work was supported by the Director, Office of Civilian Radioactive Waste Management, U.S. Department of Energy, through Memorandum Purchase Order EA9013MC5X between TRW Environmental Safety Systems Inc., and the Ernest Orlando Lawrence Berkeley National Laboratory. The support is provided to Lawrence Berkeley National Laboratory through the U.S. Department of Energy Contract No. DE-AC03-76SF00098. Technical reviews by Bill Damm and Tianfu Xu are much appreciated in addition to thoughtful discussions with both. Jens Birkholzer provided input meshes, data, and assistance with the thermohydrological model. A quality assurance review was performed by Vivi Fissekidou. TOUGHREACT was developed by Tianfu Xu and Karsten Pruess for another study. Thin sections of rock samples from the DST alcove were provided by W. Glassley, LLNL, whose ongoing cooperation is appreciated. Tashi Barnett, Colleen Haraden and Maryann Villavert gave of their time to assist in production of this report.

---

## 15. REFERENCES

- Aagaard P. and Helgeson, H.C. 1982. "Thermodynamic and Kinetic Constraints on Reaction Rates Among Minerals and Aqueous Solutions, I. Theoretical Considerations." *American Journal of Science*, 282, 237-285.
- Aja, S.U. 1995. "Thermodynamic Properties of Some 2:1 Layer Clay Minerals from Solution-Equilibration Data." *Eur. J. Mineral.*, 7, 325-333.

- Allison J.D.; Brown, D.S.; and Novo-Gradac, K.J. 1991. *MINTEQA2/PRODEFA2, A Geochemical Assessment Model for Environment Systems*. Version 3.0 Users Manual. Washington D.C.: U.S. Environmental Protection Agency.
- Apps, J.A. 1997. *Hydrochemical Analysis*. In: G.S. Bodvarsson, T.M. Bandurraga, and Y.S. Wu, eds. *The Site-Scale Unsaturated Zone Model of Yucca Mountain, Nevada, for the Viability Assessment*, Chapter 14. Yucca Mountain Project Level 4 Milestone SP24UFM4, LBNL-40376, UC-814. Berkeley, California: Lawrence Berkeley National Laboratory. DTN: LB970601233129.001(Q)
- Apps, J.A. and Chang, G.M. 1992. Correlation of the Na/K Ratio in Geothermal Well Waters with the Thermodynamic Properties of Low Albite and Potash Feldspar. In: Y.K. Kharaka and A.S. Maest, eds. *Proceedings of the 7<sup>th</sup> International Symposium on Water-Rock Interaction*, Balkema, A.A., Rotterdam; Holland, 1437-1400.
- Apps, J.A. 1970. *The Stability Field of Analcime*: Unpublished Ph.D. Thesis, Harvard University, 347p.
- Ball, J.W. and Nordstrom, D.K. 1991. *Users Manual for WATEQ4F with Revised Thermodynamic Data Base and Test Cases for Calculating Speciation of Major, Trace, and Redox Elements in Natural Waters*. Menlo Park, California: U.S. Geological Survey. Open-File Report 91-183.
- Bandurraga, T.M. and Bodvarsson, G.S. 1997. Calibrating Matrix and Fracture Properties Using Inverse Modeling. In: G.S. Bodvarsson, T.M. Bandurraga, and Y.S. Wu, eds. *The Site-Scale Unsaturated-Zone Model of Yucca Mountain, Nevada, for the Viability Assessment*, Chapter 6. Yucca Mountain Project Level 4 Milestone SP24UFM4, Report LBNL-40376, UC-814. Berkeley, California: Lawrence Berkeley National Laboratory. DTN: LB970601233129.001 (Q).
- Berman, R.G. 1988. "Internally Consistent Thermodynamic data for Minerals in the System  $\text{Na}_2\text{O}-\text{K}_2\text{O}-\text{CaO}-\text{MgO}-\text{FeO}-\text{Fe}_3\text{O}-\text{Al}_2\text{O}_3-\text{SiO}_2-\text{TiO}_2-\text{H}_2\text{O}-\text{CO}_2$ ." *J.Petrol.*, 29, 445-522.
- Birkholzer, J.T. and Tsang, Y.W. 1996. *Forecast of Thermal-Hydrological Conditions and Air Injection Test Results of the Single Heater Test at Yucca Mountain*. Yucca Mountain Project Level 4 Milestone SP918M4, Report LBNL-39789, UC-814. Berkeley, California: Lawrence Berkeley National Laboratory. MOY-970521-04.
- Birkholzer, J.T. and Tsang, Y.W. 1997. *Pretest Analysis of the Thermal-Hydrological Conditions of the ESF Drift Scale Test*. Yucca Mountain Project Level 4 Milestone SP9322M4. Berkeley, California: Lawrence Berkeley National Laboratory,
- Bish, D.L.; Carey, J.W.; Levy, S.S.; and Chipera, S.J. 1996. *Mineralogy-Petrology Contribution to the Near-Field Environment Report*. Yucca Mountain Project Milestone, LA-3668. Los Alamos, New Mexico: Los Alamos National Laboratory. UCRL-LR-

124998. Livermore, California: Lawrence Livermore National Laboratory. DTN: LASL831322AQ96.006 (Q), LASL831322AN96.001 (Non-Q).
- Bish, D.L. 1995. "Thermal Behavior of Natural Zeolites." *Natural Zeolites '93: Occurrence, Properties, and Use*. Brockport, New York, Int'l. Comm. Natural Zeolites.
- Bish, D.L. and Vaniman, D.T. 1995. *Mineralogic Summary of Yucca Mountain, Nevada*. Report LA-10543-MS. Los Alamos, New Mexico: Los Alamos National Laboratory. DTN: LA0000000000110.002 (Non-Q)
- Bish, D.L. and Chipera, S.J. 1994. *Long-Term Steam Heating of Tuffaceous Rocks*. Yucca Mountain Project Milestone Report Letter 4010. Los Alamos, New Mexico: Los Alamos National Laboratory.
- Bish, D.L., 1989. *Evaluation of Past and Future Alterations in Tuff at Yucca Mountain, Nevada, Based on the Clay Mineralogy of Drill Cores USW G-1, G-2, and G-3*. Report LA-10667-MS. Los Alamos, New Mexico: Los Alamos National Laboratory. DTN: LA000000000040.001 (Non-Q).
- Broxton, D.E.; Byers, Jr., F.M.; and Warren, R.G. 1989. *Petrography and Phenocryst Chemistry of Volcanic Units at Yucca Mountain, Nevada: A Comparison of Outcrop and Drill Hole Samples*. Report LA-11503-MS. Los Alamos, New Mexico: Los Alamos National Laboratory. DTN: LA0000000000113.002 (Non-Q)
- Broxton, D.E.; Vaniman, D.; Caporuscio, F.; Arney, B.; and Heiken, G. 1982. *Detailed Petrographic Descriptions and Microprobe Data for Drill Holes USW-G2 and UE25b-1H*. Report LA-9324-MS. Los Alamos, New Mexico: Los Alamos National Laboratory. DTN: LA0000000000112.002 (Non-Q)
- Bruton, C.J.; Glassley, W.E.; and Bourcier, W.L. 1994. *Field-Based Tests of Geochemical Modeling Codes New Zealand Hydrothermal Systems*. Report UCRL-ID-118009. Livermore, California: Lawrence Livermore National Laboratory. DTN: LL940800204241.00 (Non-Q)
- Bruton, C.J.; Glassley, W.E.; and Bourcier, W.L. 1993. *Testing Geochemical Modeling Codes Using New Zealand Hydrothermal Systems*. Report UCRL-ID-119842. Livermore, California: Lawrence Livermore National Laboratory. DTN: LL940800204241.00 (Non-Q)
- Buscheck, T.A.; Gansemer, J.; Delorenzo, T.; Nitao, J.J.; Shaffer, R.J.; Cordery, M.J.; and Lee, K.H. 1997a. *Thermal-Hydrological Models of the Distribution of Temperature, Relative Humidity, and Gas-Phase Air-Mass Fraction in Repository Drifts*. Milestone report for the CRWMS and M&O, U.S. Department of Energy, SPLD1M4 and SPLD2M4. Livermore, California: Lawrence Livermore National Laboratory.

- Buscheck, T.A.; Nitao, J.J.; Birkholzer, J.; and Tsang, Y.W. 1997b. *Recommended Guidelines for Hydrological Parameters used by TSPA-VA*. Livermore, California: Lawrence Livermore National Laboratory. September 8, 1997 memo to G.S. Bodvarsson, Lawrence Berkeley National Laboratory.
- Buscheck, T.A.; Shaffer, R.J.; Lee, K.H.; and Nitao, J.J. 1997c. *Analysis of Thermal-Hydrological Behavior During the Heating Phase of the Single-Heater Test at Yucca Mountain*. Supplemental submission of Milestone Report for the CRWMS and M&O, U.S. Department of Energy, SP9266M4. Livermore, California: Lawrence Livermore National Laboratory.
- Buscheck, T.A.; Shaffer, R.J.; and Nitao, J.J. 1997d. *Pretest Thermal-Hydrological Analysis of the Drift-Scale Thermal Test at Yucca Mountain*. Report UCRL-ID-XXXX. Livermore, California: Lawrence Livermore National Laboratory.
- Carey, J.W.; Chipera, S.J.; Vaniman, D.T.; Bish, D.L.; Viswanathan, H.S.; and Carter-Krogh, K. 1997. *Three-Dimensional Mineralogic Model of Yucca Mountain, Nevada, Rev. 1*. Report SP344BM4. Los Alamos, New Mexico: Los Alamos National Laboratory. DTN: LAJC831321DN97.009 (Non-Q). DTN: LAJC831321DQ97.008 (Q).
- Carey, J.W. and Bish, D.L. 1996. "Equilibrium in the Clinoptilolite-H<sub>2</sub>O System." *American Mineralogist*, 81, 852-952.
- Carlos, B.A.; Chipera, S.J.; and Bish D.L. 1995a. *Distribution and Chemistry of Fracture-Lining Zeolites at Yucca Mountain, Nevada*. Report LA-12977-MS. Los Alamos, New Mexico: Los Alamos National Laboratory.
- Carlos, B.A.; Chipera, S.J.; and Bish, D.L. 1995b. *Evaluation of Past and Future Alterations in Tuff at Yucca Mountain, Nevada, Based on the Clay Mineralogy of Drill Cores DSW G-1, G-2, and G-3*. Report LA-10667-MS. Los Alamos, New Mexico: Los Alamos National Laboratory.
- Carlos, B.A.; Chipera, S.J.; and Bish, D.L. and Raymond, R. 1993. "Distribution and Chemistry of Fracture-Lining Zeolites at Yucca Mountain, Natural Zeolites." *Natural Zeolites '93: Occurrence, Properties, and Use*. Brockport, New York, Int'l. Comm. Natural Zeolites.
- Carlos, B.A.; Bish, D.L.; and Chipera, S.J. 1991. "Fracture-Lining Minerals in the Lower Topopah Spring Tuff at Yucca Mountain." *Proceedings of the Second International High-Level Radioactive Waste Conference, April, 1991*. Las Vegas, Nevada: American Nuclear Society, 1, 486-493. NNA.19910206.0039, LA000000000069.001 (Non-Q).
- Carroll, S.A.; Alai, M.; and Copenhaver, S. 1996. *Amorphous Silica Precipitation Kinetics at 100°C and pH 3, 5, and 6*. Milestone for the CRWMS Management and Operating Contractor, U.S. Department of Energy. Report MOL123, OI3ALIW. Livermore,

- California: Lawrence Livermore National Laboratory. DTN: LL950613012011.001 (Non-Q).
- Carroll, S.A.; Mroczek, E.; Bourcier, W.; Alai, M.; and Ebert M. 1995. *Comparison of Field and Laboratory Precipitation Rates of Amorphous Silica from Geothermal Waters at 100°C*. Milestone report for the CRWMS Management and Operating Contractor, U.S. Department of Energy, MOL207. Livermore, California: Lawrence Livermore National Laboratory. DTN: LL950813304241.009 (Non-Q).
- Conrad, M. 1998. *Carbon Isotope Analyses of CO<sub>2</sub> Evolved During the Initial Stages of the Drift Scale Test*. Level 4 Milestone Report SP2770M4. Berkeley, California: Lawrence Berkeley National Laboratory.
- Cooper, G.S. and Smith, R.L. 1963. "Sequence of Products Formed during Denitrification of Soil in Some Diverse Western Soils." *Soil Science Society of America Proceedings*, 27, 659-662.
- CRWMS M&O. 1997. *Drift Scale Test Design and Forecast Results*. BAB000000-01717-4600-00007. Rev. 00. MOL.19980119.0021
- Daily, W.; Lin, W.; and Buscheck, T. 1985. "Hydrological Properties of Topopah Spring Tuff – Laboratory Measurements." Report UCRL-94363. Livermore, California: Lawrence Livermore National Laboratory. *Journal of Geophysical Research*, 92(B8), 7854-7864.
- Delany, J.M.; Puigdomenech, I.; and Wolery, T.J. 1986. *Precipitation Kinetics Option for the EQ6 Geochemical Reaction Path Code*. Report UCRL-53642. Livermore, California: Lawrence Livermore National Laboratory.
- DeLoach, L.; Johnson, J; Glassley, W.; and Knauss, K. 1997. *Progress Report for Plug Flow Reactor Experiments (PFR8)*. Milestone Report for the CRWMS M&O, U.S. Department of Energy SPL1CM4. Livermore, California: Lawrence Livermore National Laboratory.
- Denniston, R.F.; Shearer, C.K.; Layne, G.D.; and Vaniman, D.T. 1997. "SIMS Analysis of Minor and Trace Element Distributions in Fracture Calcite from Yucca Mountain, Nevada, U.S.A." *Geochimica et Cosmochimica Acta*, 61(9), 1803-1818.
- Eberl, D.D.; Jones, B.F.; and Khoury, H.N. 1982. "Mixed-Layer Kerolite/Stevensite from the Amargosa Desert, Nevada." *Clays and Clay Minerals*, 30(5), 321-326.
- Ehrlich R.; Etris, E.L.; Brumfield, D.; Yuan, L.P.; and Crabtree, S.J. 1991. "Petrography and Reservoir Physics III: Physical Models for Permeability and Formation Factor." *AAPG Bull*, 75, 1579-1592.
- Faure, G. 1977. *Principles of Isotopic Geology*. New York, NY: Wiley and Sons, p. 464.

- Fournier, R.O. and Rowe, J.J. 1962. "The Solubility of Cristobalite along the Three-Phase Curve, Gas Plus Liquid Plus Cristobalite." *Am. Mineralogist*, 47, 897-902.
- Gardner, R.L. 1972. "Origin of the Mormon Mesa Caliche, Clarke County, Nevada." *Geological Society of America Bulletin*, 83, 143-157.
- Garrels, R.M. 1984. "Montmorillonite / Illite Stability Diagrams." *The Clay Minerals Society*, 32(3), 161-166.
- Garrels, R.M. and Christ, C.L. 1965. *Solutions, Minerals and Equilibria*. New York: Harper and Rowe.
- Glassley, W.E. 1997a. *Chemical Composition of Water Before Contact with Repository Materials*. Milestone Report for the CRWMS M&O, U.S. Department of Energy, SPLA1M4. Livermore, California: Lawrence Livermore National Laboratory.
- Glassley, W.E. 1997b. *Models for Thermohydrochemical Alteration of Flow Pathways Above and Below the Repository*. Milestone Report for the CRWMS M&O, U.S. Department of Energy, SPL2BM4. Livermore, California: Lawrence Livermore National Laboratory.
- Glassley, W.E. 1997c. "Near-Field Environment Models." *Presentation to the Near-Field/Altered Zone Expert Elicitation Project, December 4, 1997*, Las Vegas, Nevada.
- Glassley, W.E. 1997d. *Thermochemical Analyses of the Drift-Scale Test: Mineralogical and Chemical Characteristics*. Milestone Report for the CRWMS M&O, U.S. Department of Energy, SP9320M4. Livermore, California: Lawrence Livermore National Laboratory.
- Glassley, W.E. 1997e. *Thermochemical Analysis of the Single Heater Test*, Milestone Report for the CRWMS and M&O, SP912M4. Livermore, California: Lawrence Livermore National Laboratory.
- Glassley, W.E. and DeLoach, L. 1997. *Second Quarter Results of Chemical Measurements in the Single Heater Test*. Milestone Report for the CRWMS M&O, U.S. Department of Energy, SP9240M4. Livermore, California: Lawrence Livermore National Laboratory. DTN: LL970409604244.030 (Q).
- Glassley, W.E. 1996. "Equilibrium Bounds on Water Chemistry and Mineralogical Changes Produced by Near-Field Relative Humidity Changes." *Near-Field Environment Report, Rev. 1*. Report UCRL-12498. Livermore, California: Lawrence Livermore National Laboratory.
- Glassley, W.E. and Boyd, S. 1995. *Data Report on Small Block Tests*. Yucca Mountain Project Milestone, MOL62. Livermore, California: Lawrence Livermore National Laboratory.

- Glassley, W.E. and Boyd, S. 1994a, *Preliminary Estimate of Rates and Magnitudes of Changes of Coupled Hydrological-Geochemical Properties*. Yucca Mountain Project Milestone, MOL79, Livermore, California: Lawrence Livermore National Laboratory.
- Glassley, W.E. and Boyd, S. 1994b. *Report on Near-Field Geochemistry: Water Composition Changes Due to Evaporation*, Yucca Mountain Project Milestone, MOL26, Livermore, California: Lawrence Livermore National Laboratory.
- Gottschalk, M. 1997. "Internally Consistent Thermodynamic Data for Minerals in the System  $\text{SiO}_2\text{-TiO}_2\text{-Al}_2\text{O}_3\text{-Fe}_2\text{O}_3\text{-CaO-MgO-FeO-K}_2\text{O-Na}_2\text{O-H}_2\text{O-CO}_2$ ." *European Journal of Mineralogy*, 9, 175-223.
- Grindley, G.W. and Browne, P.R.L. 1975. "Structural and Hydrological Factors Controlling the Permeabilities of Some Hot-Water Geothermal Fields." *Proceedings of the Second United Nations Symposium on the Development and Use of Geothermal Resources, May 20-22*. San Francisco, California, 377-387.
- Hardin, E.L. 1998. *Near-Field/Altered Zone Models*. Milestone Report for the CRWMS M&O, U.S. Department of Energy, SP3100M4. Livermore, California: Lawrence Livermore National Laboratory. DTN: LL980209004242.026 (Q).
- Hardin, E.L. and Chesnut, D.A. 1997. *Synthesis Report on Thermally-Driven Coupled Processes*. Level 4 Milestone Report SPL8BM4. Livermore, California: Lawrence Livermore National Laboratory.
- Harrar, J.E.; Carley, J.F.; Isherwood, W.F.; and Raber, E. 1990. *Report of the Committee to Review the Use of J-13 Well Water in Nevada Nuclear Waste Storage Investigations*. UCID-21867. Livermore, California: Lawrence Livermore National Laboratory. NNA.1910131.0274.
- Hay, R.L. and Wiggins, B. 1980. "Pellets, Ooids, Sepiolite and Silica in Three Calcretes of the Southwestern United States." *Sedimentology*, 27, 559-575.
- Helgeson, H.C.; Kirkham, D.H.; and Flowers, G.C. 1981. "Theoretical Prediction of the Thermodynamic Behavior of Aqueous Electrolytes at High pressures and Temperatures. IV. Calculation of Activity Coefficients, Osmotic Coefficients, and Apparent Molal and Standard and Relative Partial Molal Properties to the 600°C and 5 kb." *American Journal of Science*, 281, 1249-1516.
- Helgeson, H.C.; Delany, J.M.; Nesbitt, H.W.; and Bird, D.K.; 1978, "Summary and Critique of the Thermodynamic Priorities of rock forming Minerals." *American Journal of Science*, 278-A, 229.
- Helgeson, H.C. and Kirkham, D.H. 1976. "Theoretical Prediction of the Thermodynamic Behavior of Aqueous Electrolytes at High Pressures and Temperatures. III. Equation of

- State for Aqueous Species at Infinite Dilution." *American Journal of Science*, 281, 1249-1516.
- Helgeson, H.C. and Kirkham, D.H. 1974a. "Theoretical Precision of the Thermodynamic Behavior of Aqueous Electrolytes at High Pressures and Temperatures, I. Summary of the Thermodynamic/Electrostatic Properties of the Solvent." *American Journal of Science*, 274, 1089-1198.
- Helgeson, H.C. and Kirkham, D.H. 1974b. "Theoretical Prediction of the Thermodynamic Behavior of Aqueous Electrolytes at High Pressures and Temperatures. II. Debye-Hückel Parameters for Activity Coefficients and Relative Partial Molal Properties." *American Journal of Science*, 274, 1199-1261.
- Hem, J.D. 1989. "Study and interpretation of the chemical characteristics of natural water," Third Edition. U.S. Geological Survey Water-Supply Paper 2254.
- Holland, T. J. B. and Powell, R., 1990. "An Enlarged and Updated Internally Consistent Thermodynamic Dataset with Uncertainties and Correlations: the system  $K_2O-Na_2O-CaO-MgO-MnO-FeO-Fe_2O_3-Al_2O_3-TiO_2-SiO_2-C-H_2-O_2$ ." *J. Metamorphic Geology*, 8, 89-124.
- Holland, T.J.B. and Powell, R. 1990. "Equilibrium Constants Calculated using a Modified Version of SUPCRT92." *J. Metamorphic Geology*, 8, 89-124.
- Holland, T.J.B. and Powell, R. 1985. "An Internally Consistent Thermodynamic Dataset with Uncertainties and Correlations: 2. Data and Results." *J. Metamorphic Geology*, 3, 343-370.
- Johnson, J.W.; Knauss, K.G.; Glassley, W.E.; and DeLoach, L.D. 1997a. "Reactive Transport Modeling of Plug-Flow Reactor Experiments: Significance, Initial Results, and Future Applications." *Submitted to Journal of Hydrology*.
- Johnson, J.W.; Knauss, K.G.; and Glassley, W.E. 1997b. *Reactive Transport Through Topopah Spring Tuff: Summary of Initial Plug-Flow Reactor Experiments and Associated Computer Simulations*. Yucca Mountain Milestone Report, SPL1BM4. Livermore, California: Lawrence Livermore National Laboratory.
- Johnson, T.M. and DePaolo, D.J. 1994. "Interpretation of Isotopic Data in Groundwater Systems: Model Development and Application to Sr Isotopic Data from Yucca Mountain." *Water Resour. Res.*, 30, 1571-1587.
- Johnson, J.W; Oelkers, E.H.; and Helgeson, H.C. 1992. "Equilibrium Constants Calculated with, and Data from, SUPCRT92." *Computers and Geosciences*, 18, 899-947.
- Kennedy, G.C. 1950. "A Portion of the System Silica-Water." *Econ. Geol.*, 45(7), 629-653.

- Kharaka, Y.K.; Gunter, W.D.; Aggarwal, W.E.; Perkins, H.; and DeBraal, J.D., 1988. "SOLMINEQ.88: A Computer Program for Geochemical Modeling of Water-Rock Interactions." *U.S. Geological Survey Investigations Report*, 88-4277.
- Khoury, H.N.; Eberl, D.D. and Jones, B.F. 1982. "Origin of Magnesium Clays from the Amargosa Desert, Nevada." *Clays and Minerals*, 30(5), 327-336.
- Kitahara, S. 1960a. "Solubility of Quartz in Water at High Temperatures and Pressures." *Rev. Phys. Chem. Japan*, 30, 109-114.
- Kitahara, S. 1960b. "The Polymerization of Silica Acid Obtained by the Hydrothermal Treatment of Quartz and the Solubility of Amorphous Silica." *Rev. Phys. Chem. Japan*, 30, 131-137.
- Knauss, K.G. and Copenhaver, S.A. 1995. *Progress Report on Hydrothermal Alteration of Vitric Tuff from Yucca Mountain*. Livermore, California: Lawrence Livermore National Laboratory. DTN: LL950613812011.000.
- Knauss, K. and Wolery, T. 1988. *The Dissolution Kinetics of Quartz as a Function of pH and Time at 70°C*. Report UCRL-96071. Livermore, California: Lawrence Livermore National Laboratory 1987. *Geochimica et Cosmochimica Acta*, 52(1), 43-53. DTN: LL941100404241.006.
- Knauss, K.G.; Beiriger, W.J.; and Peifer, D.W. 1987. *Hydrothermal Interaction of Solid Wafers of Topopah Spring Tuff with J-13 Water and Distilled Water at 90°C and 150°C Using Dickson-Type, Gold-Bag Rocking Autoclaves: Long-Term Experiments*. Report UCRL-53722. Livermore, California: Lawrence Livermore National Laboratory. DTN: LL940800904241.002 (Non-Q).
- Knauss, K. 1986. *Zeolitization of Glassy Topopah Spring Tuff Under Hydrothermal Conditions*. Report UCRL-94664, Livermore, California: Lawrence Livermore National Laboratory. *In proceedings from Materials Resources Symposium*, 84, 737-745.
- Knauss, K.G. and Peifer D.W. 1986. *Reaction of Vitric Topopah Spring Tuff and J-13 Ground Water under Hydrothermal Conditions, Using Dickson-Type, Bold-Bag Rocking Autoclaves*. Report UCRL-53795. Livermore, California: Lawrence Livermore National Laboratory. DTN: LLLLYMP9305206.00 (Non-Q).
- Knauss, K.G.; Delany, J.M.; Beiriger, W.J.; and Peifer D.W. 1986. "Hydrothermal Interaction of Topopah Spring Tuff with J-13 Water as a Function of Temperature." *In proceedings from Mat. Res. Soc. Symp.*, 44, 539-546.
- Knauss, K.G.; Beiriger, W.J.; and Peifer, D.W. 1985a. *Hydrothermal Interaction of Crushed Topopah Spring Tuff and J-13 Water at 90°C, 150°C and 250°C Using Dickson-Type, Gold-Bag Rocking Autoclaves*. Report UCRL-52560. Livermore, California: Lawrence Livermore National Laboratory.

Knauss, K.G.; Beiriger, W.J.; and Peifer, D.W. 1985b *Hydrothermal Interaction of Solid Wafers of Topopah Spring Tuff with J-13 Water and Distilled Water at 90°C, 150°C and 250°C Using Dickson-Type Gold Bag Rocking Autoclaves*. Report UCRL-53630. Livermore, California: Lawrence Livermore National Laboratory. DTN: LL940800404241.001 (Non-Q).

Knauss, K.G.; Beiriger, W.J.; Peifer, D.W.; and Piwinski, A.J. 1985c. *Hydrothermal Interaction of Solid Wafers of Topopah Spring Tuff with J-13 Water and Distilled Water at 90°C, 150°C, and 250°C, Using Dickson-Type, Gold-Bag Rocking Autoclaves*. Report UCRL-53645. Livermore, California: Lawrence Livermore National Laboratory. DTN: LLLLYMP9305205.000 (Non-Q).

Knauss, K.G. and Beiriger W.B. 1984. *Report on Static Hydrothermal Alteration Studies of Topopah Spring Tuff wafers in J-13 water at 1500C*. Report UCRL-53576. Livermore, California: Lawrence Livermore National Laboratory.

Knauss, K.G.; Delany, J.M.; Beiriger, W.J.; and Peifer D.W. 1984. *Hydrothermal Interaction of Topopah Spring Tuff with J-13 water as a Function of Temperature*. Report UCRL-90853. Livermore California: Lawrence Livermore National Laboratory. Boston, Massachusetts. *In Proceedings of the Materials Research Society Meeting, 44*, 539-546.

Kulik, D.A. and Aja, S.U. 1997. The Hydrothermal Stability of Illite: Implications of Empirical Correlations and Gibbs Energy Minimization. *In*: D.A. Palmer and D.J. Wesolowski, eds. *Proceedings of the Fifth International Symposium on Hydrothermal Reactions*. Tennessee, U.S., 288-292.

LaCamera, R.J. and Westenburg, C.L. 1992. *Selected ground-water data for Yucca Mountain region, Southern Nevada and Eastern California, through December 1992*. U.S. Geological Survey Report USGS OFR 94-54.

Lebron, I. and Suarez, D.L. 1996. "Calcite Nucleation and Precipitation Kinetics as Affected by Dissolved Organic Matter at 25°C and pH > 7.5." *Geochimica et Cosmochimica Acta*, 60(15), 2765-2776.

Levy, D.B.; Amrhein, C.; Anderson, M.A.; and Daoud, A.M. 1995. "Coprecipitation of Sodium, Magnesium, and Silicon with Calcium Carbonate." *Soils Science Society of American Journal*, 59(5), 1258-1267.

Lin, W. 1997. *Status Report of the Single Heater Test: Chapter 4. Integrated Analyses*. Milestone Report for the CRWMS and M&O, U.S. Department of Energy, SP9266M4. Livermore, California: Lawrence Livermore National Laboratory.

Lin, W.; Roberts, J.; Glassley W.; and Ruddle, D. 1997. "Fracture-Matrix Permeability at Elevated Temperatures." *Presentation to the Near-Field/Altered Zone Expert Elicitation Project, November 8, 1997*, San Francisco, California.

- Lin, W. and Roberts, J.J. 1996. *Chapter 2: Laboratory-Determined Hydrological Properties and Processes, Near-Field Environment Report, Rev. 1*. Report UCRL-124998. Livermore, California: Lawrence Livermore National Laboratory.
- Lin, W.; Roberts, J.J.; Glassley, W.; and Ruddle, D. 1995. *The Effect of Rock-Water Interaction on Permeability*. Report UCRL-JC-119574, Livermore California: Lawrence Livermore National Laboratory. *International Congress on Rock mechanics, Tokyo, Japan*. (volume and page numbers not available at this time). DTN: LL950916504242.018.
- Lin, W. and Daily, W.D. 1991. *Variation of Permeability with Temperature in Fractured Topopah Spring Tuff Samples*. Report UCRL-JC-104765. Livermore, California: Lawrence Livermore National Laboratory, *In Proceedings from Second Annual International High Level Radioactive Waste Management*. Las Vegas, Nevada: American Nuclear Society, La Grange Park, Illinois, 988-993.
- Lin, W.; Ramirez, A.; and Watwood, D. 1991. *Temperature Measurements from a Horizontal Heater Test in G-tunnel*. Report UCRL-JC-106693. Livermore, California: Lawrence Livermore National Laboratory.
- Lin, W. 1990. *Variation of Permeability with Temperature in Fractures Topopah Spring Tuff Samples*. Report UCRL-JC-104765. Livermore, California: Lawrence Livermore National Laboratory.
- Lin, W. and Daily, W.D. 1989. *Laboratory Study of Fracture Healing in Topopah Spring Tuff – Implications for Near Field Hydrology*. Report UCRL-100624, Livermore, California: Lawrence Livermore National Laboratory. American Nuclear Society, La Grange Park, Illinois: *Proceedings from Topical Meeting on Nuclear Waste Isolation in the Unsaturated Zone, Focus '89, September 17-21*, Las Vegas, Nevada.
- Lin, W. and Daily, W.D. 1988. *Hydrological Properties of Topopah Spring Tuff Under a Thermal Gradient: Laboratory Results*. Report UCRL-96926. Livermore, California: Lawrence Livermore National Laboratory. *Intl. J. Rock Mech.*, 27(5), 373-385. DTN: LL940800504242.000. DTN: LL940800704242.002.
- Lin, W. and Daily, W. 1984. *Transport Properties of Topopah Spring Tuff*. Report UCRL-53602. Livermore, California: Lawrence Livermore National Laboratory.
- Machette, M.N. 1985. "Calico Soils of the Southwestern United States." *Geological Society of America Special Paper*, 203, 1-21.
- MacKenzie, F.T. and Gees, R. 1971. "Quartz Synthesis at Earth-Surface Conditions." *Science*, 173, 533-535.
- Matyskiela, W. 1997. "Silica Redistribution and Hydrologic Changes in Heated Fractured Tuff." *Geology Report*, 25(12), 1115-1118.

- McFadden, L.D. and Tinsley, J.C. 1985. "Rate and Depth of Pedogenic-Carbonate Accumulation in Soils: Formulation and Testing of a Compartment Model." *Geological Society of America Special Paper*, 203, 23-41.
- Mehran, M.; and Tanji, K.K. 1974. "Computer Modeling of Nitrogen Transformations in Soils." *J. Environ. Qual.*, 3(4), 391-396.
- Miyamoto, S. and Pingitore, N.E. 1992. "Predicting Calcium and Magnesium Precipitation in Saline Solutions Following Evaporation." *Soil Sci. Soc. Am. J.*, 56, 1767-1775.
- Moore, D.E.; Morrow, C.A.; and Byerlee, J.D. 1986. "High-Temperature Permeability and Groundwater Chemistry of Some Nevada Test Site Tuffs." *Journal of Geophysical Research*, 91(B2), 2163-2171.
- Moore, D.E.; Morrow, C.A.; and Byerlee, J.D. 1985. *Permeability and Fluid Chemistry Studies of the Topopah Spring Member of the Paintbrush Tuff, Nevada Test Site: Part II*. Report UCRL-15667. Livermore, California: Lawrence Livermore National Laboratory.
- Morey, G.W.; Fournier, R.O. and Rowe, J.J. 1964. "The Solubility of Amorphous Silica at 25°C." *Journal of Geophysical Research*, 69, 1995-2002.
- Morey, G.W.; Fournier, R.O. and Rowe, J.J. 1962. "The Solubility of Quartz in Water in the Temperature Interval from 25° to 300°C." *Geochimica et Cosmochimica Acta*, 26, 1029-1043.
- Moridis, G.J.; Apps, J.A.; and Bodvarsson, G.S. 1997. "<sup>14</sup>C Data Analysis Using the UZ Model. In: G.S. Bodvarsson, T.M. Bandurraga, and Y.S. Wu, eds. *The Site-Scale Unsaturated Zone Model of Yucca Mountain, Nevada, for the Viability Assessment*, Chapter 18. Yucca Mountain Project Level 4 Milestone SP24UFM4, LBNL-40376, UC-814. Berkeley, California: Lawrence Berkeley National Laboratory.
- Morrow, C.A.; Moore, D.E.; and Byerlee, J.D. 1984. "Permeability and Pore-Fluid Chemistry of the Topopah Spring Member of the Paintbrush Tuff, Nevada Test Site, in a Temperature Gradient: Application to Nuclear Waste Storage." *Proceedings of the Materials Research Society Symposium*, 26, 883-890. Boston, Massachusetts.
- Mucci, A.; and Morse, J.W. 1983. "The Incorporation of Mg<sup>2+</sup> and Sr<sup>2+</sup> into Calcite Overgrowths: Influences of Growth Rate and Solution Composition." *Geochimica et Cosmochimica Acta*, 47, 217-233.
- Neymark, L.A.; Marshall, B.D.; Kwak, L.M.; Futa, K.; and Mahan, S.A. 1995. *Geochemical and Pb, Sr, and O Isotopic Study of the TIVA Canyon Tuff and Topopah Spring Tuff, Yucca Mountain, Nye County, Nevada*. Open File Report 95-134. Denver, Colorado: U.S. Geological Survey. DTN: GS941208314211.005 (Non-Q).

- Nordstrom, D.K.; Plummer, N.; Langmuir, S.; Busenberg, E.; May, H.M.; Jones, B.J.; and Parkhurst, D.L. 1990. Revised Chemical Equilibrium Data for Major Water–Mineral Reactions and Their Limitations. In: D.C. Melchoir, and R.L. Bassett, eds. *Chemical Modeling of Aqueous Systems II*. American Chemical Society, Washington, D.C..
- Okamoto, G.; Takeski, O.; and Katsumi, G. 1957. "Properties of Silica in Water." *Geochimica et Cosmochimica Acta*, 12, 123-321.
- Oversby, V.M. 1985. *The Reaction of Topopah Spring Tuff with J-13 Water at 150°C-Samples from Drill Cores USW G-1, USW GU-3, USW G-4 and UE-25h#1*. Report UCEL-53629. Livermore, California: Lawrence Livermore National Laboratory.
- Oversby, V. 1984a. *Reaction of the Topopah Spring Tuff with J-13 water at 120°C*. Report UCRL-53574. Livermore, California: Lawrence Livermore National Laboratory.
- Oversby, V.M. 1984b. *Reaction of the Topopah Spring Tuff with J-13 Well Water at 90°C and 150°C*. Report UCRL-53552. Livermore, California: Lawrence Livermore National Laboratory.
- Paces, J.B.; Marshall, B.D.; Whelan, J.F.; Neymark, L.A.; and Peterman, Z.E. 1998. *Summary of Subsurface Calcite and Opal Deposits and Estimates of the Probable Distribution and Isotopic Compositions of Hydrogenic Minerals along the East-West Cross Drift, Yucca Mountain, Nevada*. Open File Report. Denver, Colorado, U.S. Geological Survey. DTN: GS980308315215.009 (Q).
- Parkhurst, D.L. 1990. Ion Association Models and Mean Activity Coefficients of Various Salts. In: D.C. Melchior and R.L. Bassett, eds. *Chemical Modeling in Aqueous Systems II*. Washington, D.C.: American Chemical Society, American Chemical Society Symposium Series, 416, 30-43.
- Parkhurst, D.L.; Thorstenson, D.C.; and Plummer, L.N. 1980. *PHREEQE-A Computer Program for Geochemical Calculations*. U.S. Geological Survey Water-Resources Investigation, 80-96.
- Parson, M. and Garvin, G. 1992. "Hydrologic Constraints on Petroleum Generation within Continental Rift Basins." *Theory and Application to the Rhine Graben, American Association of Petroleum Geologists Bulletin*, 76, 468-488.
- Plummer, L.N.; and Busenberg, E. 1982. "The Solubilities of Calcite, Aragonite and Vaterite in CO<sub>2</sub>- H<sub>2</sub>O Solutions between 0 and 90° C, and an Evaluation of the Aqueous Model for the System CaCO<sub>3</sub> -CO<sub>2</sub> -H<sub>2</sub>O." *Geochimica et Cosmochimica Acta*, 46(6), 1011-1040.
- Pokrovskii, V.A. and Helgeson, H.C. 1995. "Thermodynamic Properties of Aqueous Species and the Solubilities of Minerals at High Pressures and Temperatures: The System Al<sub>2</sub>O<sub>3</sub>-H<sub>2</sub>O-NaCl." *Am. J. Sci.*, 295, 1255-1342.

- Pruess, K.; Simmons, A.; Wu, Y.S.; and Moridis, G.J. 1996. *TOUGH2 Software Qualification Report*. Report LBL-38383. Berkeley, California: Lawrence Berkeley National Laboratory. MOL19960610.0010-0020.
- Pruess K. 1991. *TOUGH2—A General Purpose Numerical Simulator for Multiphase Fluid and Heat Flow*. Report LBL-29400, UC-814. Berkeley, California: Lawrence Berkeley National Laboratory. NNA.1940202.0088.
- Ramirez, A.L.; Buscheck, T.A.; Carlson, R.; Daily, W.; Latorre, V.R.; Lee, K.; Kin, W.; Mao, N.; Towse, D.; Towse, T.S.; and Watwood, D. 1989. *Prototype Heater Test of the Environment Around a Simulated Waste Package*. Report UCRL-101693. Livermore, California: Lawrence Livermore National Laboratory.
- Ramirez, A.L.; Carlson, R.C.; and Buscheck, T.A. 1991. *In Situ Changes in the Moisture Content of Heated, Welded Tuff Based on Thermal Neutron Measurements*. Report UCRL-104715. Livermore, California: Lawrence Livermore National Laboratory.
- Reda, D.C. 1985. *Liquid Permeability Measurements of Densely Welded Tuff Over the Temperature Range 25° to 90°C*. Report SAND85-2482. Albuquerque, New Mexico: Sandia National Laboratories.
- Reed, M.H. 1988. *Yucca Mountain Boiling Studies*. Series of Unpublished Reports from M.H. Reed. Eugene, Oregon: The University of Oregon to Mifflin and Associates, Engineers, Las Vegas, Nevada.
- Reed, M.H. 1982. "Calculation of Multicomponent Chemical Equilibria and Reaction Processes in Systems Involving Minerals, Gases, and an Aqueous Phase." *Geochimica et Cosmochimica Acta*, 46, 513-548.
- Rimstidt, J.D. 1997. "Quartz Solubility at Low Temperatures." *Geochimica et Cosmochimica Acta*, 61(13), 2553-2558.
- Rimstidt, J.D.; and Barnes, H.L. 1980. "The Kinetics of Silica-Water Reactions." *Geochimica et Cosmochimica Acta*, 44, 1683-1699.
- Roberts, S. and Viani, B. 1997a. *Mineral Abundances for Samples from Instrumented Boreholes in the Access Drift Scale Test*. Yucca Mountain Project Level 4 Milestone, SP9511M4. Livermore, California: Lawrence Livermore National Laboratory. DTN: LL980106404244.050(Q).
- Roberts, S. and Viani, B. 1997b. *Mineral Abundances from Six Chemistry (SEAMIST) holes in the Drift Scale Heater Test area of the Exploratory Studies Facility*. Yucca Mountain Project Level 4 Milestone, SP9510M4. Livermore, California: Lawrence Livermore National Laboratory. DTN: LL980106404244.050(Q).

- Robie, R.A. and Hemingway, B.C. 1995. "Thermodynamic Properties of Minerals and Related Substances at 298.15K and 1 Bar ( $10^5$  Pascals) and at Higher Temperatures." *U.S. Geological Survey Bulletin*, 461. Reston, Virginia, U.S. Geological Survey.
- Rosenberg, P.E.; Kittrick, J.A.; and Sass, B.M. 1985. "Implications of Illite/Smectite Stability Diagrams: A Discussion." *Clays and Clay Minerals*, 33(6), 561-562.
- Rousseau, J.P.; Kwicklis, E.M.; and Gillies, D.C., eds. 1996 (In Press). *Hydrogeology of the Unsaturated Zone, North Ramp Area of the Exploratory Studies Facility, Yucca Mountain, Nevada*, USGS-WRIR-98-4050 Yucca Mountain Project Milestone 3GUP667M (formerly 3GUP431M). Submitted for publication as a Water-Resources Investigations Report, Denver, Colorado: U.S. Geological Survey. GS960908312232.014 (Q).
- Scheel, L.D.; Fleshier, E.; and Klemperer, F.W. 1953. "Toxicity of Silica, I: Silica Solutions." *Arch. Ind. Hvg. Occupation Med.*, 8, 564-573.
- Shock, E.L. and Helgeson, H.C. 1990. "Calculations of the Thermodynamic and Transport Properties of Aqueous Species at High Pressure and Temperatures: Standard Partial Molal Properties of Organic Species." *Geochimica et Cosmochimica Acta*, 54, 915-945.
- Shock, E.L. and Helgeson, H.C. 1988. "Calculation of Thermodynamic and transport Properties of Aqueous Species at high Pressure and Temperatures: Correlation Algorithms for Ionic Species and Equations of State Predictions to 5kb and 1000° C." *Geochimica et Cosmochimica Acta*, 52, 2009-2036.
- Shock, E.L.; Sassani, D.C.; Willis, M.; and Sverjensky, D.A. 1997. "Inorganic Species in Geologic Fluids: Correlations Among Standard Modal Thermodynamic Properties of Aqueous Ions and Hydroxide Complexes." *Geochimica et Cosmochimica Acta*, 61(5), 907-950.
- Siever, R. 1962. "Silica Solubility, 0°- 200° C, and the Diagnosis of Siliceous Sediments." *J. Geol.*, 70, 127-150.
- Simmons, A.M. and Glassley, W.E. 1998. "Fracture Mineral Evolution Affecting Flow Around a Potential Repository," American Nuclear Society, *Proceedings of the 8th Annual International High-Level Radioactive Waste Conference, May 11-14, 1998*, Las Vegas, Nevada.
- Sonnenthal, E.L.; Ahlers, C.F.; and Bodvarsson, G.S. 1997a. Fracture and Fault Properties for the UZ Site-Scale Flow Model. In: G.S. Bodvarsson, T.M. Bandurraga, and Y.S. Wu, eds. *The Site-Scale Unsaturated Zone Model of Yucca Mountain, Nevada, for the Viability Assessment*, Chapter 7. Yucca Mountain Project Level 4 Milestone SP24UFM4. Report LBNL-40376, UC-814. Berkeley, California: Lawrence Berkeley National Laboratory. LB970601233129.001 (Q).

- Sonnenthal, E.L.; DePaolo, D.J.; and Bodvarsson, G.S. 1997b. Modeling the Strontium Geochemistry and Isotopic Ratio in the Unsaturated Zone. In: G.S. Bodvarsson, T.M. Bandurraga, and Y.S. Wu, eds. *The Site-Scale Unsaturated Zone Model of Yucca Mountain, Nevada, for the Viability Assessment*, Chapter 17. Yucca Mountain Project Level 4 Milestone SP24UFM4. Report LBNL-40376, UC-814. Berkeley, California: Lawrence Berkeley National Laboratory. LB970601233129.001 (Q).
- Sonnenthal, E. and Ortoleva, P.J. 1994. "Numerical Simulations of Overpressured Compartments in Sedimentary Basins, in Basin Compartments and Seals." In: P.J. Ortoleva and Z. Al-Shaieb, eds. *American Association of Petroleum Geologists Memoir*, 61, 403-416.
- Spycher, N.S. and Reed, M.H. 1992. "Microcomputer-Based Modeling of Speciation and Water-Mineral-Gas Reactions Using Programs SOLVEQ and CHILLER." In Y.K. Kharaka and A.S. Maest eds. *Proceedings of the 7<sup>th</sup> International Symposium on Water-Rock Interaction*, 1087-1090. Balkema, A.A., Rotterdam: Holland.
- Steeffel, C.I. and Lasaga, A.C. 1994. "A Coupled Model for Transport of Multiple Chemical Species and Kinetic Precipitation/Dissolution Reactions with Applications to Reactive Transport in Single Phase Hydrothermal Systems." *Am. J. Sci.*, 294, 529-592
- Steeffel, C.I. and Yabusaki, S.B. 1996. *OS3D/GIMRT: Software for Modeling Multicomponent -Multidimensional Reactive Transport*, Richland, Washington: Pacific Northwest Laboratory, Battelle Memorial Institute.
- Stellavato, N. and Montazer, P. 1998. Environmental gases, permeability, and thermal conductivity tests at Borehole ONC#1, Yucca Mountain, Nevada. In: *High Level Waste Management. Proceedings of the Eighth International Conference, May 11-14, 1998*, La Grange Park, Illinois, USA: American Nuclear Society, Inc. 5-8.
- Stober, W., 1967. "Formation of Silicic Acid in Aqueous Suspensions of Different Silica Modifications: Equilibrium Concepts in Natural Water Systems." *Advan. Chem. Ser.*, 67, 161-182.
- Stoessell, R.K. 1988. "25°C and 1 atm Dissolution Experiments of Sepiolite and Kerolite." *Geochimica et Cosmochimica Acta*, 52, 365-374.
- Suarez, D. L.; Wood, J.D.; and Ibrahim, I. 1992. "Re-Evaluation of Calcite Supersaturation in Soils." *Soil Sci. Soc. Am. J.*, 56, 1776-1784.
- Sverjensky, D.A.; Shock, E.L.; and Helgeson, H.C. 1997. "Prediction of the Thermodynamic Properties of Aqueous Metal Complexes to 1000°C and 5 kb." *Geochimica et Cosmochimica Acta*, 61(7), 1359-1412.

- Tarshis, A.L. 1982. *Electron Microscopic Examination of Zeolitization and Cooling Devitrification in Silicic Volcanic Rocks*. Ph.D. Thesis. Santa Cruz, California: University of California at Santa Cruz.
- Tester, J.W.; Worley, G.W.; Robison, B.A.; Grigsby, C.O.; and Feerer, J.L. 1994. "Correlating Quartz Dissolution Kinetics in Pure Water from 25 to 625°C." *Geochimica et Cosmochimica Acta*, 58(11), 2407-2420.
- Tsang, Y.W. and Birkholzer, J.T. 1997. *Interpreting the Thermal-Hydrological Response of the ESF Single Heater Test*. Yucca Mountain Project Level 4 Milestone SP9267M4. Berkeley, California: Lawrence Berkeley National Laboratory. MOL.19971204.0759.
- U.S. Department of Energy, 1995. *Modeling and Testing Thermohydrologic Processes in the Yucca Mountain Site Characterization Project*. Yucca Mountain Site Characterization Project Report (Draft). MOL. 19980219.1111 (TBV).
- Vaniman, D.T. and Chipera, S.J. 1996. "Paleotransport of Lanthanides and Strontium Recorded in Calcite Compositions from Tuffs at Yucca Mountain, Nevada, U.S.A." *Geochimica et Cosmochimica Acta*, 60(22), 4417-4433.
- VanLier, J.A.; de Bruyn, P.L.; and Overbeck, J.T. 1960. "The Solubility of Quartz," *J. Phys. Chem.*, 64, 1675-1682.
- Veblel, M.A. 1989. "Effect of Chemical Affinity on Feldspar Hydrolysis Rate in Two Natural Weathering Systems." *Chem. Geol.*, 78, 245-253.
- Viani, B.E. and Bruton, C. J. 1992. *Modeling fluid-rock interaction at Yucca Mountain, Nevada: a Progress Report*. Report UCRL-109221. Livermore, California: Lawrence Livermore National Laboratory.
- Walther, J.V. and Helgeson, H.C. 1977. "Calculation of the Thermodynamic Properties of Aqueous Silica and the Solubility of Quartz and its Polymorphs at High Pressures and Temperatures." *American Journal of Science*, 277(10), 1315-1351.
- Weyl, P.K. 1959. "Pressure Solution and the Force of Crystallization." *J. of Geophysical Research*, 64,2001-2025.
- Wilder, D. (ed.). 1996. *Near-Field and Altered Zone Environment Report*, UCRL-LR-124998, v.2, rev. 1. Livermore, California: Lawrence Livermore National Laboratory.
- Wolery, T.J. 1993. *EQ3/6, A Software Package for Geochemical Modeling of Aqueous Systems: Package Overview and Installation Guide (Version 7.0)*, Report UCRL-MA-110662, Pt. I. Livermore, California: Lawrence Livermore National Laboratory. NNA.19921023.0028.

- Wolery, T.J. 1992. *EQ3NR, A Computer Program for Geochemical Aqueous Speciation-Solubility Calculations: Theoretical Manual, User's Guide and Related Documentation (Version 7.0)*, Report UCRL-MA-110662, Pt. III. Livermore, California: Lawrence Livermore National Laboratory. NNA.19921218.0010.
- Wolery, T.J. and Daveler, S.A. 1992. *EQ6, A Computer Program for Reaction Path Modeling of Aqueous Geochemical Systems: Theoretical Manual, User's Guide, and Related Documentation (Version 7.0)*, Report UCRL-MFA-110662, Pt. IV. Livermore, California: Lawrence Livermore Laboratory Report. NNA19939127.0030.
- Wu, Y.S.; Ahlers, C.F.; Fraser, P.; Simmons, A.; and Pruess, K. 1996. *Software Qualification of Selected TOUGH2 Modules*. Report LBL-39490 UC-800. Berkeley, California: Lawrence Berkeley National Laboratory. MOL.19970219.0100-0105.
- Xu, T.; Gerard, F.; Pruess, K.; and Brimhall, G. 1998a. "Introducing Reactive Solute Transport to TOUGH2: Application to Supergene Copper Enrichment." *Proceedings of the TOUGH Workshop '98*, Berkeley, California: Lawrence Berkeley National Laboratory.
- Xu, T.; Gerard, F.; Pruess, K.; and Brimhall, G. 1998b. (In preparation). *An Efficient Algorithm for Subsurface reactive Transport of Water-Rock-Gas Interaction Under Equilibrium and Kinetic Conditions*. Berkeley, California: Lawrence Berkeley National Laboratory
- Xu, T.; Gerard, F.; Pruess, K.; and Brimhall, G. 1997. *Modeling Non-Isothermal Multiphase Multi-species Reactive Chemical Transport in Geologic Media*. Report LBNL-40504, UC-400. Berkeley California: Lawrence Berkeley National Laboratory.
- Xu, T. 1996. *Modeling Non-Isothermal Multicomponent Reactive Solute Transport Throughout Variably Saturated Porous Media*. Ph.D. Dissertation. La Corunia, Spain: University of La Corunia.
- Yang, I.C.; Rattray, G.W.; and Yu, P. 1996a. *Interpretation of Chemical and Isotopic Data from Boreholes in the Unsaturated Zone at Yucca Mountain*. U.S. Geological Survey Water Resources Investigation Report 96-4058. Denver, Colorado: U.S. Geological Survey. DTN: GS970108312271.001 (Q).
- Yang, I.C.; Yu, P.; Rattray, G.W.; and Thorstenson, D.C. 1996b. *Hydrochemical Investigations and Geochemical Modeling in Characterizing the Unsaturated Zone at Yucca Mountain, Nevada*. U.S. Geological Survey Water Resources Investigation Report 96-?????. Denver, Colorado: U.S. Geological Survey.
- Yang, I.C. 1992. "Flow and Transport through Unsaturated Rock—Data from Two Test Holes, Yucca Mountain, Nevada." *Proceedings of the Third Annual International High-Level Radioactive Waste Management Conference, 1*, 732-737. Las Vegas, Nevada: American Nuclear Society. NNA19930112.0137, GS920908312272.011 (Non-Q).

Yang, I.C.; Turner, A.K.; Sayre, T.M.; and Montazer, P. 1988. *Triaxial-Compression Extraction of Pore Water from Unsaturated Tuff, Yucca Mountain, Nevada*. U.S. Geol. Surv. Water Resour. Invest. Rep. 88-4189. Denver, Colorado; U.S. Geological Survey. GS90090123344G.001 (Non-Q), NNA.890309.0161.

**16. FIGURES (APPENDIX A)**

---

**16. FIGURES (APPENDIX A)**



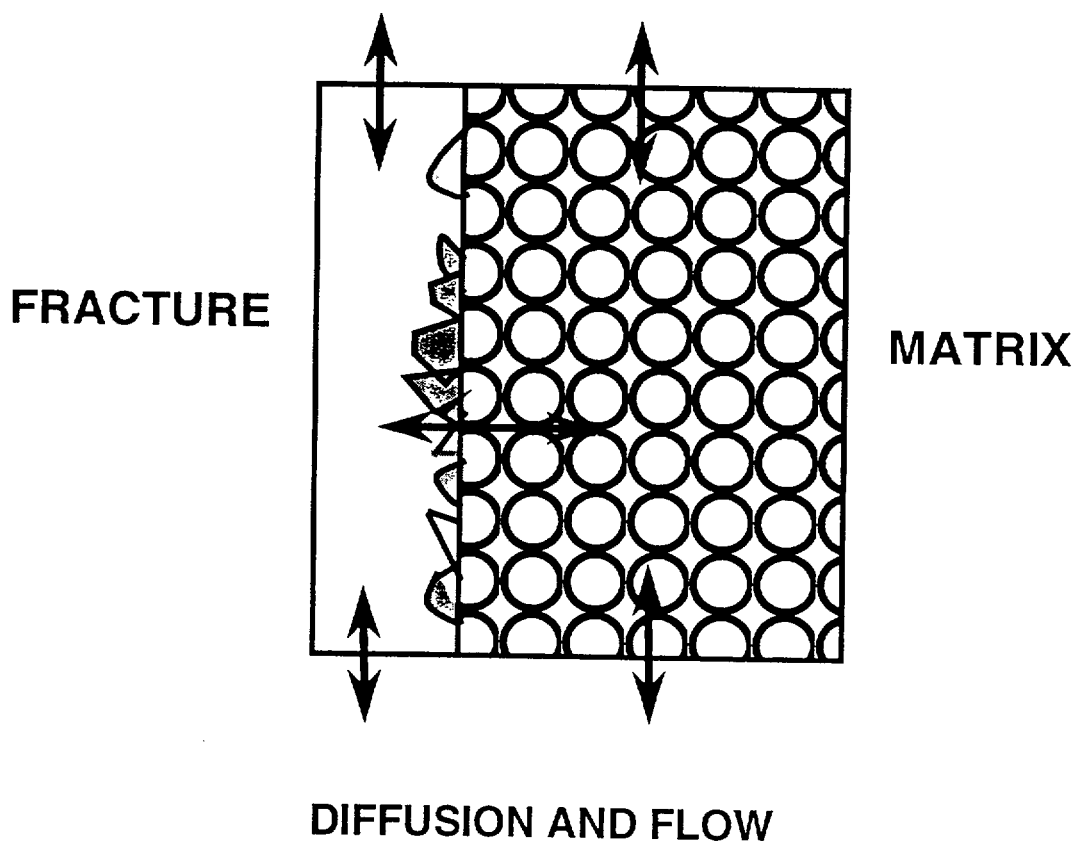


Figure 5.1 Dual permeability concept for reaction-transport models.

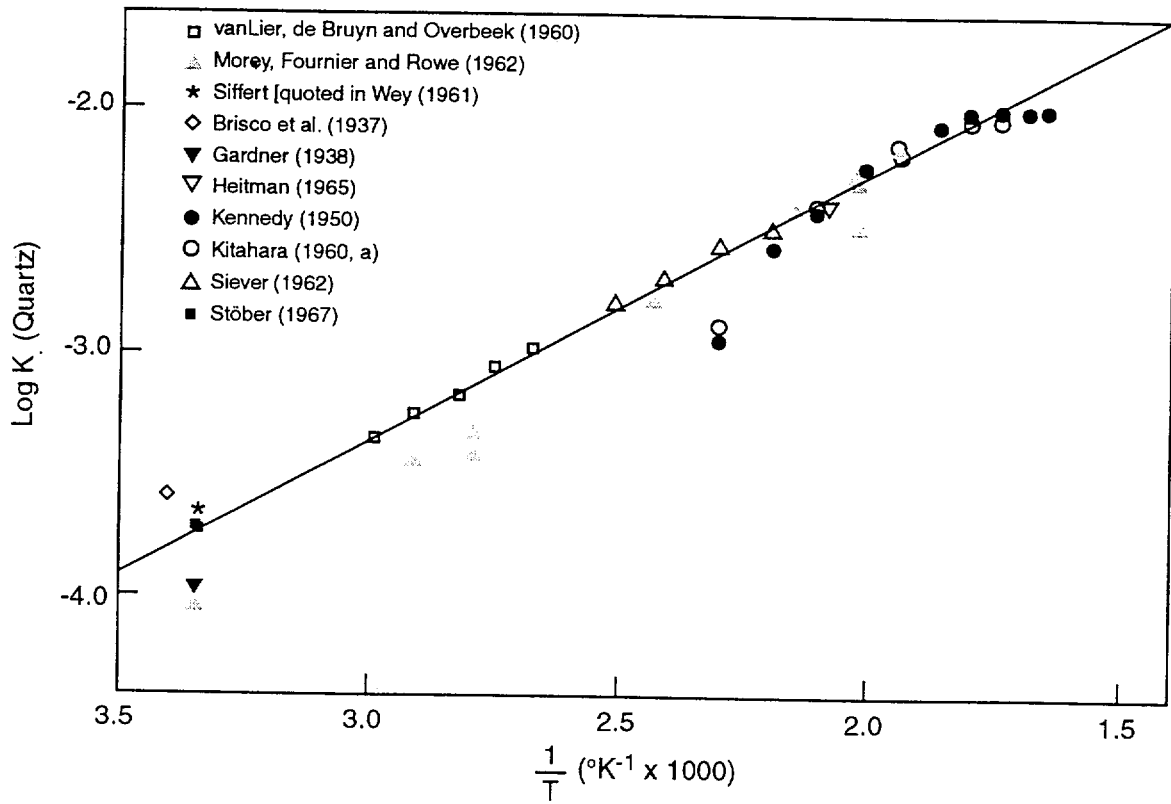


Figure 6.1 The solubility of quartz as a function of temperature. The continuous line through the data is a linear regression of logK (quartz) versus 1/T (K) (after Apps, 1970).

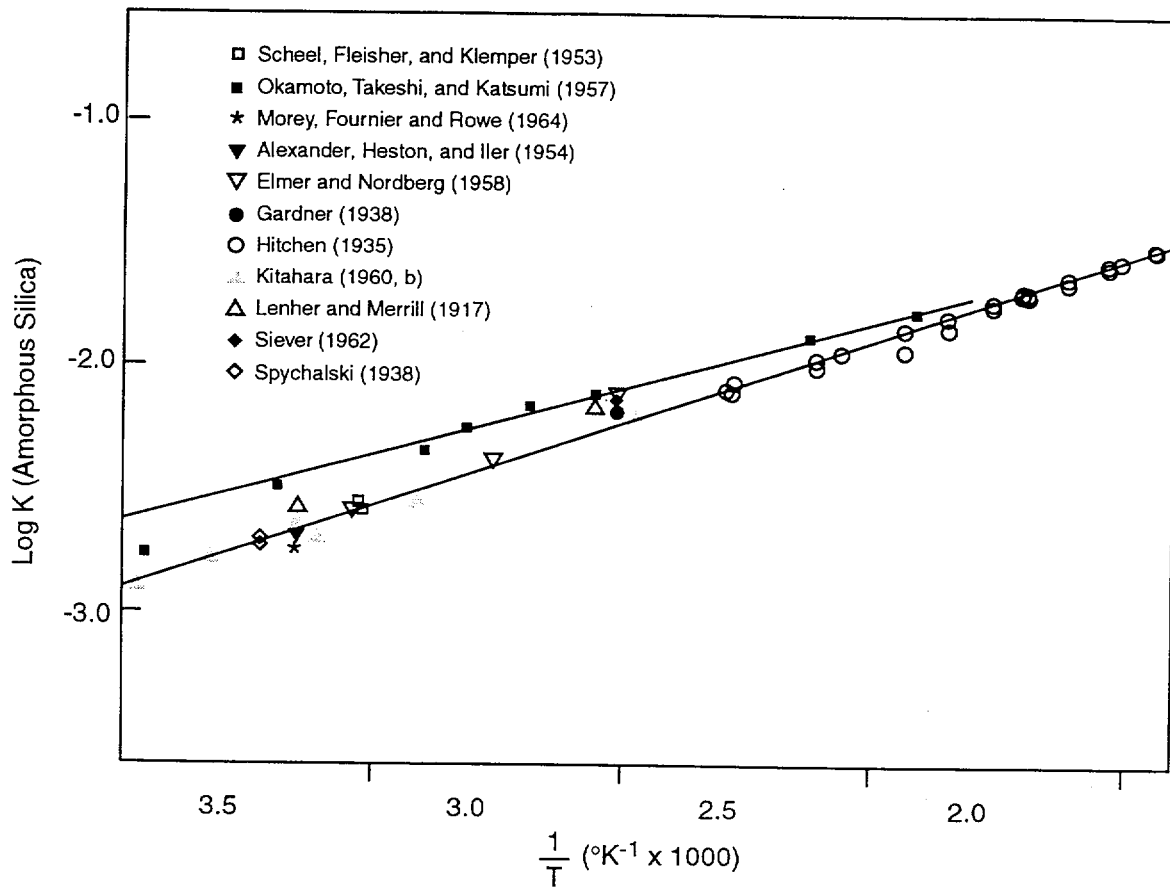


Figure 6.2 The solubility of amorphous silica as a function of temperature. The continuous line through the data is a linear regression of  $\log K$  (am.  $\text{SiO}_2$ ) versus  $1/T$  (K) (after Apps, 1970).

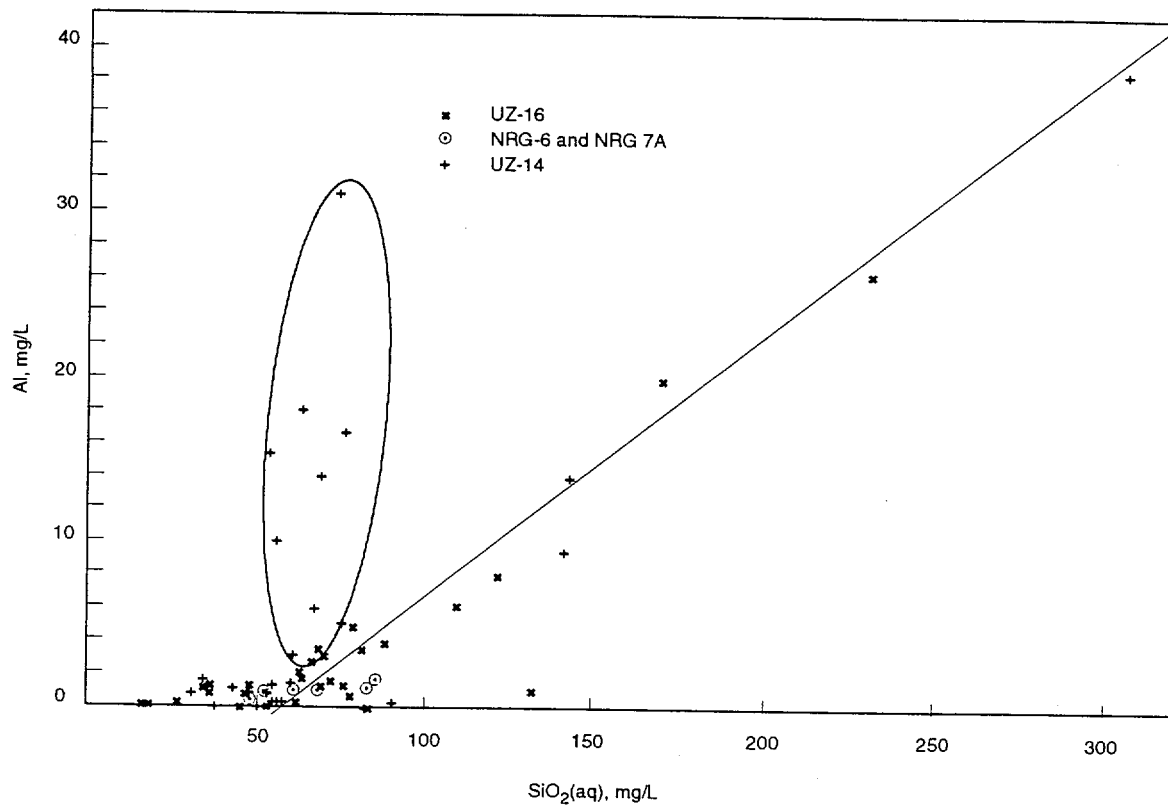


Figure 7.1 Plot to illustrate the corrections applied to pore water SiO<sub>2</sub> (aq) concentrations due to the dissolution of clay particulates during chemical analysis.

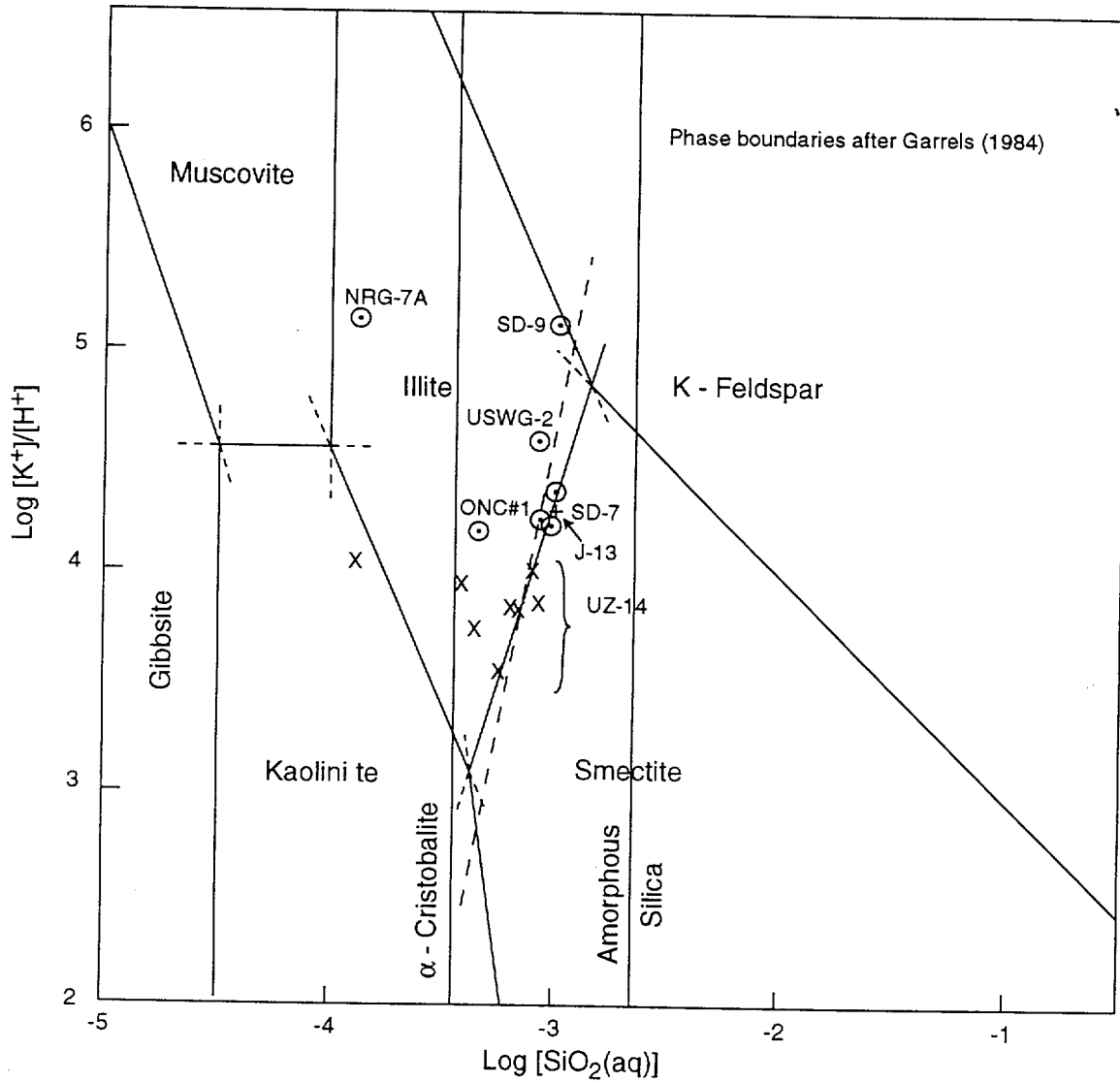


Figure 7.2 The  $\text{log[K}^+]/[\text{H}^+]$  versus  $\text{log[SiO}_2(\text{aq})]$  activity diagram at 25°C showing the phase boundaries calculated by Garrels (1984), upon which are superimposed the corresponding log activity ratios calculated for perched waters from Yang et al. (1996a). The dashed line represents the idealized slope of the illite/smectite phase boundary based on the stoichiometry of I/S phases by Aja (1995).

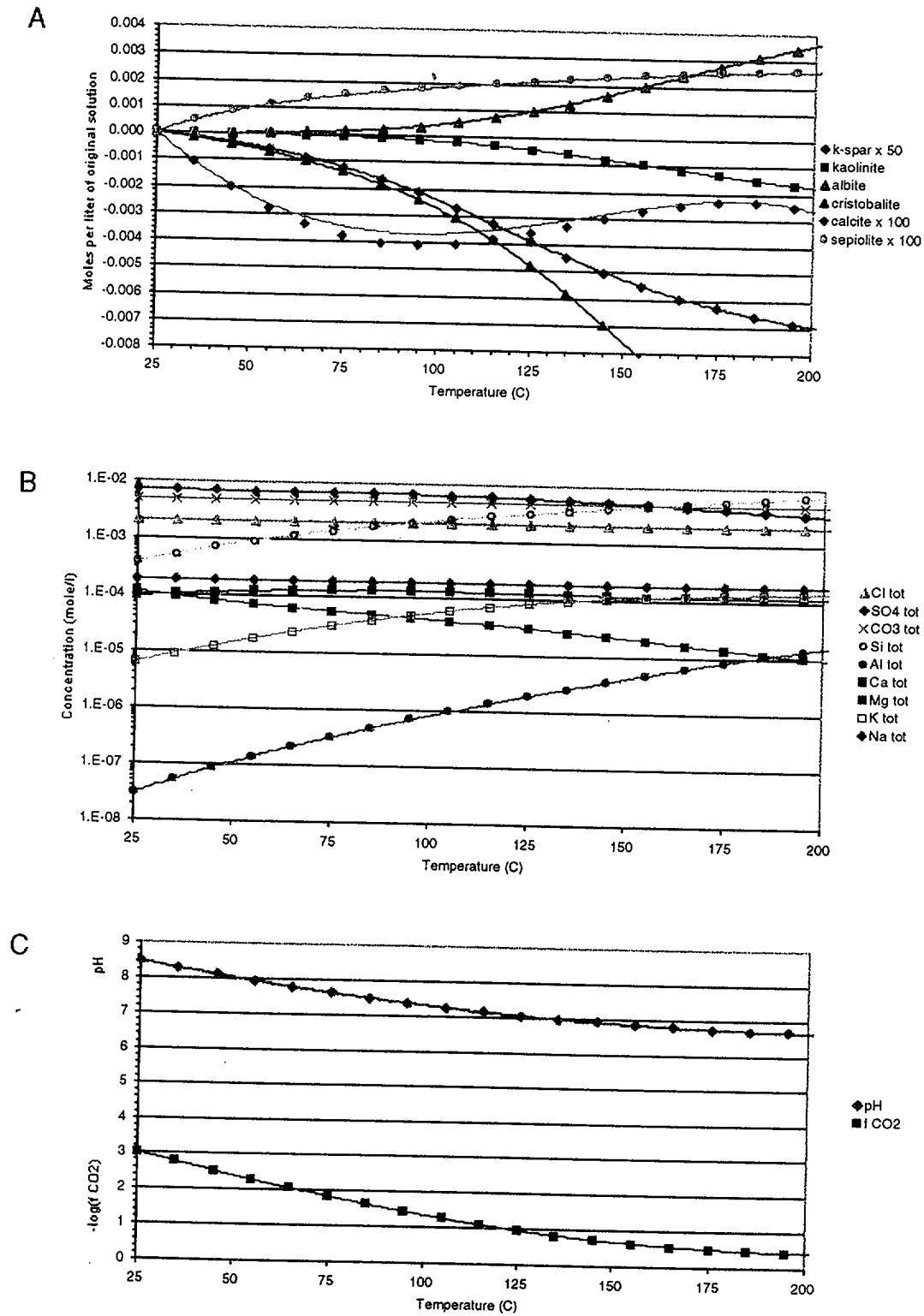


Figure 9.1 Benchmark heating simulations: (a) mineral amounts (positive for precipitation, negative for dissolution), (b) total aqueous concentrations, and (c) pH and  $f\text{CO}_2$  calculated with TOUGHREACT (solid lines) and CHILLER (symbols). No gas phase is present. Equilibrium is assumed.

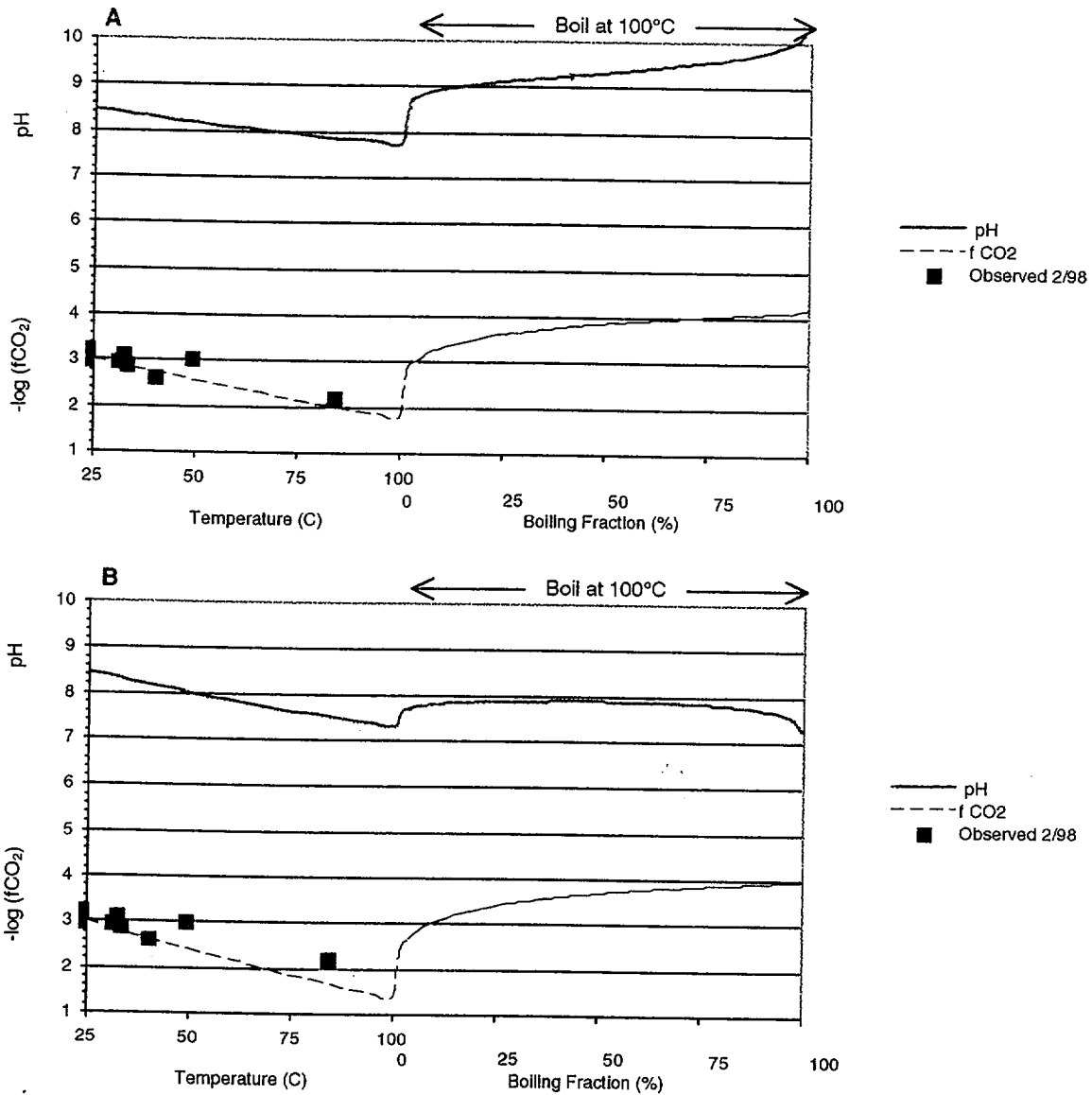


Figure 11.8 Equilibrium boiling simulation: pH and  $f\text{CO}_2$  computed with (a) Case-1 mineral assemblage (no Al-silicates) and (b) Case-2 mineral assemblage (with Al-silicates). The solution is heated from 25 to 100° C then allowed to boil at a pressure near 1 atm until reaching a final boiling fraction of 99.7 percent. A closed system is assumed.

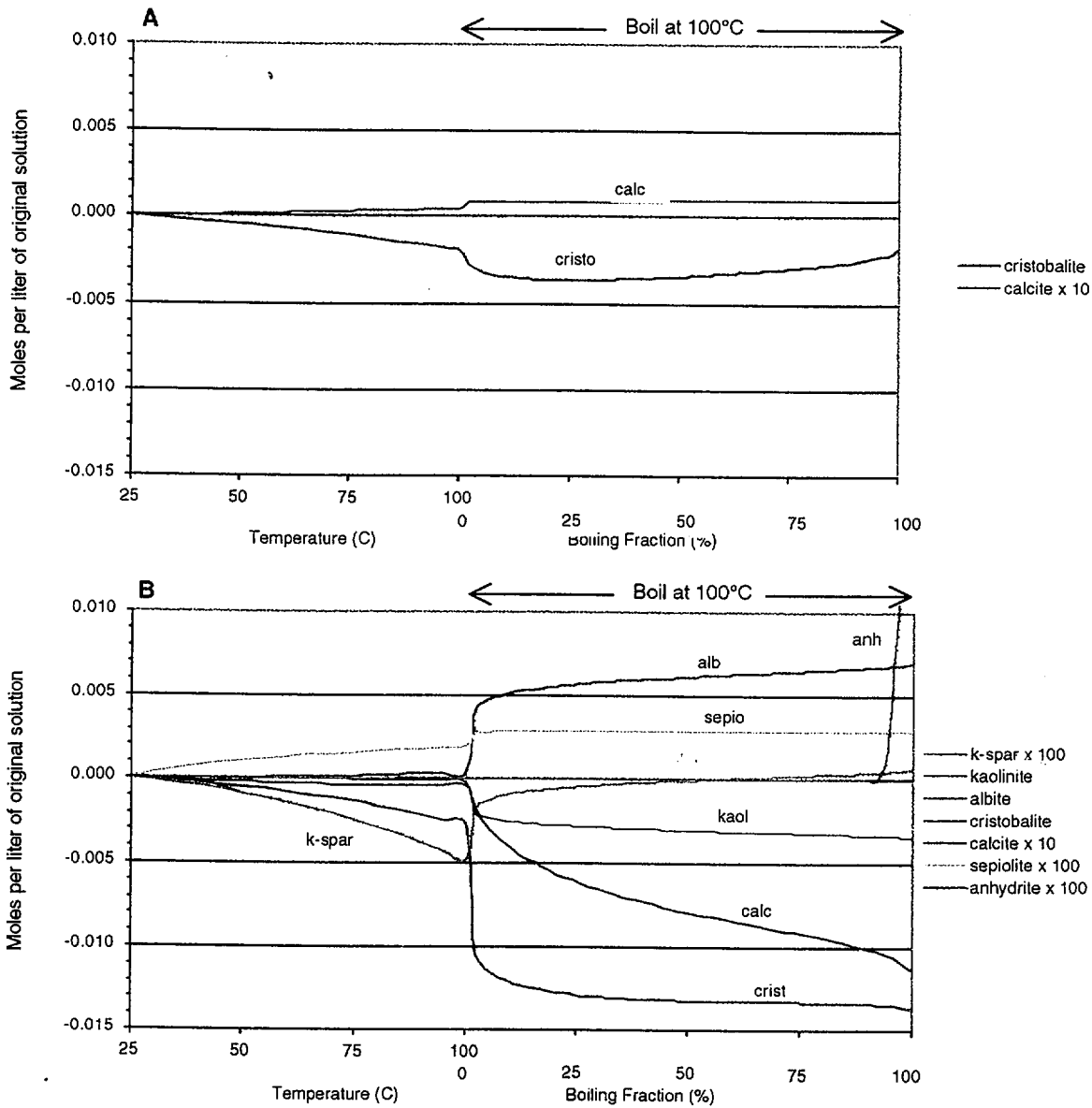


Figure 11.9 Equilibrium boiling simulation: mineral amounts (positive for precipitation, negative for dissolution) computed with (a) Case-1 mineral assemblage (no Al-silicates) and (b) Case-2 mineral assemblage (with Al-silicates). The solution is heated from 25 to 100 °C then allowed to boil at a pressure near 1 atm until reaching a final boiling fraction of 99.7 percent. A closed system is assumed.

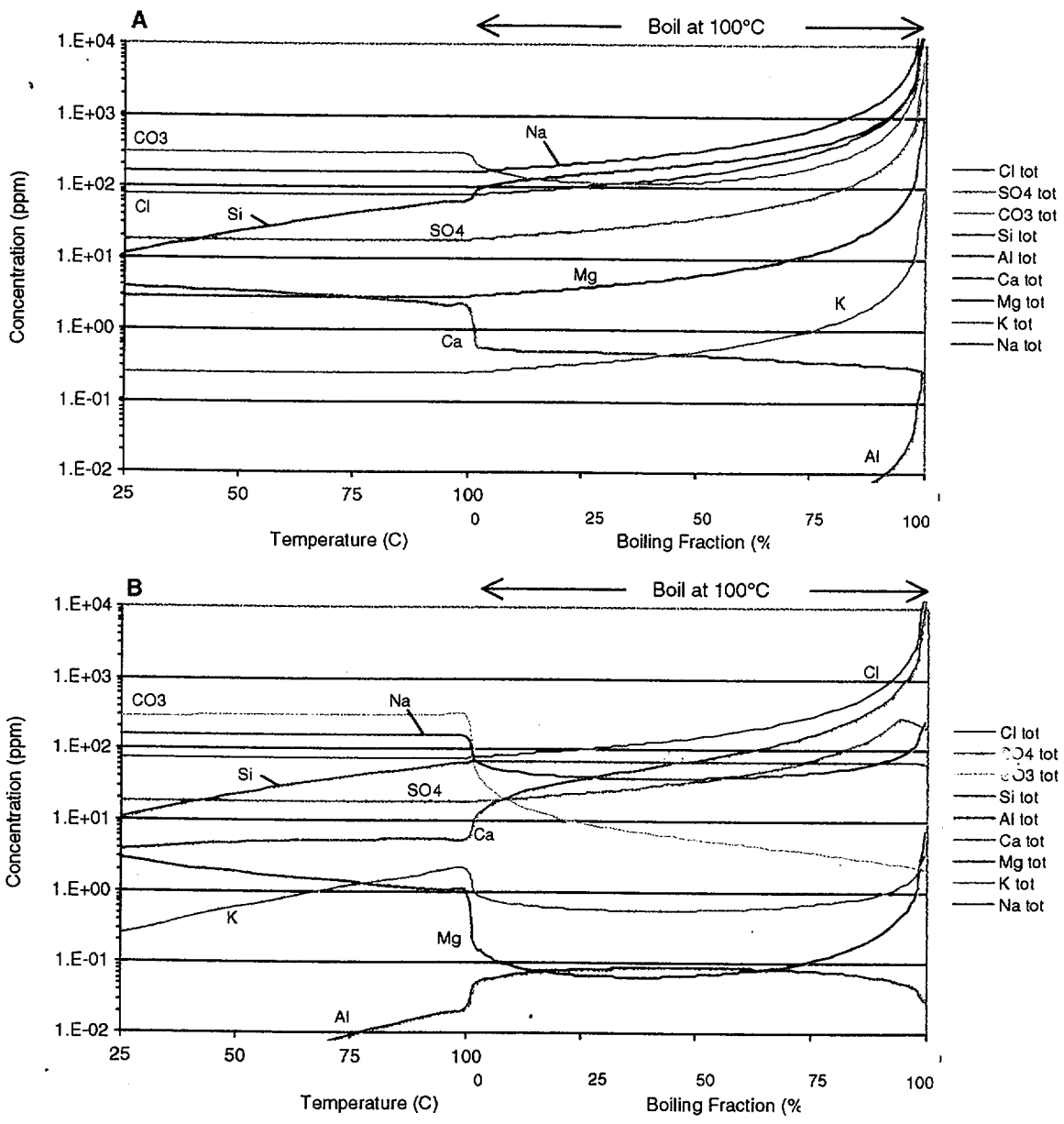


Figure 11.10 Equilibrium boiling simulation: total aqueous concentrations computed with (a) Case-1 mineral assemblage (no Al-silicates) and (b) Case-2 mineral assemblage (with Al-silicates). The solution is heated from 25 to 100° C then allowed to boil at a pressure near 1 atm until reaching a final boiling fraction of 99.7 percent. A closed system is assumed.

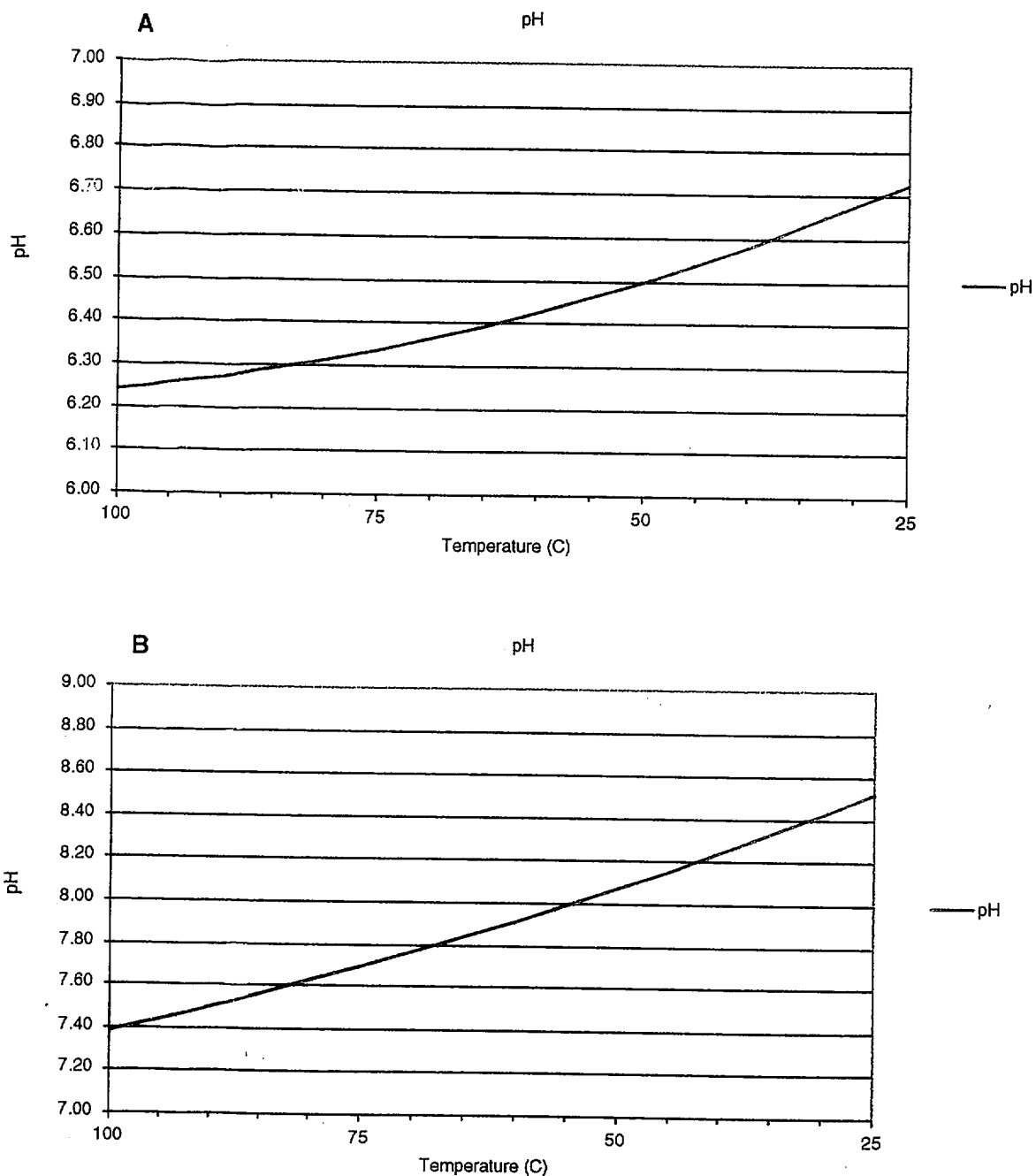


Figure 11.11 Equilibrium gas condensation simulation: pH computed with (a) Case-1 mineral assemblage (no Al-silicates) and (b) Case-2 mineral assemblage (with Al-silicates). The gas condensate is cooled from 100° C to 25° C at a pressure near 1 atm. A closed system is assumed.

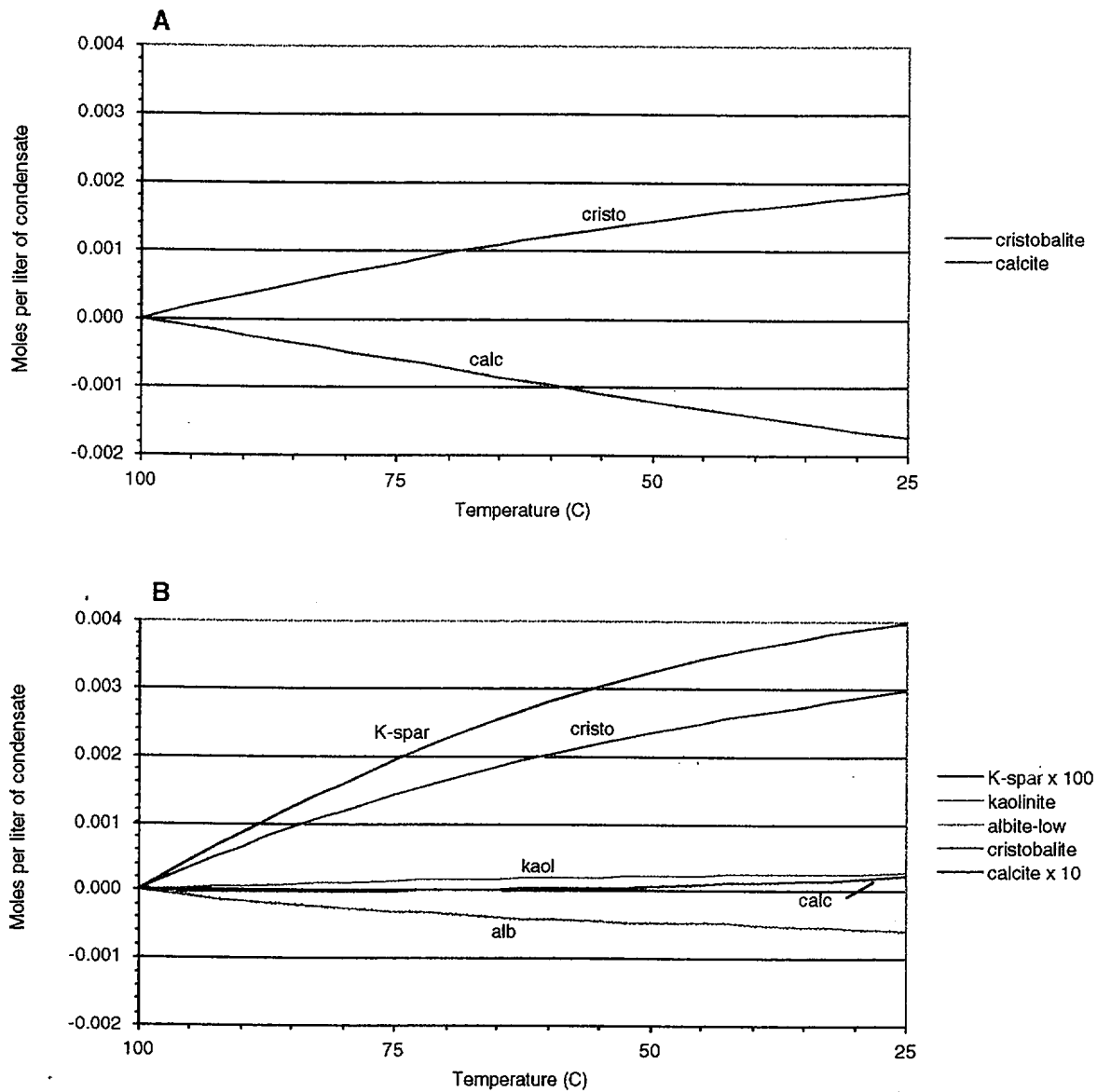


Figure 11.12 Equilibrium gas condensation simulation: mineral amounts (positive for precipitation, negative for dissolution) computed with (a) Case-1 mineral assemblage (no Al-silicates) and (b) Case-2 mineral assemblage (with Al-silicates). The gas condensate is cooled from 100° C to 25° C at a pressure near 1 atm. A closed system is assumed.

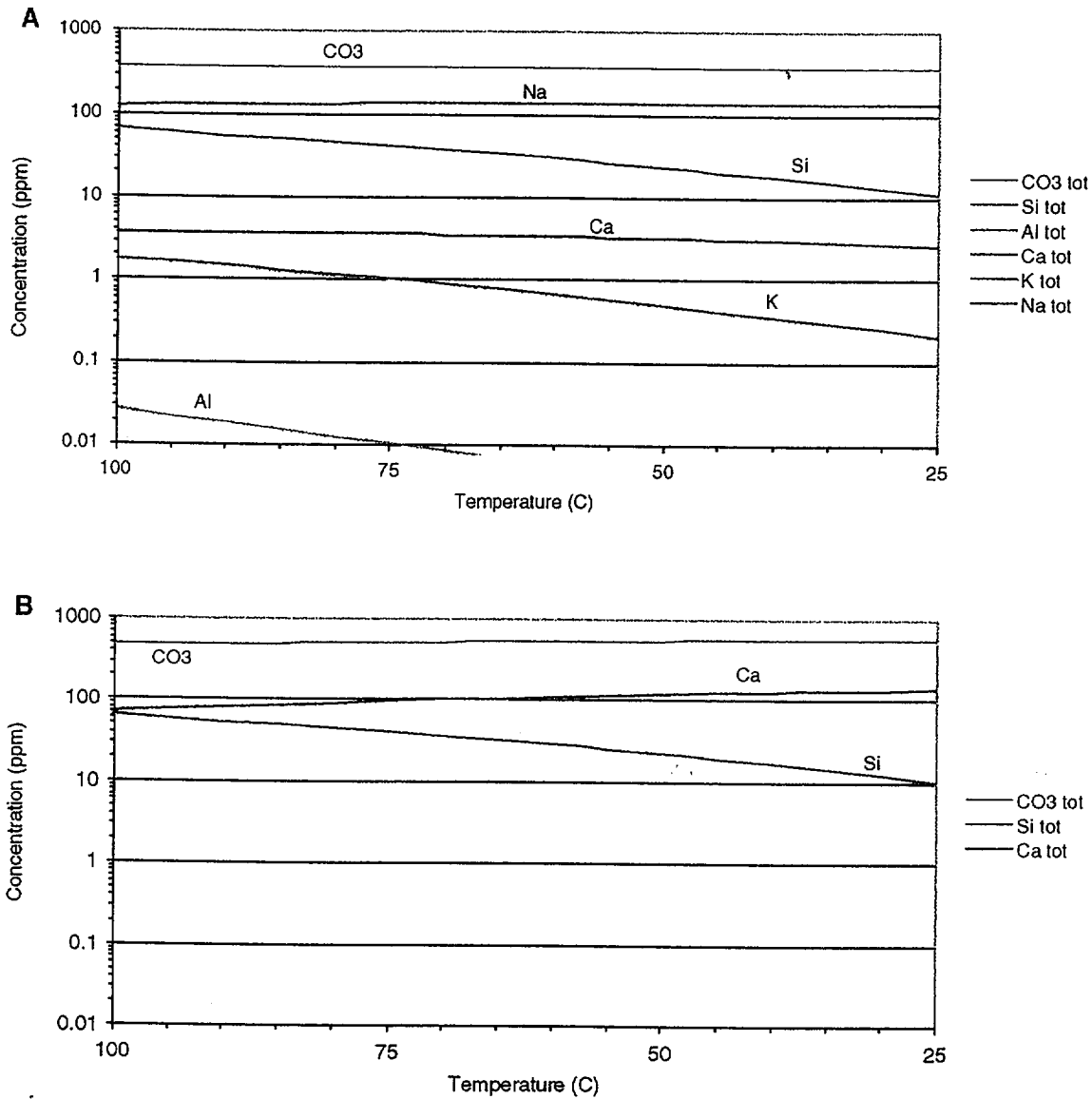


Figure 11.13 Equilibrium gas condensation simulation: total aqueous concentrations computed with (a) Case-1 mineral assemblage (no Al-silicates) and (b) Case-2 mineral assemblage (with Al-silicates). The gas condensate is cooled from 100° C to 25° C at a pressure near 1 atm. A closed system is assumed.

### DRIFT-SCALE TEST MESH

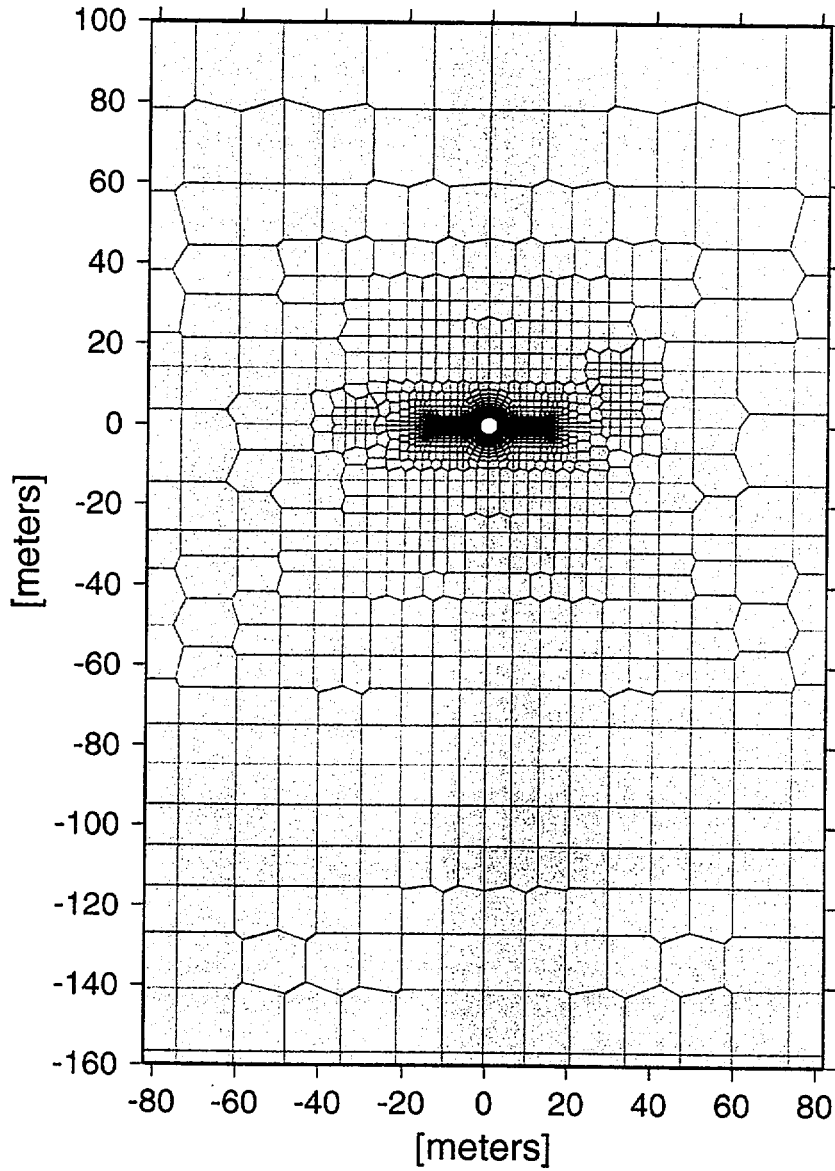


Figure 12.1 2-D Drift-scale test mesh for 2-D dual permeability model (Birkholzer and Tsang, 1997).

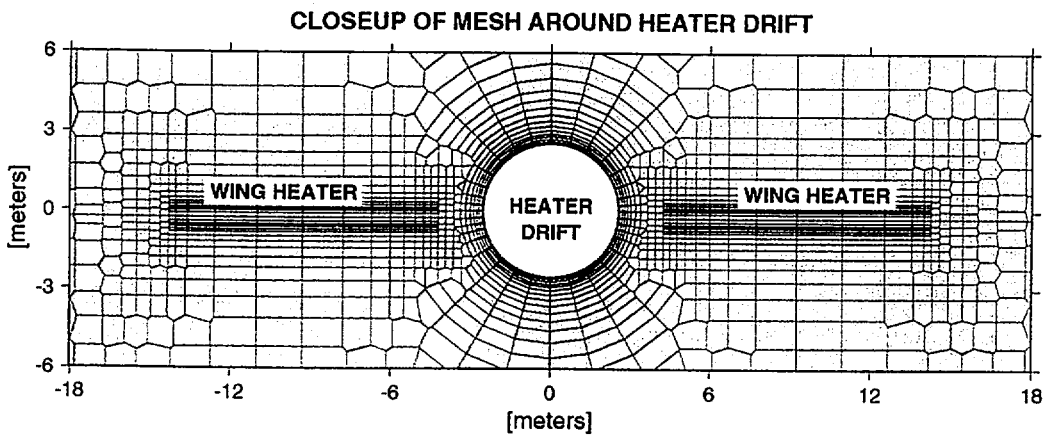


Figure 12.2 Close-up view of region around central drift heater and wing heaters, showing local grid refinement.

### DRIFT-SCALE TEST MESH

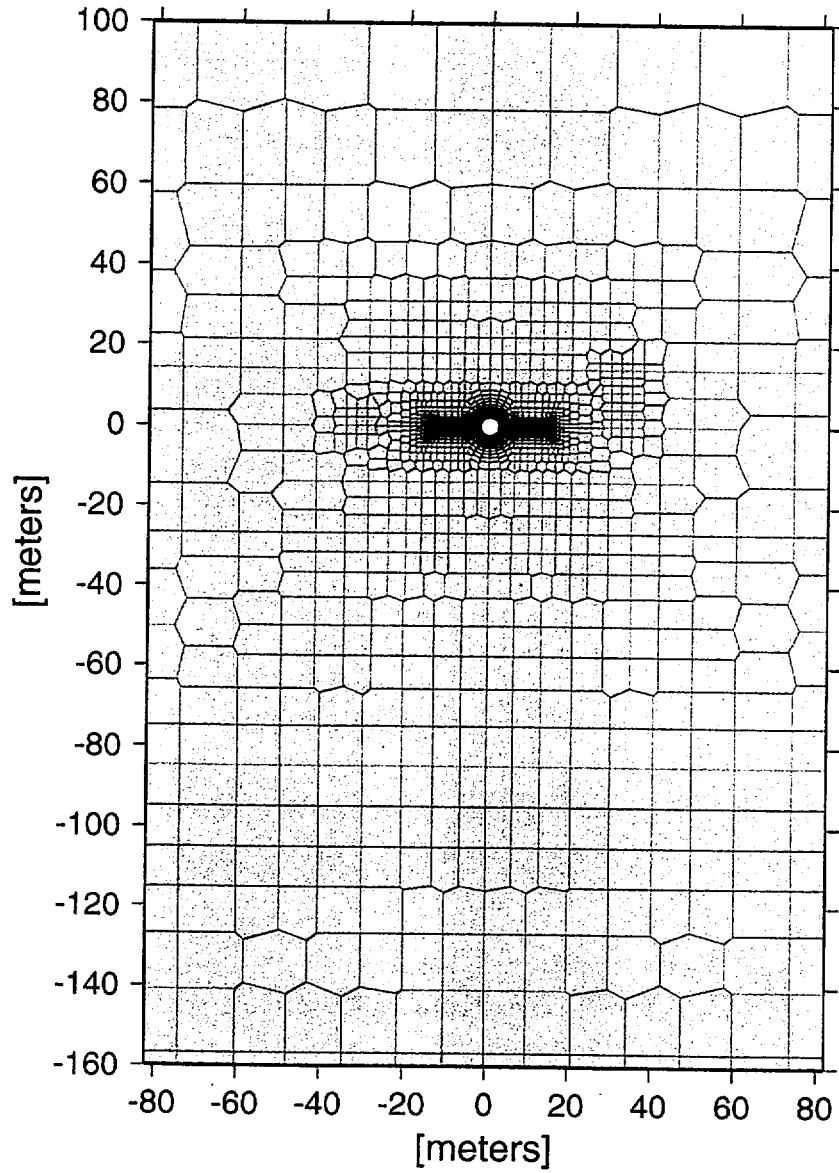


Figure 12.1 2-D Drift-scale test mesh for 2-D dual permeability model (Birkholzer and Tsang, 1997).

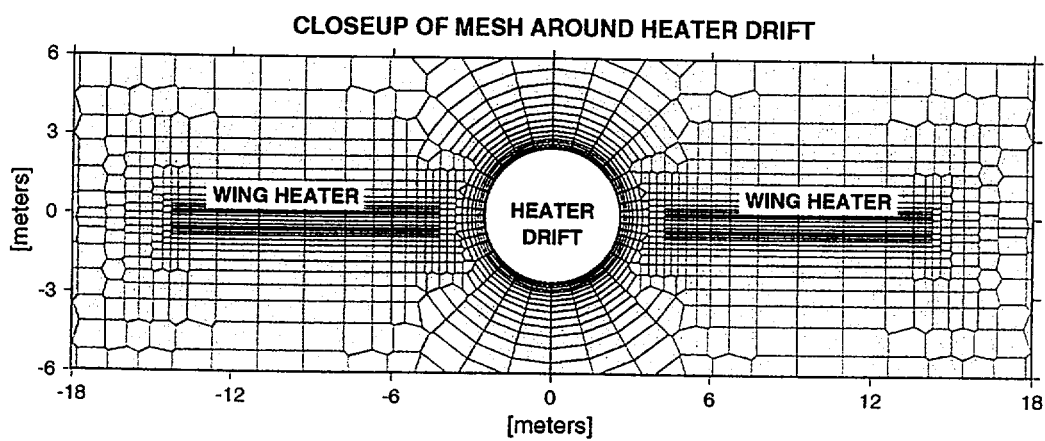


Figure 12.2 Close-up view of region around central drift heater and wing heaters, showing local grid refinement.

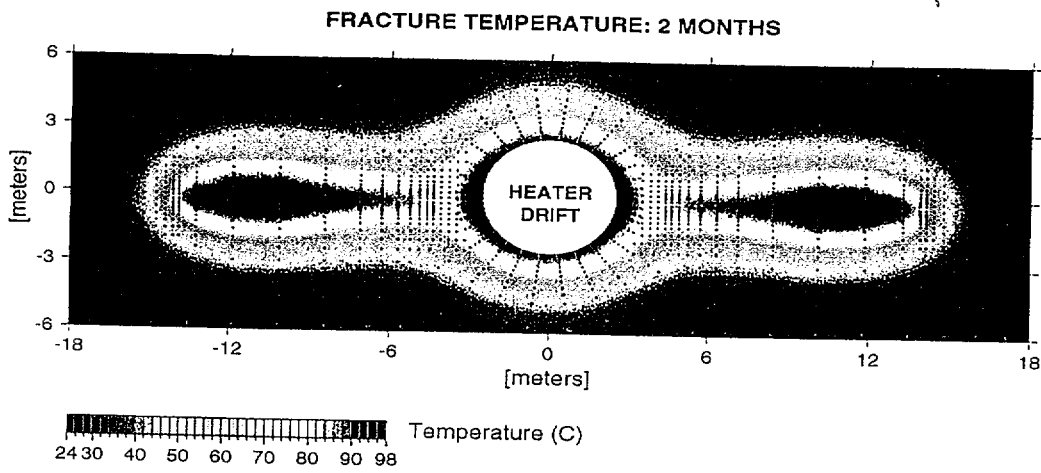


Figure 13.1 Temperature in fractures after two months of heating, for DST-1.

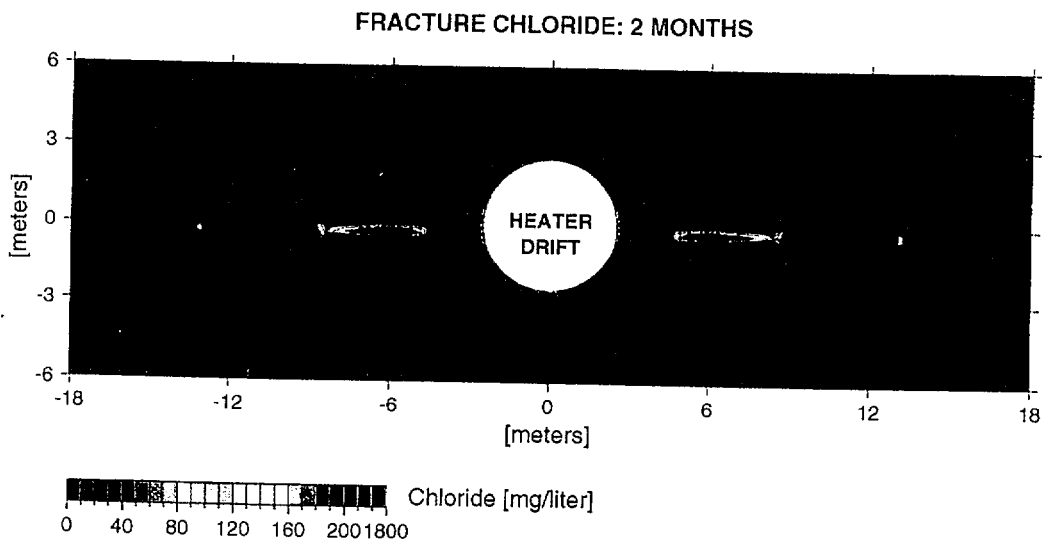


Figure 13.2 Chloride concentration in fracture pore water, for DST-1.

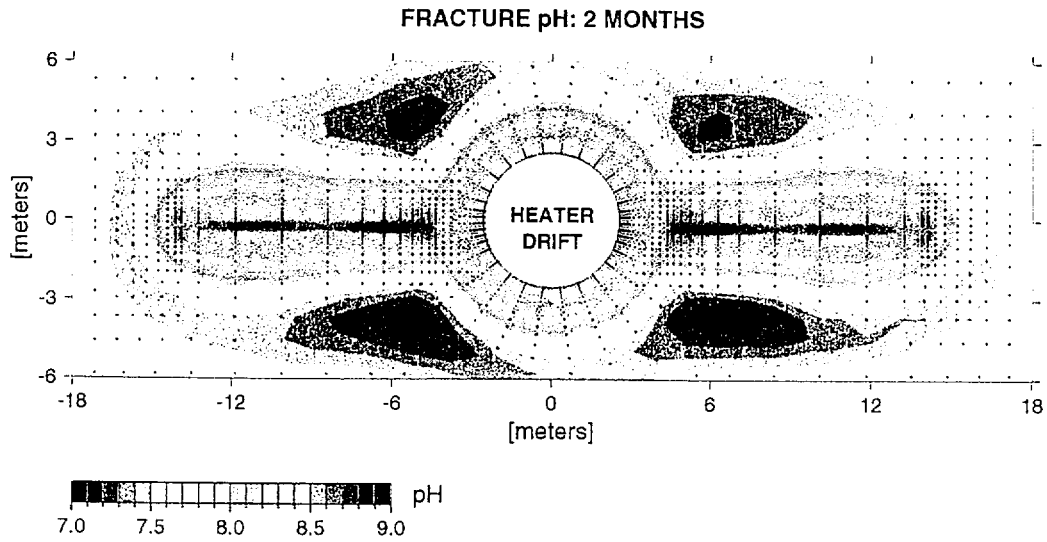


Figure 13.5 Pore water pH in fractures, for DST-1.

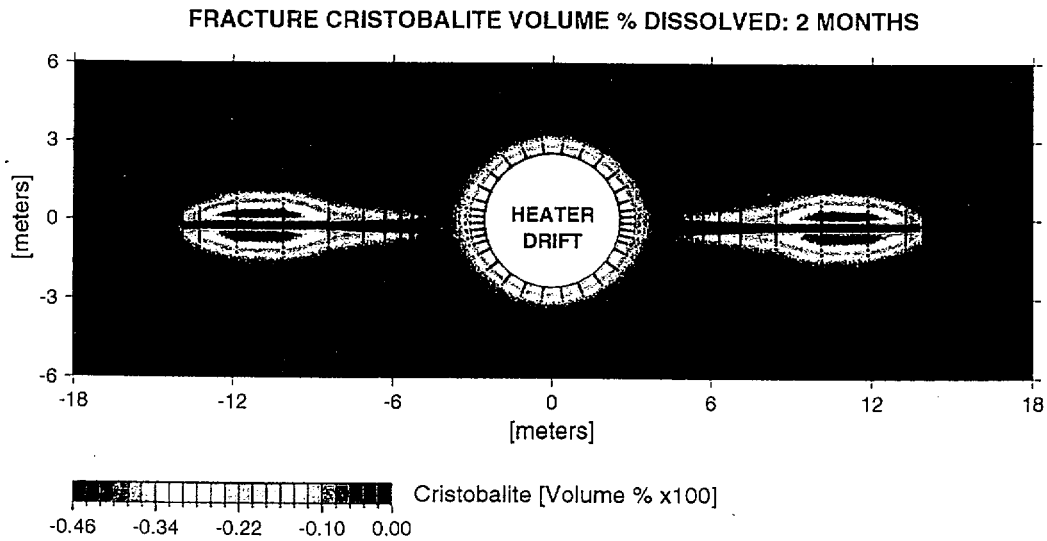


Figure 13.6 Volume percent change in cristobalite (x100) in fractures, for DST-1.

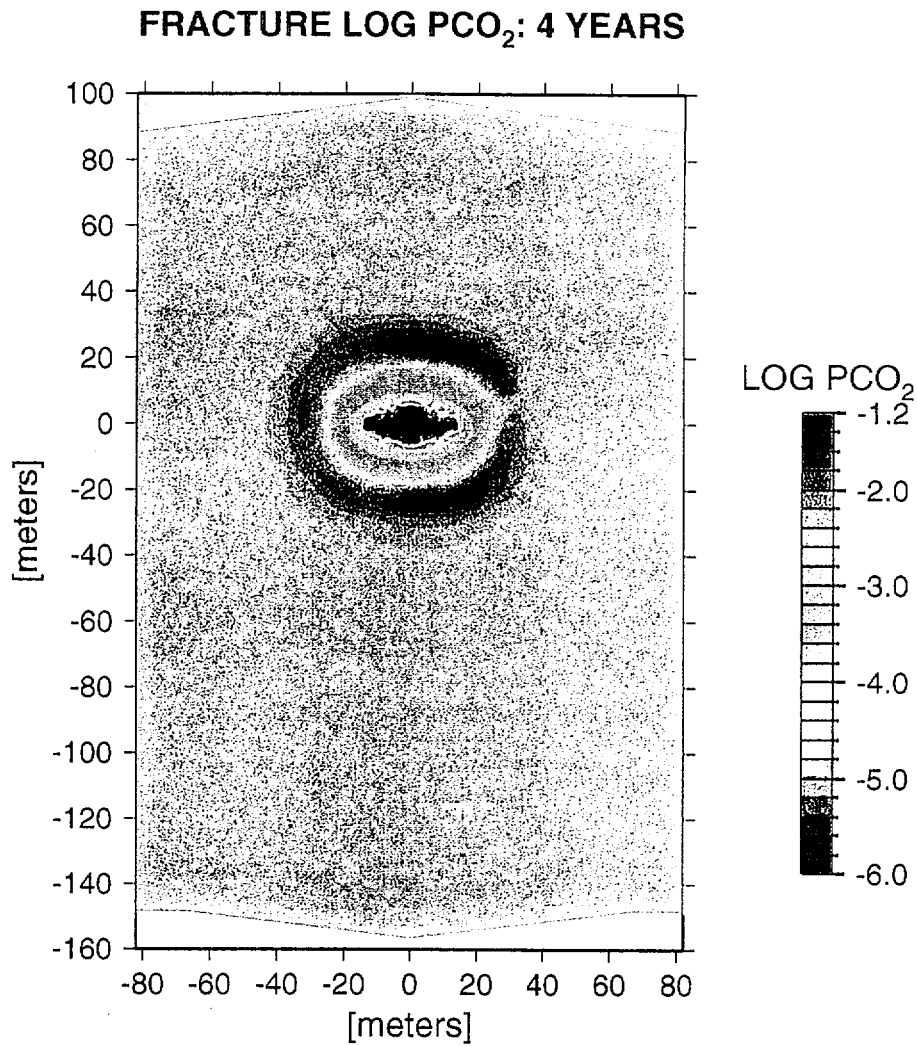


Figure 13.7 Simulation DST-1a. Log partial pressure of CO<sub>2</sub> in the gas phase in fractures at the end of the 4 year heating cycle of the DST.

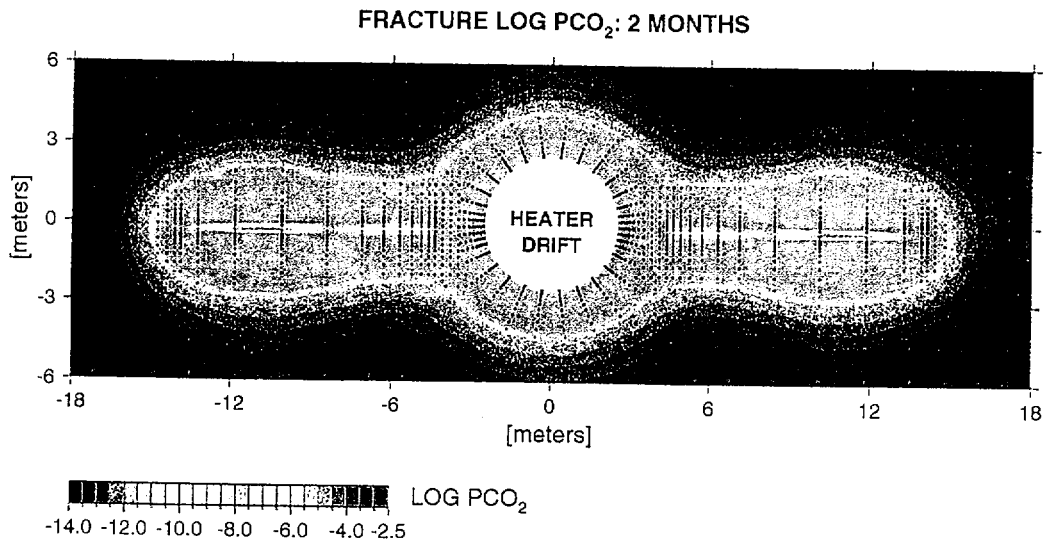


Figure 13.8 Partial pressure of CO<sub>2</sub> in the gas phase in fractures (log PCO<sub>2</sub>), for DST-2.

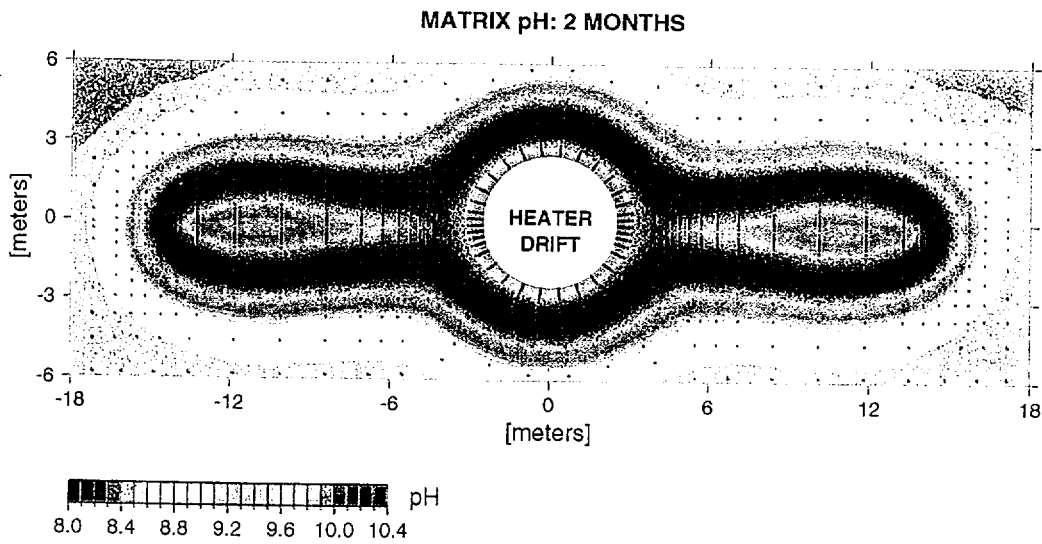


Figure 13.9 Pore water pH in the matrix, for DST-2.

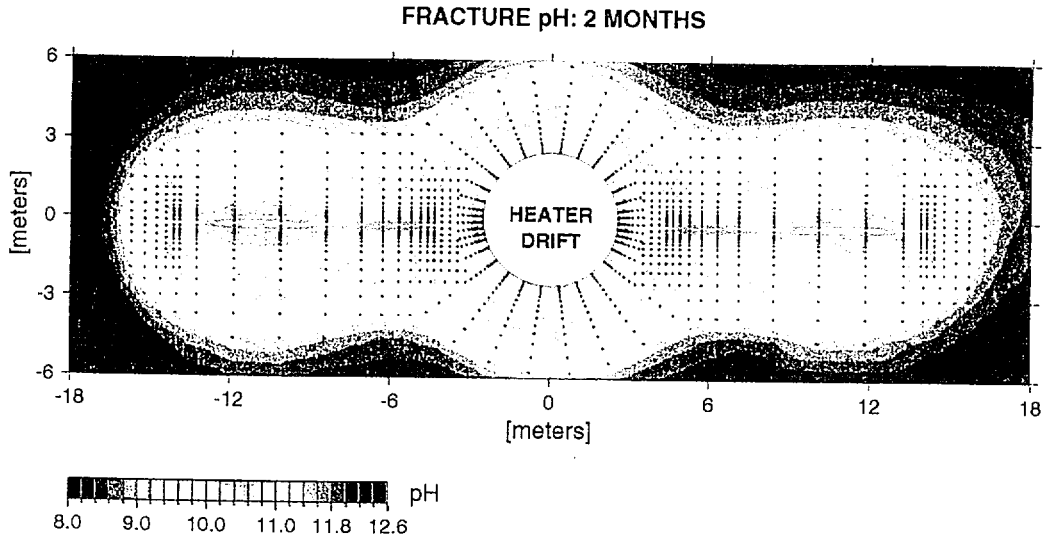


Figure 13.10 Pore water pH in fractures, for DST-2.

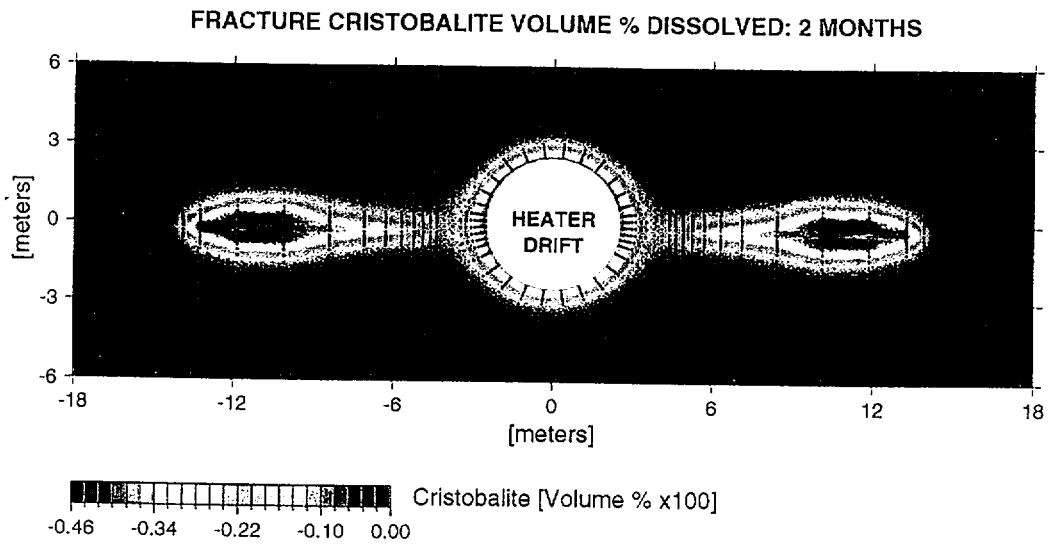


Figure 13.11 Volume percent change (x100) in cristobalite in fractures, for DST-2.

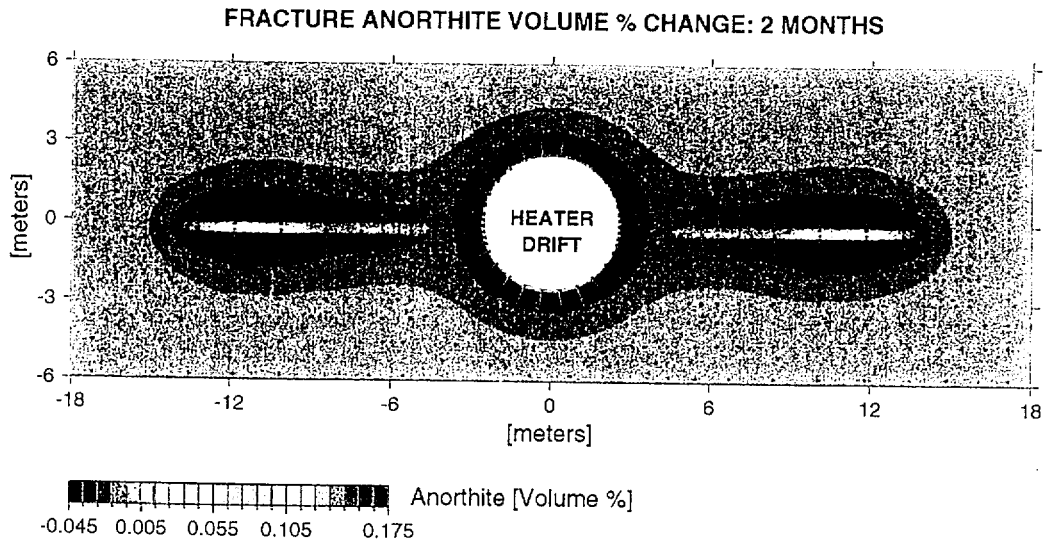


Figure 13.14 Volume percent change in anorthite in fractures, for DST-2.

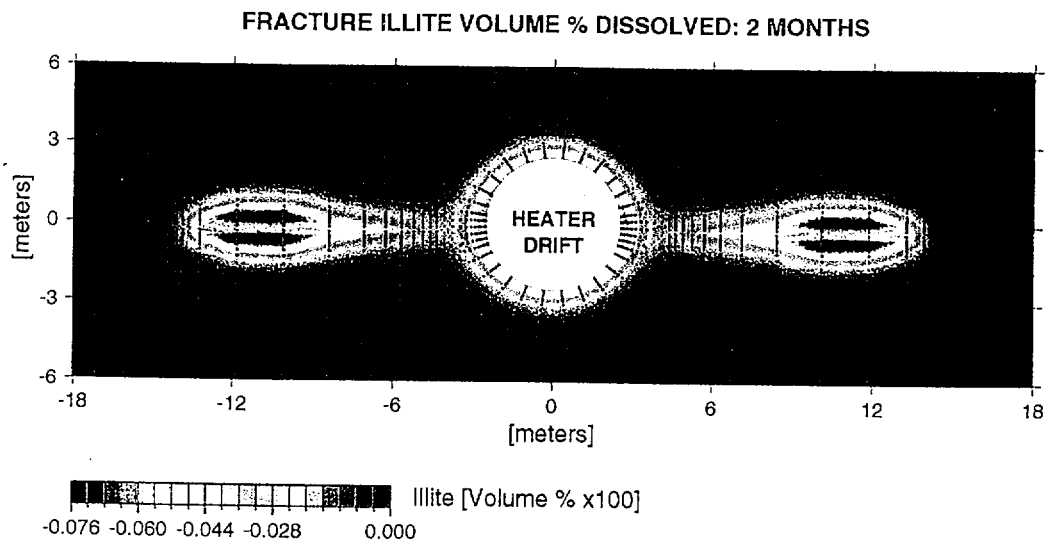


Figure 13.15 Volume percent change (x100) in illite in fractures, for DST-2.

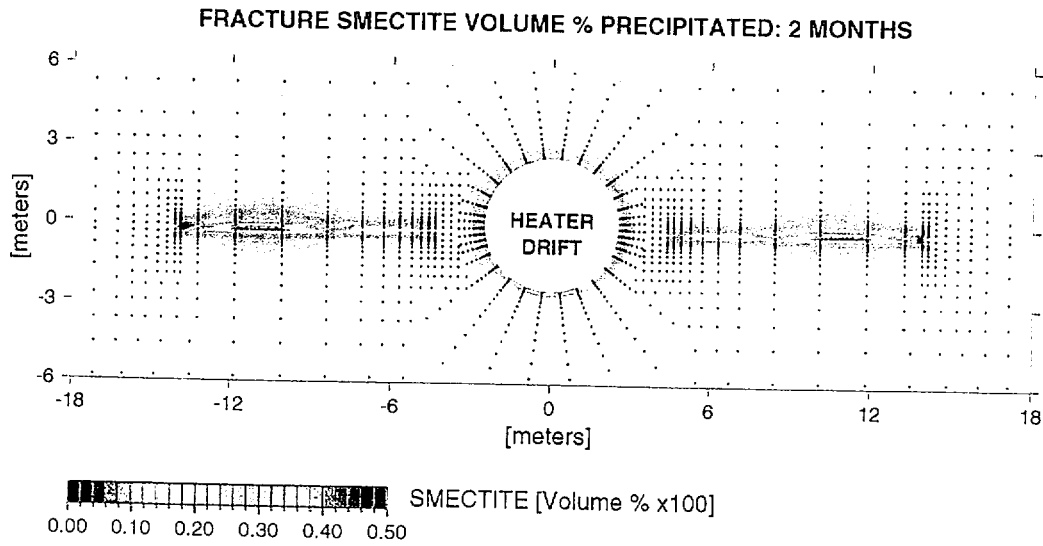


Figure 13.16 Volume percent change (x100) in smectite in fractures. Smectite is given as the sum of the Mg, Ca, Na, and K endmembers, for DST-2.

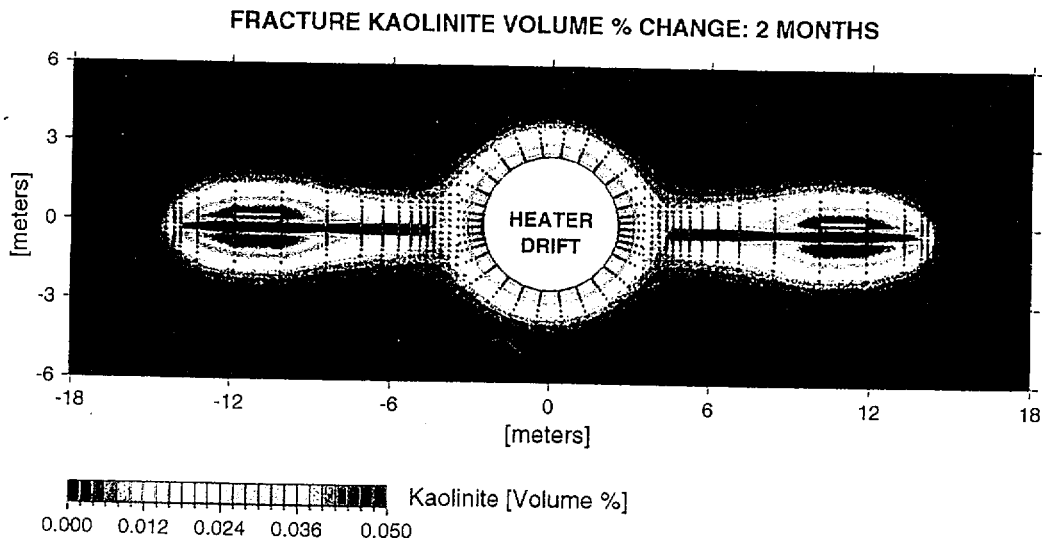


Figure 13.17 Volume percent change in kaolinite in fractures, for DST-2.

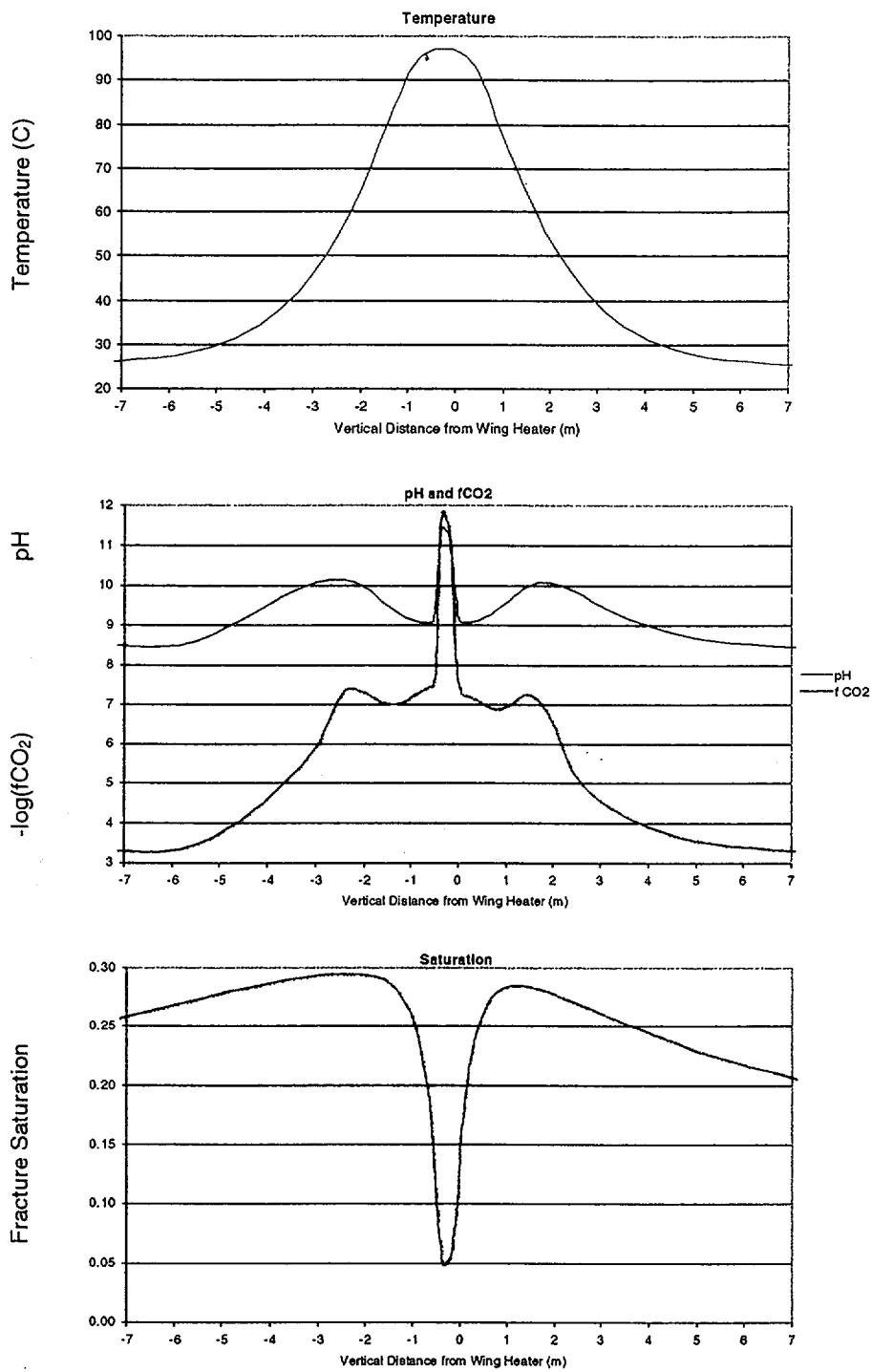


Figure 13.18 Temperature, pH, PCO<sub>2</sub>, and liquid saturation in fractures for a vertical profile through a wing heater (about 12 m to the left of the drift) in the DST-2 simulation.

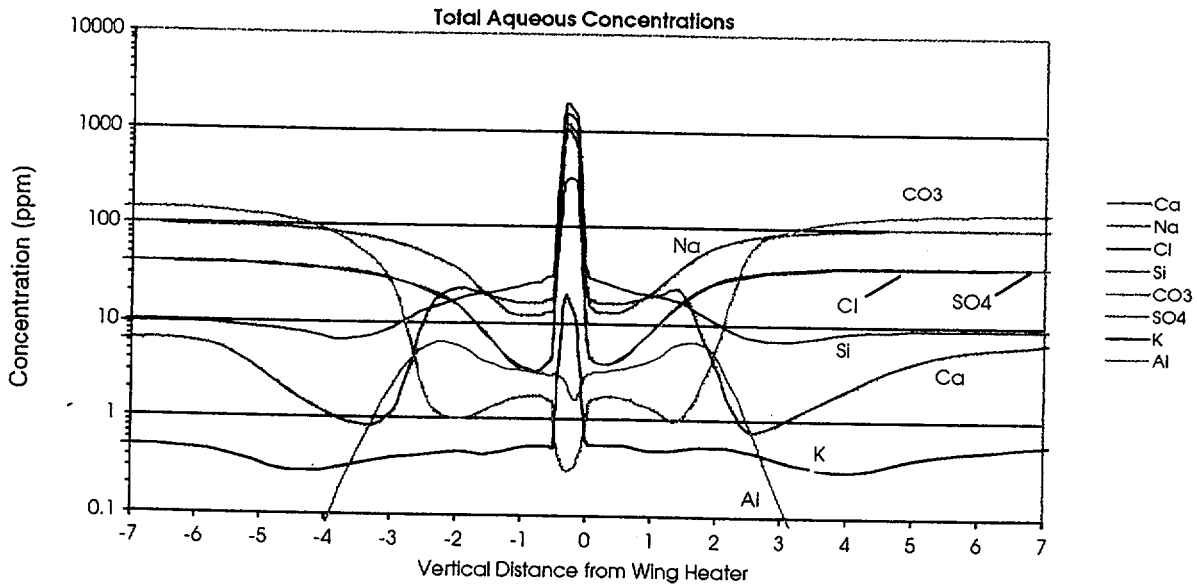
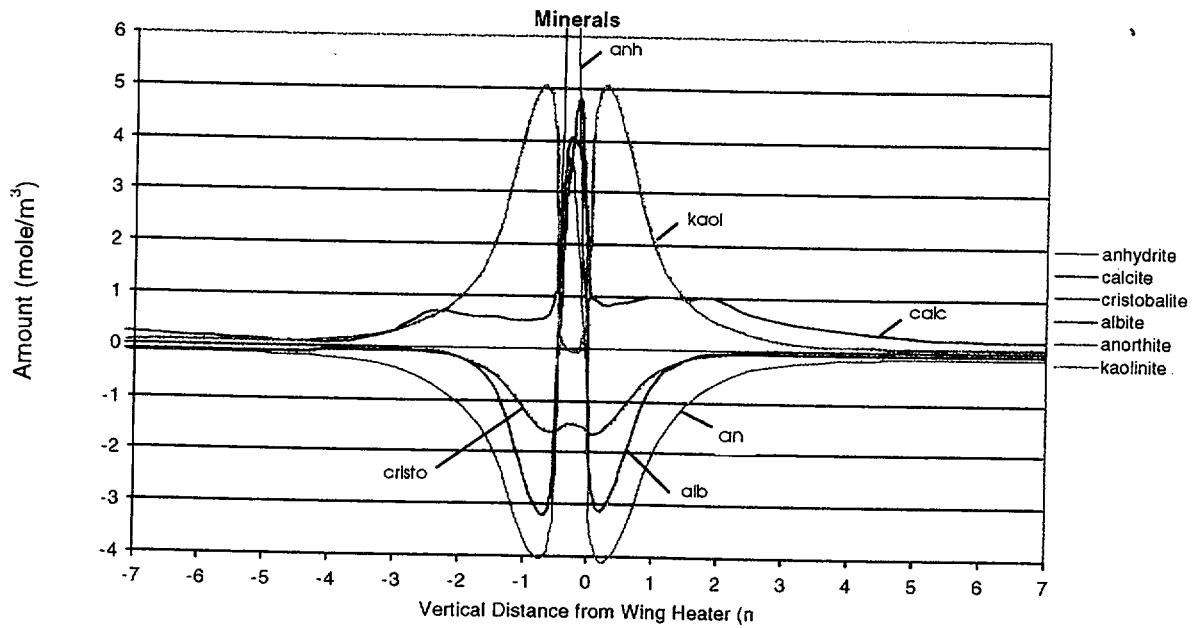


Figure 13.19 Major reacting minerals (cumulative change) and aqueous species concentrations in fractures for a vertical profile through a wing heater (about 12 m to the left of the drift) in the DST-2 simulation.

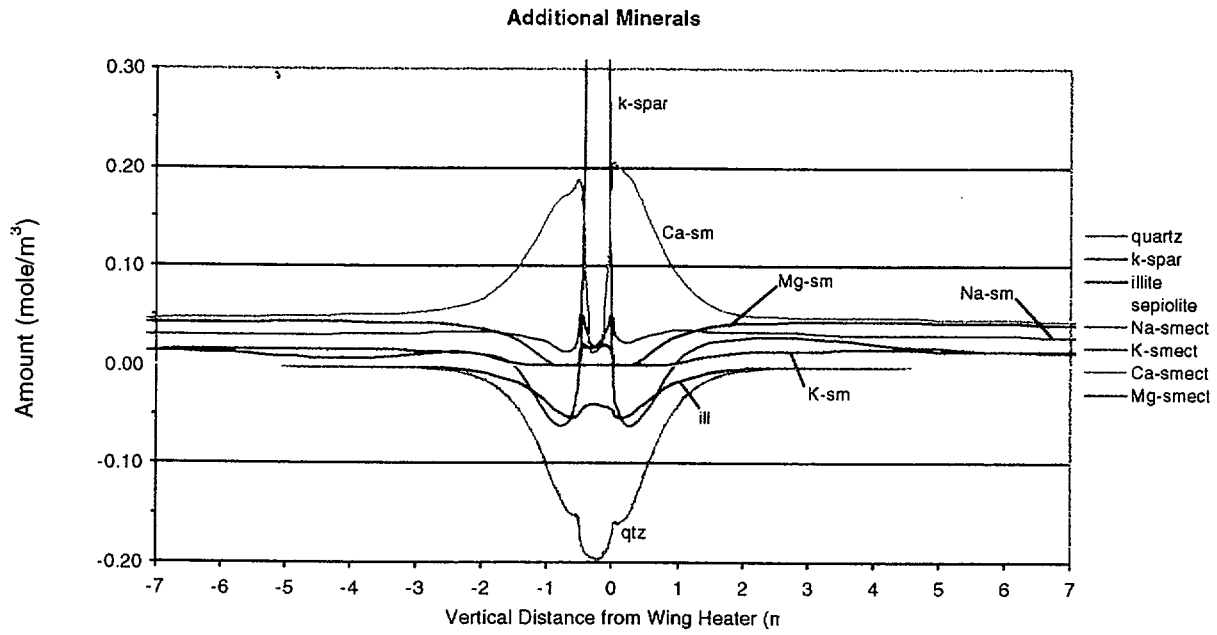


Figure 13.20 Other less volumetrically important minerals (cumulative change) in fractures for a vertical profile through a wing heater (about 12 m to the left of the drift) in the DST-2 simulation.

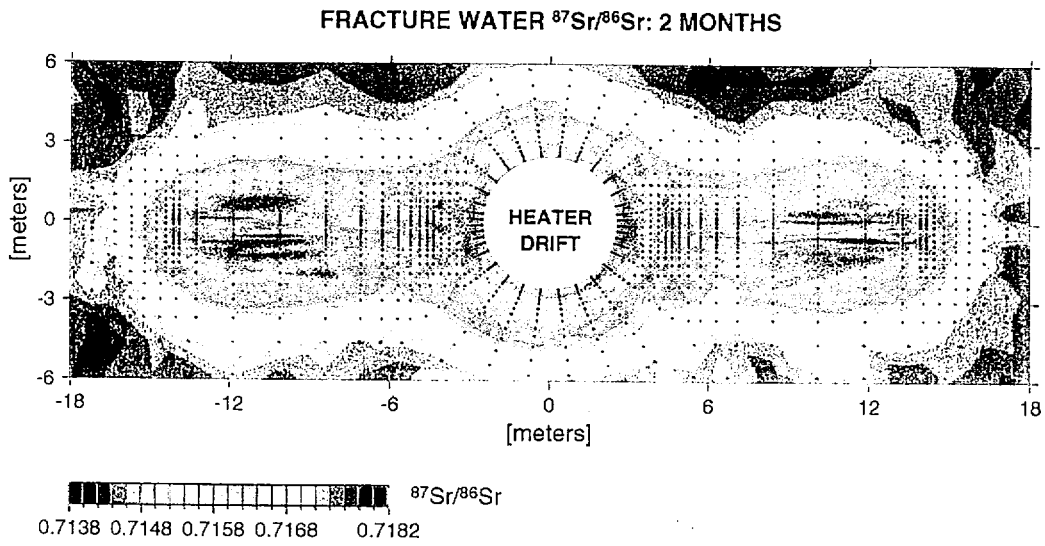


Figure 13.21  $^{87}\text{Sr}/^{86}\text{Sr}$  ratio in fracture pore water.

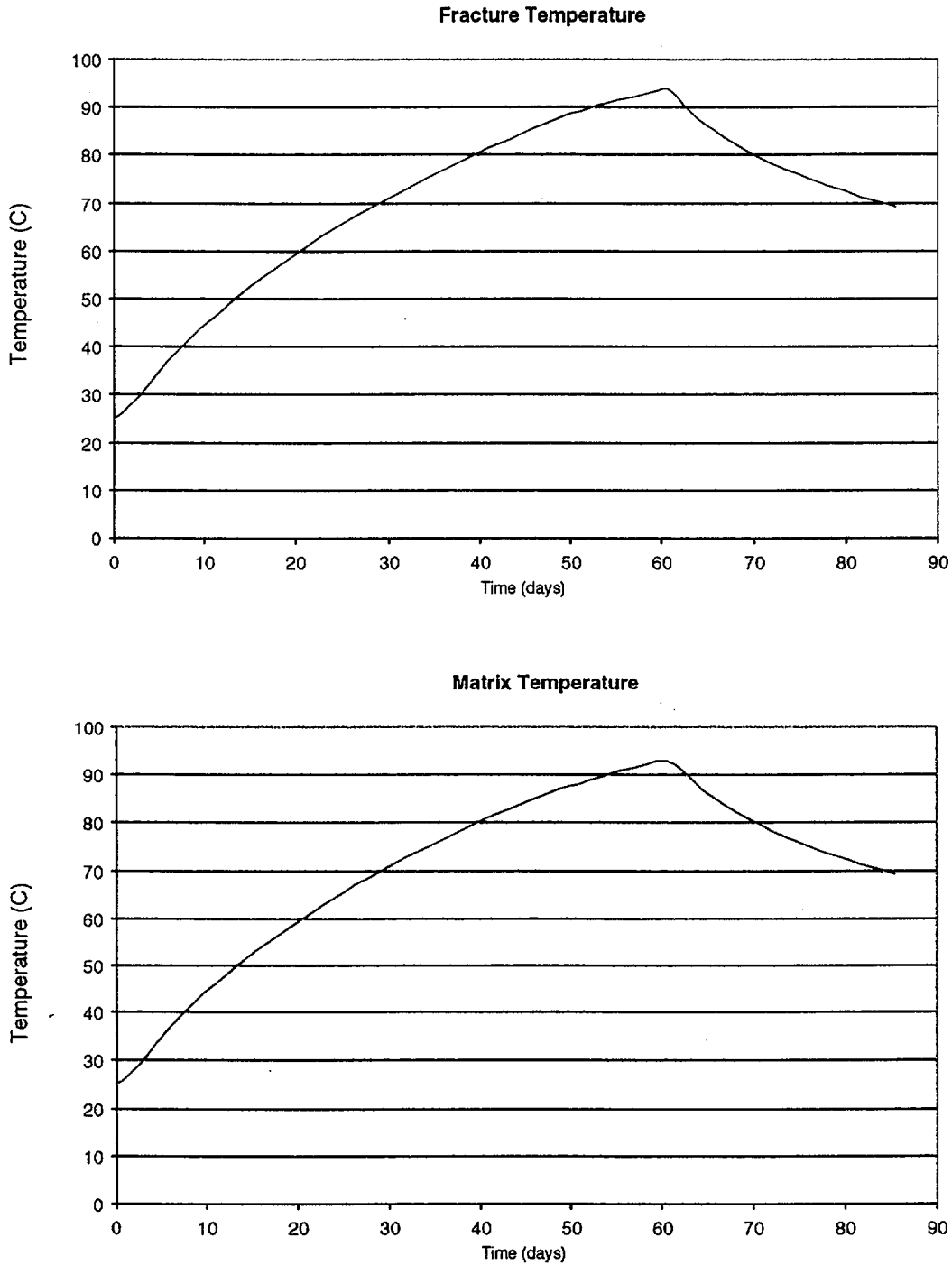


Figure 13.22 Fracture and matrix temperatures as a function of time for the DST-3 simulation. Cooldown starts at 60 days.

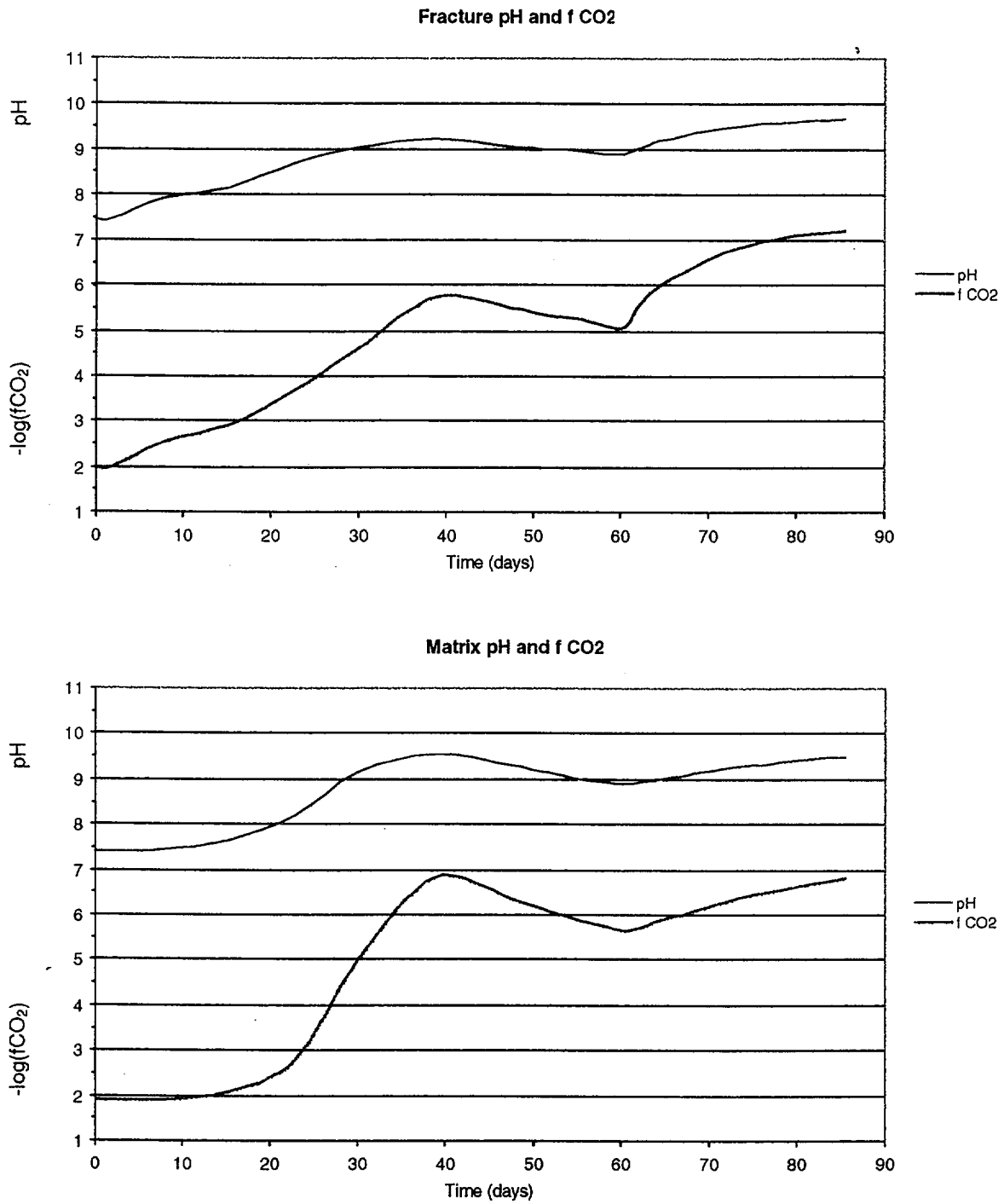


Figure 13.23 Fracture and matrix pH and fCO<sub>2</sub> as a function of time for the DST-3 simulation. Cooldown starts at 60 days.

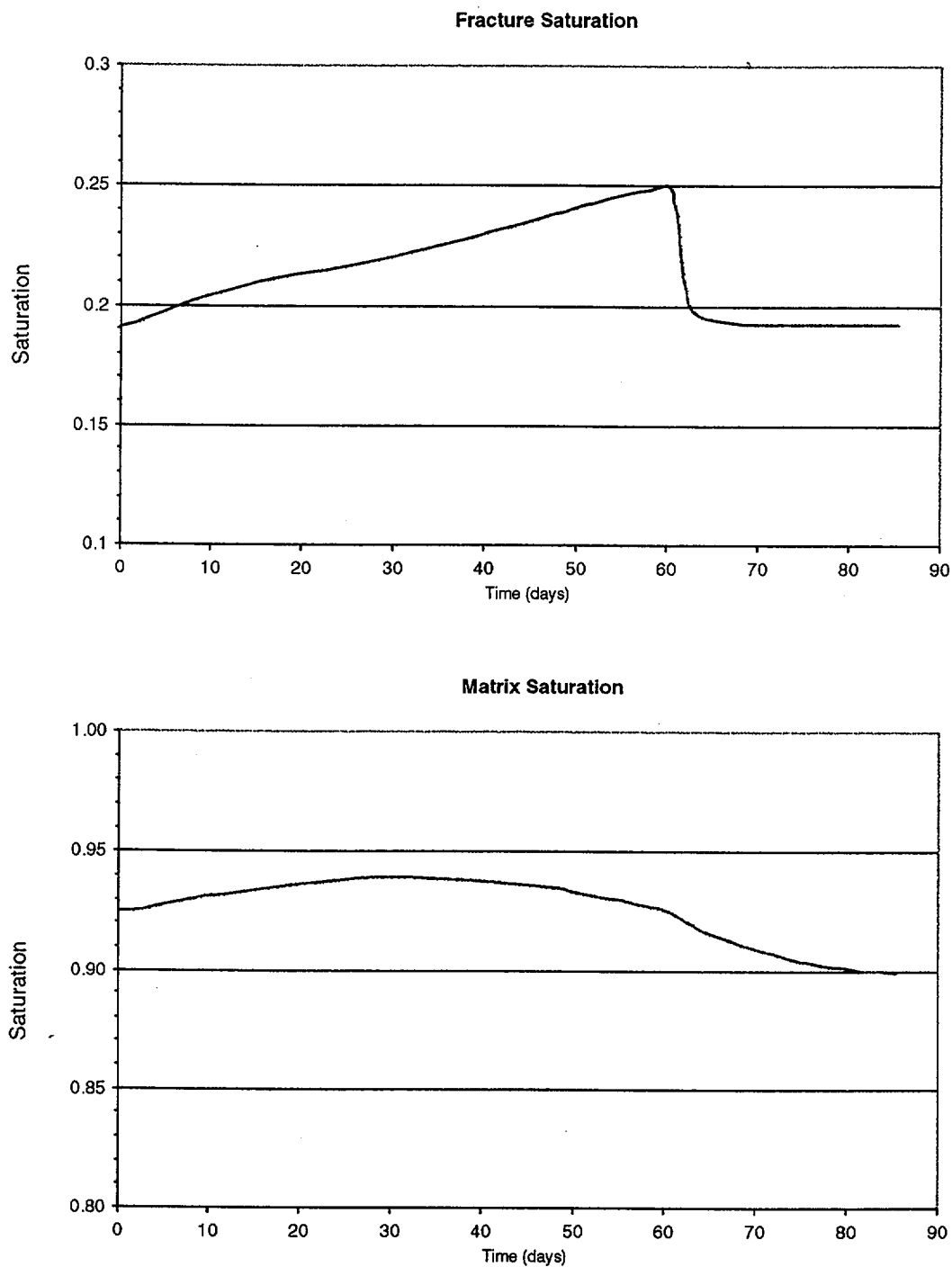


Figure 13.24 Fracture and matrix liquid saturation as a function of time for the DST-3 simulation. Cooldown starts at 60 days.

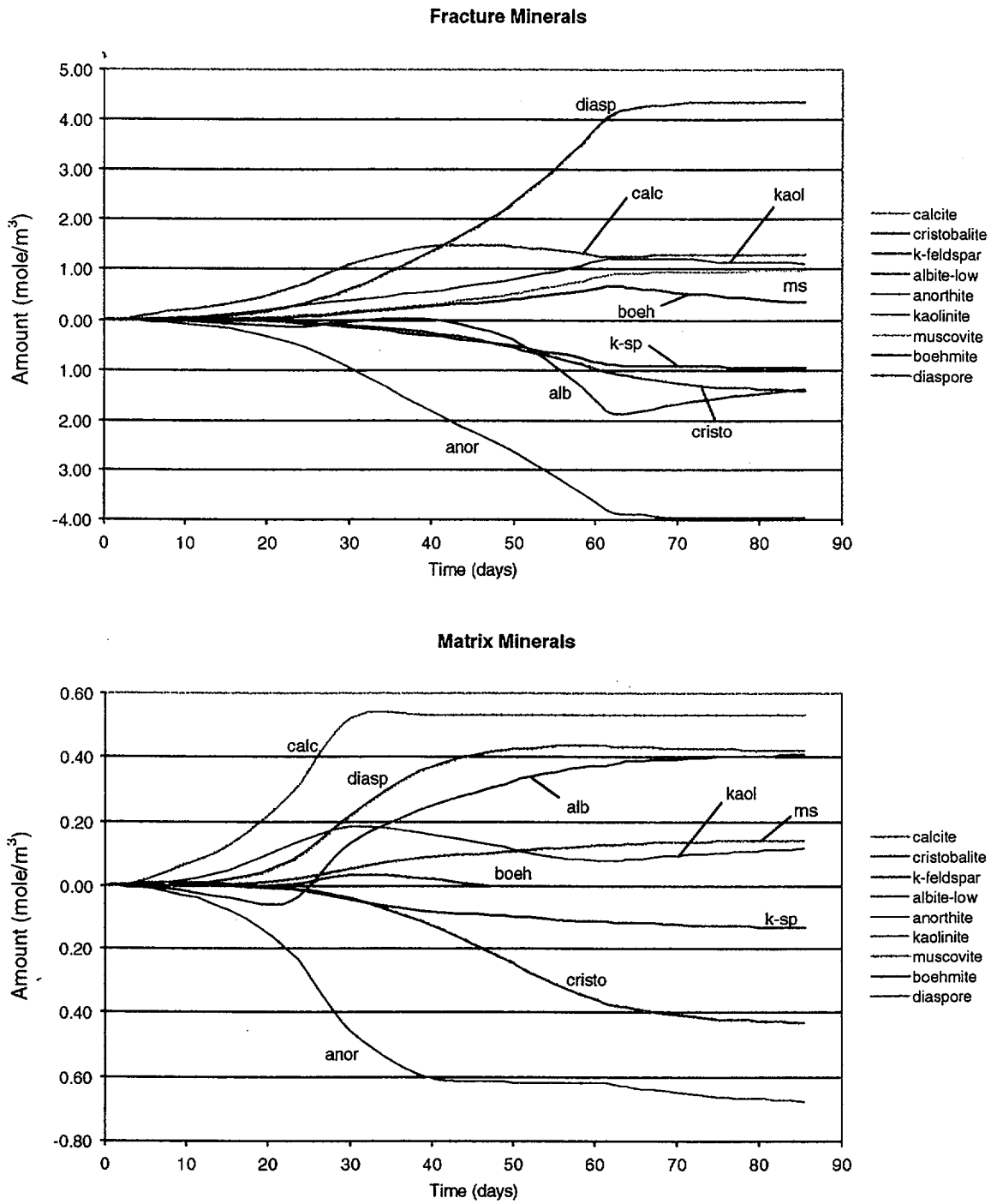


Figure 13.25 Major reacting minerals (cumulative change) in fractures and matrix as a function of time for the DST-3 simulation. Cooldown starts at 60 days.

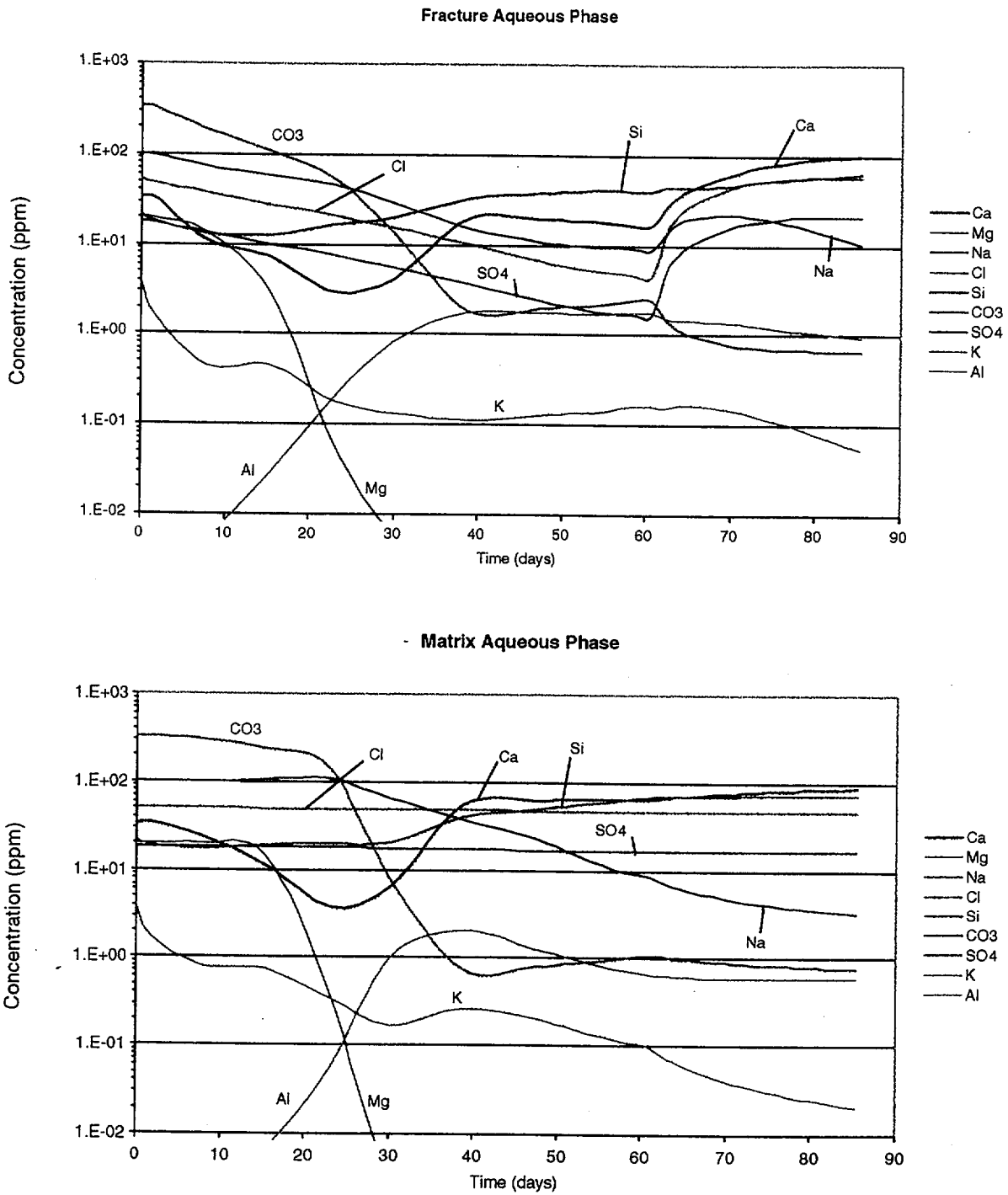


Figure 13.26 Aqueous species concentrations in fractures and matrix as a function of time for the DST-3 simulation. Cooldown starts at 60 days.

### FRACTURE CRISTOBALITE: 8 YEARS

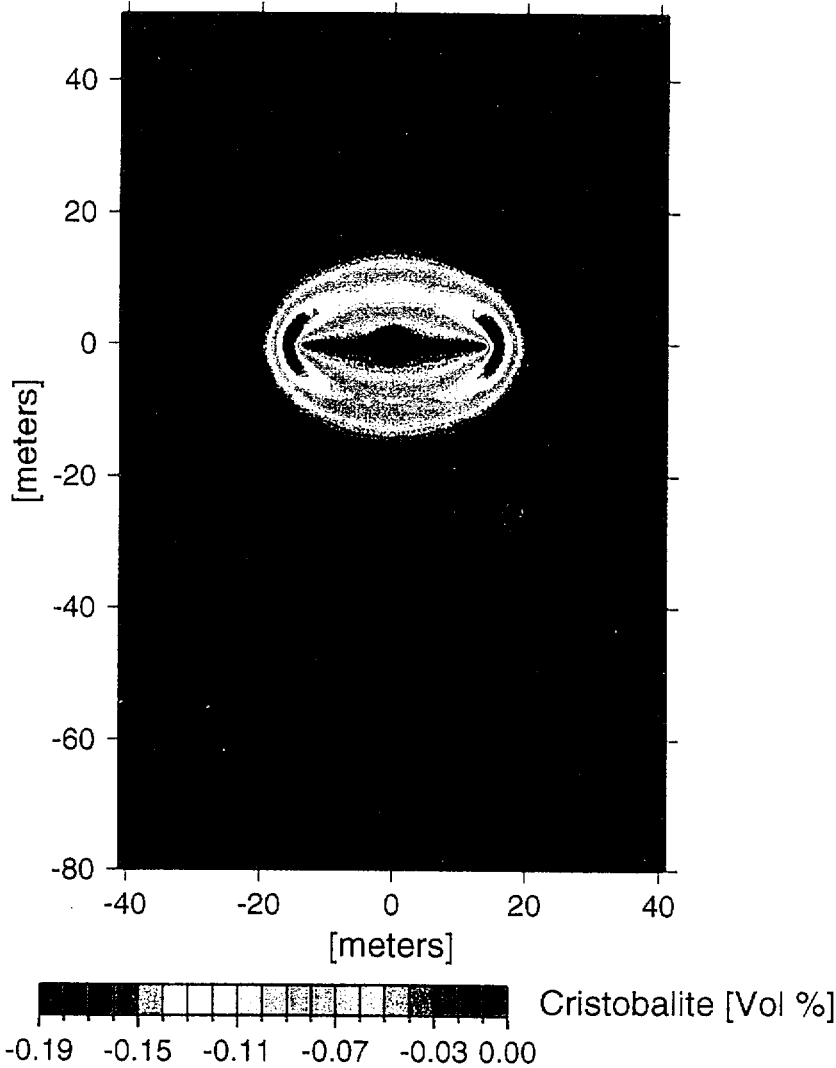


Figure 13.27 Simulation DST-4. Cristobalite dissolved in fractures at the end of the 8-year planned DST.

### FRACTURE AMORPHOUS SiO<sub>2</sub> : 8 YEARS

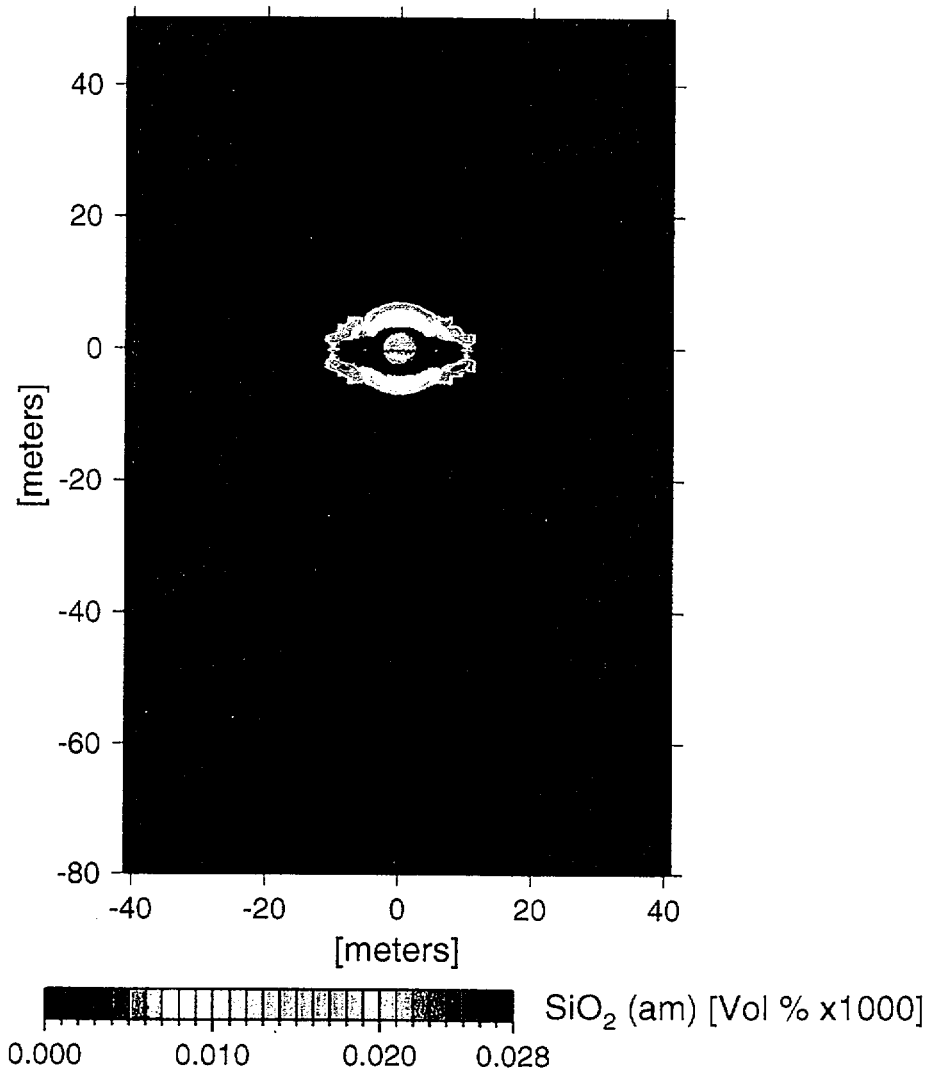


Figure 13.28 Simulation DST-4. Amorphous silica precipitated in fractures at the end of the 8-year planned DST.

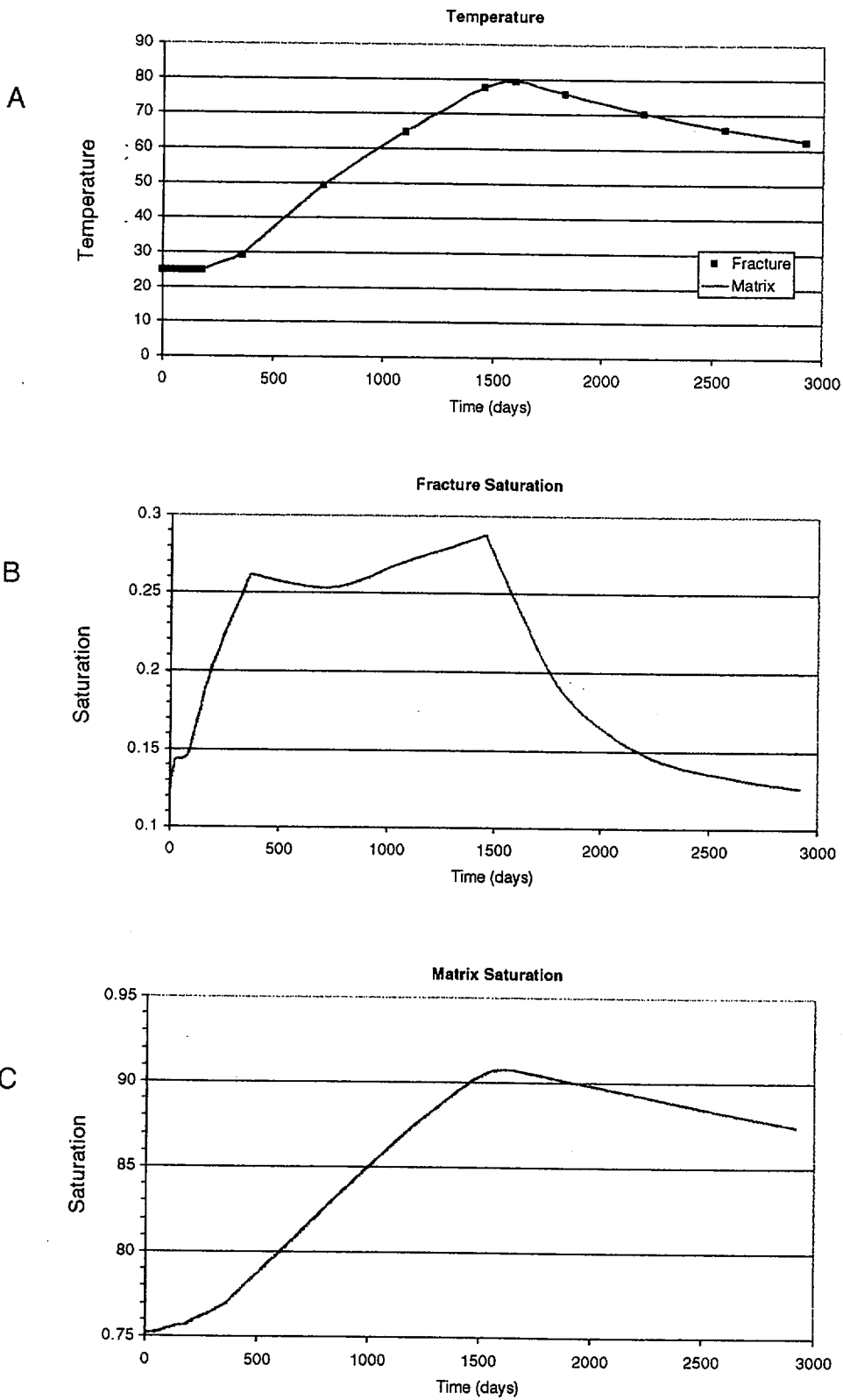


Figure 13.29 Simulation DST-4. a). Temperature in fractures and matrix in one node in the condensate region over the full 8-year heating and cooling phases of the DST. b). Liquid saturation in fractures. c). Liquid saturation in matrix.

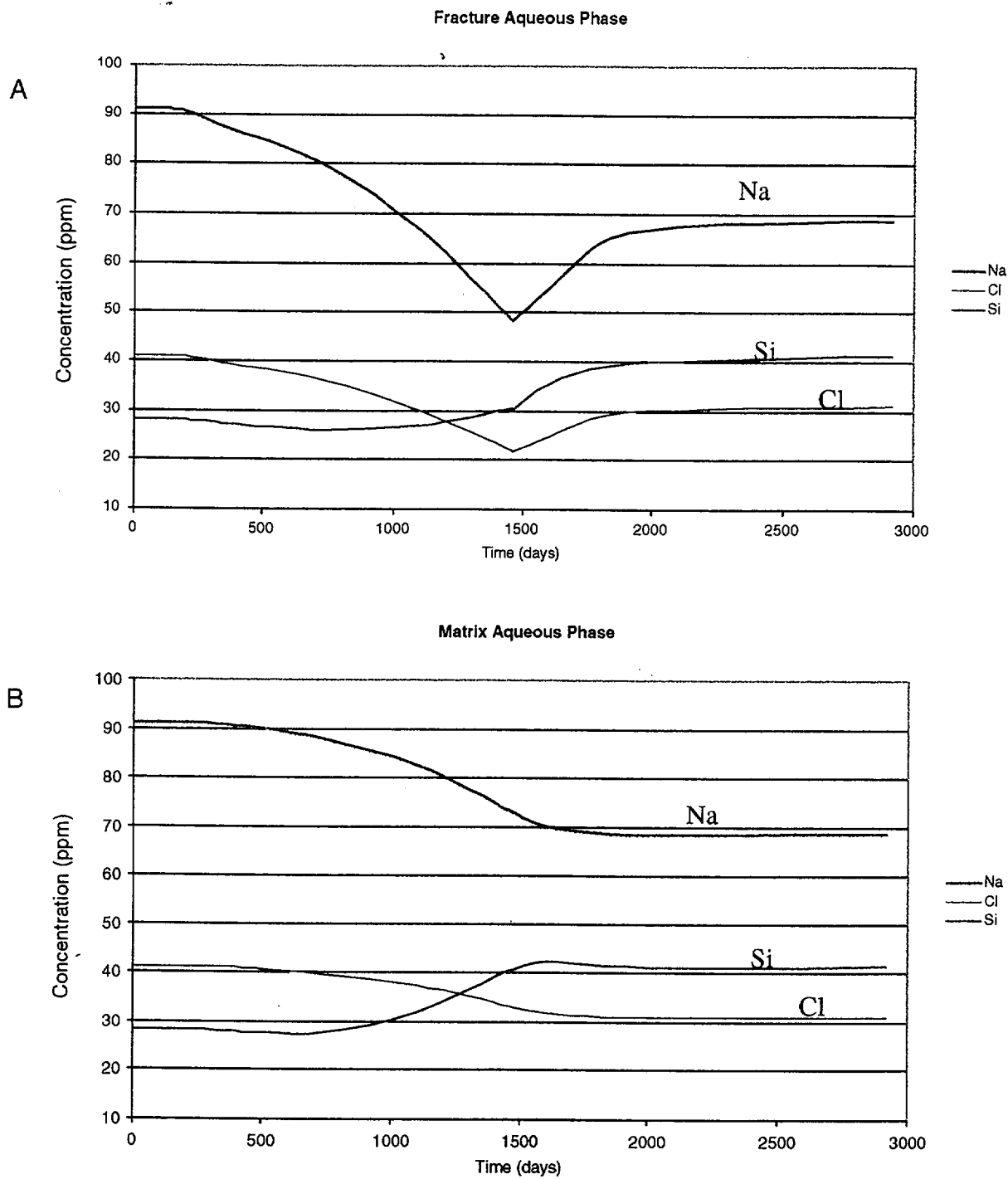
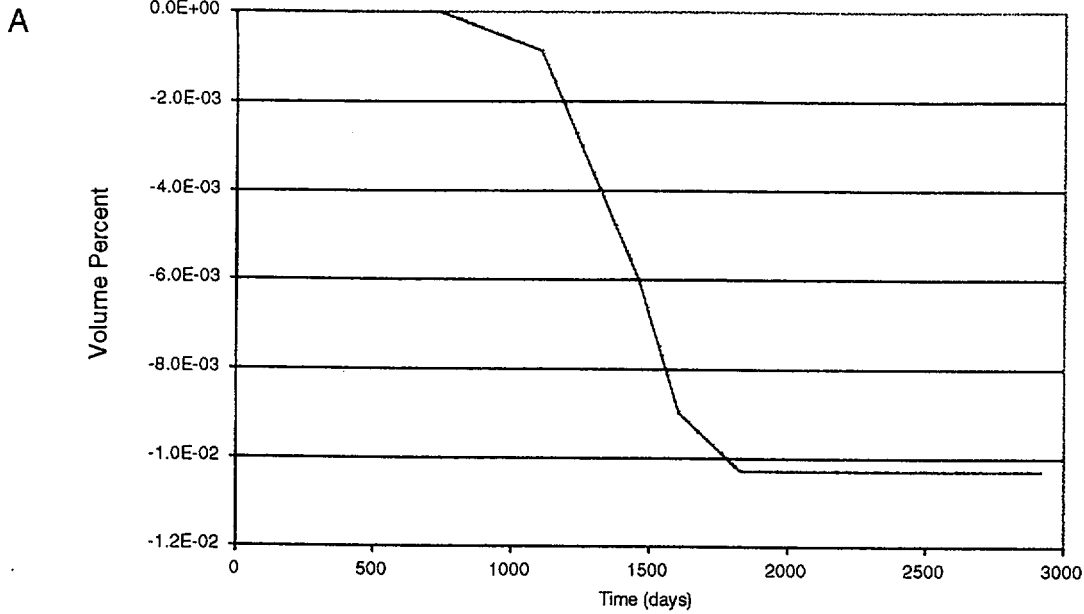


Figure 13.30 Simulation DST-4. a). Concentrations of aqueous species in fractures over the full 8-year heating and cooling phases of the DST. b). Concentrations of aqueous species in the matrix.

Fracture Minerals



Matrix Minerals

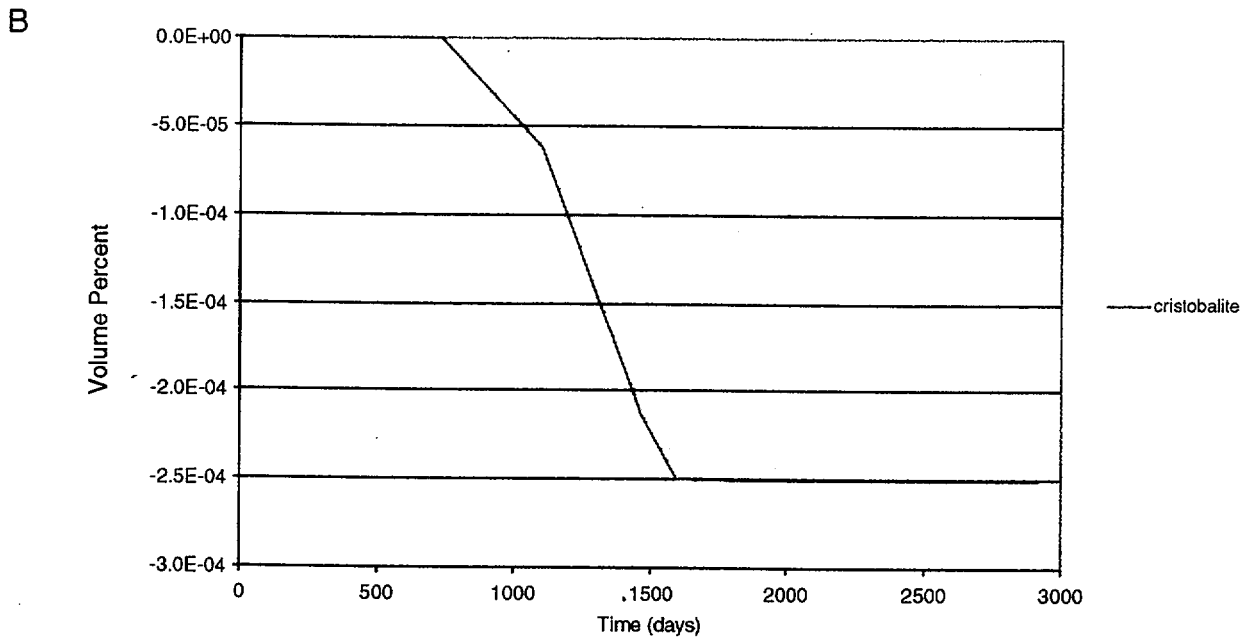


Figure 13.31 Simulation DST-4. a). Volume percent dissolution of cristobalite in fractures over the full 8-year heating and cooling phases of the DST. b). Volume percent dissolution of cristobalite in the matrix.